A DISSERTATION FOR THE DEGREE OF DOCTOR OF PHILOSOPHY

Preparation and Characterization of Porous Sheet with Cellulose Nanofibrils and its Potential Application

다공성 셀룰로오스 나노피브릴 시트의 제조 및 특성 구명과 적용성 연구

Advisor Professor : Dr. Hye Jung Youn

by Kyujeong Sim

PROGRAM IN ENVIRONMENTAL MATERIALS SCIENCE
DEPARTMENT OF FOREST SCIENCES
GRADUATE SCHOOL
SEOUL NATIONAL UNIVERSITY

February, 2016

ABSTRACT

Preparation and Characterization of Porous Sheet with Cellulose Nanofibrils and its Potential Application

Kyujeong Sim
Program in Environmental Materials Science
Department of Forest Sciences
Graduate School
Seoul National University

Cellulose nanofibrils (CNF) are renewable and biodegradable material with high mechanical strength and specific surface area. CNF has a width below 100 nm and the length is several micrometers. It is necessary to remove water from CNF suspension by dewatering and drying to utilize as a value-added product because CNF suspension has a lot of water. By dewatering and drying, the CNF can be converted to porous products. It is crucial to understand and control the nanostructure of porous CNF material. In this study, porous CNF sheet was prepared and its characteristics depending on the physicochemical properties of fiber and suspension, and drying condition were investigated. In the first, the effects of preparation conditions such as nanofibrillation degree of fibers, sheet forming condition, drying condition on the structural properties of CNF sheet were investigated. In the second, the properties of CNF suspension and CNF sheet were investigated depending on the degree of flocculation or dispersion of CNF by changing the electrical charge or surface tension of suspension. Further, the potential application of the porous CNF sheet as an air filter media was examined.

The CNF sheet with low density and high porosity could be prepared by supercritical drying, solvent exchange drying, and freeze drying due to the inhibition of hydrogen bonds and a low shrinkage during drying. The room temperature drying and hot pressing produced a very dense structure. Porosity of the CNF sheets was affected by the degree of nanofibrillation and dewatering as well as drying condition. The CNF sheet consisted of mainly mesopores in BET analysis. The CNF sheets showed a high tensile strain at break.

The degree of flocculation or dispersion of CNF was varied by controlling the electrical charge of CNF or surface tension of suspension. The electrical charge of CNF was controlled by chemical treatment (carboxymethylation and TEMPO-mediated oxidation) and chemical additive (salt), and their effects on the characteristics of CNF suspension and sheet were investigated. Carboxymethylation was carried out on pulp fibers as a pre-treatment before preparation of CNF. The gel-like and translucent CNF hydrogel was obtained. The viscosity of CNF suspension was increased by carboxymethylation due to the increased electrostatic repulsion, and the drainage rate was decreased significantly. The freeze dried sheet showed higher transparency than untreated CNF sheet. TEMPO-mediated oxidation was carried out as a post-treatment of CNF. The density of sheet made of TEMPO-oxidized CNF was increased with the amount of oxidizing agent. The flocculation of CNF was caused by the addition of salt because the degree of compression of electrical double layer changed by adsorption of cations onto CNF, which depends on the type and concentration of salt. Viscosity, storage modulus, and yield stress of the CNF suspension increased with an increase in ionic strength of suspension, showing more solid-like behavior. Bivalent cations were more effective for increasing network strength and

dewatering at a small addition amount of salt compared to monovalent cations. The flocculation degree of nanofibrils affected the porous structure of CNF sheet. The surface tension of suspension was changed by the addition of surfactant. The total drained water content and drainage rate were increased with the decreased in surface tension of water. The highly porous CNF sheet was produced by decreasing the surface tension of water, showing the maximum porosity of 91%.

To investigate the applicability of porous CNF sheet as a filter media, the porous sheet with high mechanical strength was prepared with natural pulp fibers or polyethylene terephthalate (PET) by adding CNF, and its characteristics were evaluated. The apparent density and porosity of porous sheets changed with relation to the morphology of the mixed fibers and drying methods. The tensile properties of the sheets were improved by the addition of CNF. The applicability of porous sheets as a filter media was examined by evaluating the filtration efficiency and pressure drop. The filtration efficiency of CNF-contained sheet greater than 99.97% was achieved by supercritical drying. The high pressure drop during filtration would be solved by surface treatment and controlling the fiber dimension. The porous CNF sheet is expected to be used as substrate for nanocomposite, water membrane filter as well as air filter media depending on its pore characteristics.

Keywords : Cellulose nanofibrils (CNF), sheet, pore, drying, flocculation, chemical treatment, salt, surfactant, rheological properties, dewatering, air filter

Student number : 2009-21202

List of Papers

This dissertation is written based on the following published papers:

Paper I

Effect of the number of passes through grinder on the pore characteristics of nanofibrillated cellulose mat

Kyujeong Sim, Jaeho Ryu, and Hye Jung Youn

Journal of Korea TAPPI (SCOPUS), 45(1):35-41 (2013)

-Designed and performed the experiments, wrote the paper.

Paper II

Structural characteristics of nanofibrillated cellulose mats: Effect of preparation conditions

Kyujeong Sim, Jaeho Ryu, and Hye Jung Youn

Fibers and Polymers (SCIE), 16(2):294-301 (2015)

-Designed and performed the experiments, wrote the paper.

Paper III

Surface modification of cellulose nanofibrils by carboxymethylation and TEMPO-mediated oxidation

Kyujeong Sim, Hye Jung Youn, and Yeonhee Jo

Journal of Korea TAPPI (SCOPUS), 47(2):42-52 (2015)

-Designed and performed the experiments, wrote the paper.

Paper IV

Flocculation behavior of cellulose nanofibrils under different salt conditions and its impact on network strength and dewatering ability

Kyujeong Sim, Jegon Lee, Hyeyoon Lee, and Hye Jung Youn

Cellulose (SCI), 22(6):3689-3700 (2015)

-Designed and performed the experiments, wrote the paper.

Paper V

Preparation of porous sheets with high mechanical strength by the addition of cellulose nanofibrils

Kyujeong Sim, and Hye Jung Youn

Cellulose (SCI), Accepted (2016.01.20), DOI 10.1007/s10570-016-0865-6

-Designed and performed the experiments, wrote the paper.

Table of Contents

Chapter 4

Chapter 5

List of Table

List of Figures

Chapter 1

Introduction

1. Introduction

Cellulose is the most abundant natural organic material and is a linear polysaccharide composed of D-anhydroglucopyranose units linked by 1, 4-β-glycosidic bonds (Klemm et al. 1998). Cellulose has been used in many applications because of its advantages such as biocompatibility, biodegradability, thermal and chemical stability, high strength, durability, and flexibility (Zugenmaier 2008; Deng et al. 2009). Individual cellulose molecular chains are aggregated together by van der Waals forces, and intra- and inter-molecular hydrogen bonds. The cellulose molecular chains then form larger units called microfibrils. The width of microfibrils ranges from 2 to 20 nm, significantly depending on their origin (Pääkkö et al. 2007; Iwamoto et al. 2008; Wågberg et al. 2008; Habibi et al. 2010) and they have several micrometers in length. Microfibrils show outstanding elastic modulus of 138 GPa (Iwamoto et al. 2007). Cellulose nanofibrils (CNF) consist of microfibrils or their aggregates by diminishing size of the cellulose fibers. Since the ‘nano’ concept has received the spotlight in many scientific studies, CNF also has drawn great attention in the cellulose research fields based on earlier studies and technologies.

CNF can be obtained by mechanical treatment, typically in aqueous suspension. The first report on preparation of microfibrillated cellulose (MFC) suspension was in 1983 by Turbak et al. (1983) and Herrick et al. (1983). The wood pulp fiber suspension was passed several times through a high pressure homogenizer, and then the cellulose fibrils that are nanometers in width were produced. Besides the high pressure homogenizer (Nakagaito and Yano 2004;

Iwamoto et al. 2005; Stenstad et al. 2008), other methods such as microfluidizing (Zimmermann et al. 2004; Aulin et al. 2010b; Taipale et al. 2010) and grinding (Taniguchi and Okamura 1998; Abe et al. 2007; Nogi et al. 2009; Ifuku and Saimoto 2012) have been reported to obtain CNF suspension. Various mechanical, chemical or enzymatic pretreatment also have been conducted in order to produce more homogeneous CNF and reduce energy consumption in CNF production (Zimmermann et al. 2004; Henriksson et al. 2007; Saito et al. 2007; Isogai et al. 2011).

The size reduction from milliscale to nanoscale in width by mechanical shearing offers new potential with unique properties such as a high aspect ratio, high mechanical strength, and high surface area (Iwamoto et al. 2007; Rodionova et al. 2011; Xhanari et al. 2011). Therefore, CNF has been considered as a potential material for various industrial fields. The application of CNF as a strength-enhancement additive in biocomposite materials has been studied (Hubbe et al. 2008; Siqueira et al. 2010; Siró and Plackett 2010). In addition, CNF can be applicable to packaging and display substrates. CNF has been reported to create dense film, which provides barrier and optical transparency properties (Fukuzumi et al. 2009; Syverud and Stenius 2009; Okahisa et al. 2009; Aulin et al. 2010; Zheng et al. 2013). The study on medicine (Bhattacharya et al. 2012; Cai et al. 2014; Plackett et al. 2014) and paper coating (Dimic-Misic et al. 2013; Lavoine et al. 2014) has been also reported.

Because CNF is generally produced by mechanical shearing of pulp fibers in aqueous suspension at low consistency (<3%), proper processes of

suspension such as casting, dewatering or drying are required for the use of CNF. An aqueous CNF suspension can be easily converted to dense product (film or composite) by conventional heat drying. In case of porous products (foam or sheet), however, the appropriate drying condition is necessary to control hydrogen bonding during drying. The porous products, especially sheet form, based on CNF have a potential as a filter media, separator of secondary lithium-ion batteries, substrate for biocomposites, and so on. It is crucial to prepare and control the structure of the porous CNF product. To control the nanostructure, it is necessary to understand how processing condition affect the product structure.

Chemical treatment or various additives such as polyelectrolyte, salt, and surfactant can affect the structure of nanofibril network because CNF has electrical charge in water. The effect of polyelectrolyte addition on the network properties of CNF suspension has been investigated (Ryu 2013). However, the effects of surface modification or additives on characteristics of porous product after drying were not examined. Moreover, understanding and controlling the rheological properties of CNF suspension is important. It would be useful to predict the network structure of the CNF suspension and the final product, as well as the behavior of CNF in the pumping, shearing and forming processes.

Exploring the applicability of porous CNF product is another major global concern. As is already mentioned, the porous CNF product has a potential in various fields. It is expected that the end use of porous CNF product can be varied depending on its pore characteristics. One of them, for

example, is filter media. Many industrial fields including the hospital, semiconductor, pharmaceutical, and food sectors, need to remove the pollutants from the air or water to maintain a clean environment during work or the manufacture of products (Barhate and Ramakrishna 2007). Pollutants can be removed with various types of filter media. It is necessary to use appropriate filter media depending on pollutant type and size. The filter media used for air filtration are categorized according to their filtration efficiency (e.g., medium, HEPA (high efficiency particulate air), and ULPA (ultra low penetration air) filters) (Yun et al. 2007; BS-EN1822-1 2009). Water filtration is classified according to pollutant size because most types of pollutants exist in the form of particles (Gopal et al. 2006; Sundarrajan et al. 2013). Generally, the removal of pollutants greater than 100 μm in diameter is classified as particle filtration. The removal of particles that range from 0.1 μm to 10 μm and from 0.01 μm to 0.1 μm is classed as micro- and ultrafiltration, respectively. Nanofiltration means a filtration process that removes particles that are 0.001 – 0.01 μm in diameter. Substances with a diameter of less than 0.001 μm can be removed by reverse osmosis filtration. Contrary to filter media made of synthetic fibers based on petrochemical polymers, porous sheet with cellulose fiber and CNF promises us the eco-friendly filter media. To utilize the porous CNF sheet as filter media, the filtration performance depending on the pore characteristics should be carried out preferentially.

2. Objectives

The objective of this study is to understand the effect of the physicochemical properties of fiber and suspension, and drying condition on the characteristics of CNF suspension and CNF sheet. To find out key factor for preparing porous sheet from CNF suspension, the CNF sheets were prepared depending on various preparation conditions and its characteristics were investigated. It is easy to make a film with CNF by casting and room temperature drying, which resulted in a very dense structure with high transparency. To create a porous structure, however, it is crucial to determine a proper preparation condition in order to control hydrogen bonding during drying. Nanofibrillation of fibers, dewatering, drying methods, chemical treatment, additives, and mixing of other fibers were examined as factors to control suspension network and fibrils bonding. The properties of suspension and porous CNF sheet were investigated. In addition, the potential application of porous CNF sheet was explored. This study mainly consists of three parts:

– In the first part, the structural properties of CNF sheet were investigated depending on the degree of nanofibrillation of fibers, sheet forming condition, and drying condition.

– In the second part, the effect of the degree of flocculation or dispersion of CNF on the properties of CNF suspension and CNF sheet was investigated. The degree of flocculation or dispersion of CNF was controlled by changing the electrical charge or surface tension. The electrical charge of CNF was varied by chemical treatment or controlling the ionic strength of suspension

with salt. Surface tension of suspension was changed by surfactant. The suspension properties were investigated in terms of rheological properties and dewatering ability of CNF suspension.

– In the last part, the porous sheets were prepared by mixing other fibers with CNF and then, the applicability of the porous CNF sheet was examined to suggest its potential application.

Chapter 2

Literature Reviews

1. Preparation of CNF and its Characteristics

Strong mechanical shearing action is necessary to fibrillate the cellulose pulp fibers into nano-sized dimension in width. Generally, CNF has the width below 100 nm and the length is several micrometers. The preparation of CNF using a high pressure homogenizer, a microfluidizer, and a grinder has been reported.

The microfibrillated cellulose (MFC) was reported firstly in 1983 by Turbak et al. (1983) and Herrick et al. (1983). The wood pulp fibers were fibrillated to nanosize under a high pressure and shearing action. The refining has been generally used together as a mechanical pre-treatment before homogenizing (Nakagaito and Yano 2005; Stenstad et al. 2008). A microfluidizer has been also used to prepare CNF as pulp fibers are passed through a narrow tube with high speed (Zimmermann et al 2004; Aulin et al. 2010b). In the grinder, CNF is prepared as the pulp fibers suspension is passed between two grinder stones. Abe et al. (2007) obtained the CNF with about 15 nm in width from softwood pulp fibers by grinding. Iwamoto et al. (2005) integrated the refining, homogenizing and grinding, resulting in the CNF width ranged from 50 nm to 100 nm.

CNF can be also prepared by chemical treatment such as TEMPO (2,2,6,6-tetramethylpiperidine-1-oxyl radical)-mediated oxidation. TEMPO is a stable radical and soluble well in water. In 1995, de Nooy et al. (1995) applied TEMPO-mediated oxidation on polysaccharides such as starch and pullulan for the first time. The C-6 hydroxyl group of cellulose is substituted

to carboxylic acid group by TEMPO-mediated oxidation. The increased electrostatic repulsion by carboxylic acid group made the cellulose fibers fibrillate to cellulose nanofibrils (Isogai et al. 2011). TEMPO-mediated oxidation can occur under both alkali and acidic conditions. TEMPO, NaBr, and NaClO are used in alkali condition (pH 10 ~ 11) at room temperature (Saito and Isogai 2004; Saito et al. 2006; Saito et al 2007; Okita et al. 2010). In the case of acidic condition, TEMPO, NaClO, and $NaClO_2$ are used and the reaction occurs at 40°C or 60°C with buffer solution of pH 4.8 or 6.8 (Saito et al. 2009; Tanaka et al. 2012). The TEMPO-oxidized cellulose nanofibers (TOCNs) can be obtained after mechanical shearing followed by centrifugation. The TOCNs are well dispersed with an increase in substituted carboxylic acid content, resulting in the highly transparent suspension (Saito et al. 2007). It has been reported that the film made of TOCNs showed the transmittance of 80% - 90% and excellent barrier property (Fujisawa et al. 2011; Fukuzumi et al. 2013).

TEMPO-mediated oxidation has been also used as pre- or post-treatment for preparing of cellulose nanofibrils. Besbes et al. (2011) could overcome the problem in yield decrease and reduced the passes number of homogenizing by TEMPO-mediated oxidation as pre-treatment. Silva et al. (2012) conducted TEMPO-mediated oxidation on homogenized cellulose nanofibrils as post-treatment and then, the relatively more homogeneous substitution of carboxylic acid group on cellulose could be achieved.

2. Potential Application of CNF

2.1 Nanocomposites

Nanocomposite consists of two-phase materials that one of them has at least nanoscale dimension (1 – 100 nm) (Siró and Plackett 2010). A single cellulose nanofibril has a high mechanical strength and its network has a high specific surface area (Iwamoto et al. 2007; Rodionova et al. 2011; Xhanari et al. 2011). Because of these attractive characteristics, numerous studies on utilization of CNF as reinforcing filler have been reported. Besides a superior strength property, CNF also has a thermal stability and lower density than metal and glass. Therefore, it may be achieved to prepare the light-weight nanocomposite with high strength using CNF as filler. However, CNF has hydrophilic nature because of the great amount of hydroxyl group on cellulose surface so that it is difficult to disperse CNF homogeneously in organic solvent or non-polar polymer solution, resulting in a low miscibility or compatibility with polymer matrix when preparing nanocomposites. To overcome this shortage, the studies on surface modification (hydrophobization) of CNF have been performed.

Various chemical groups may be substituted to hydroxyl groups on cellulose surface. Acetylation is one of the methods to hydrophobize the cellulose surface. The studies on acetylation of bacterial cellulose have been reported firstly. Kim et al. (2001) acetylated some part of bacterial cellulose and reported the changes in physical properties without morphological change. The acetylated bacterial cellulose also had an improved resistance on thermal

degradation (Nogi et al. 2006). The properties of biocomposite made of bacterial cellulose were affected by substitution of acetyl group (Ifuku et al. 2007). In case of CNF made by mechanical shearing action, Iwatake et al. (2008) reported that the surface acetylation of microfibrillated cellulose (MFC) improved the mechanical and thermal properties of MFC/PLA composite. The acetylated MFC was dispersed well in PLA solution and the composite properties were changed depending on the MFC addition level and degree of substitution (Tingaut et al. 2010; Bulota et al. 2012). The preparation of MFC film which showed a high surface contact angle without morphological change and strength reduction has been reported (Rodionova et al. 2011).

Silylation has been considered for hydrophobization of cellulose surface. The dispersibility of nanofibrils in organic solvents and the degree of film hydrophobicity by silylation has been studied (Goussé et al. 2004; Andresen et al. 2006). Aulin et al. (2010b) prepared the freeze dried CNF aerogels by chemical vapor deposition (CVD) with 1H,1H,2H,2H-perfluorodecyltrichlorosilane (PFOTS) and evaluated the degree of hydrophobization by XPS analysis. The aerogel showed the contact angle of greater than 90°.

The surface of MFC can also be hydrophobized by grafting of epoxy group with gylcidyl methacrylate (Stenstad et al. 2008). This method has an advantage that the chemical reaction for hydrophobicity is conducted in the water, not in organic solvent.

The cellulose nanofibrils can be hydrophobized by cationic polyelectrolytes or surfactants because the CNF has a negative charge in water. The water resistance of CNF film was increased by adsorption of cationic surfactant, e.g., cetyltrimethylammonium bromide (CTAB), onto cellulose nanofibrils (Xhanari et al. 2011). The hydrophilic nature of cellulose nanofibrils increased again because the CTAB formed bilayer above critical micelle concentration. Karppinen et al. (2011) adsorbed the two types of methacrylate polymers onto the MFC surface and evaluated the rheological properties of suspensions. One type (PDMQ) increased the network strength of MFC suspension by increasing the polymer dosage, and the other type (PSMA13Q containing hydrophobic segments) decreased the yield stress of MFC suspension, resulting in fluid-like property.

2.2 Film with transparency and barrier property

CNF has a nano-sized dimension in width below 100 nm. Therefore, it is expected that highly transparent film could be prepared because the dimeters less than one-tenth of visible light wavelength does not affect light scattering (Yano et al. 2005; Abe et al. 2007). CNF suspension can be converted to optically transparent film by casting of diluted suspension or drying of vacuum filtered sheet. Fukuzumi et al. (2009) prepared the transparent films with TEMPO-oxidized cellulose nanofibers from softwood and hardwood fibers, resulting in that the UV-Vis transmittance of 20 μm thick films was about 90% and 78% at 600 nm, respectively. According to Nogi et al. (2009), the surface smoothness of film affected the light scattering and transparency. The light transmittance of surface-polished CNF film was 71.6% at a

wavelength of 600 nm. When the acrylic resin A600 was coated on the film surface, the transmittance was increased up to 89.7% (Nogi and Yano 2009). Recently, Oji Holdings Corporation successfully prepared highly transparent film with 91.4% transmittance by using the chemically modified CNF (Shimaoka 2015). The transparent film has a potential to utilize as a substrate of display media (Okahisa et al. 2009). They succeeded in depositing the organic light-emitting diode (OLED) on CNF nanocomposite, which has flexibility, low thermal expansion, and high optical transparency.

CNF film has a barrier property on oxygen by strong hydrogen bonds between nanofibrils. The barrier property of CNF film is beneficial to packaging for foods and medicines. The TOCN-coated PLA film showed a very low oxygen permeability (1 mL m^{-2} day^{-1} Pa^{-1}), whereas the only PLA film had an oxygen permeability of 746 mL m^{-2} day^{-1} Pa^{-1} (Fukuzumi et al. 2009). However, CNF film with high carboxylic acid content is expected to have a low water vapor barrier property in comparison to petrochemical plastics. Spence et al. (2011) decreased the water vapor transmission rate (WVTR) of MFC film by the addition of fillers or coating with beeswax, paraffin, and starch. The WVTR of CNF film was also decreased with addition of nanoclay (Aulin et al. 2012), layered silicates (Ho et al. 2012), and hydrophobization (Rodionova et al. 2011).

2.3 Aerogels

Aerogel is porous material produced from a gel by replacing the liquid with air without collapsing the network. It has extremely low density, high

specific surface area, and low thermal conductivity. Aerogel has potential applications such as gas or liquid adsorption, thermal and acoustic insulation, and so on (Aaltonen and Jauhiainen 2009; Sehaqui et al. 2011a). Aulin et al. (2010) reported CNF aerogels with high porosity by freeze drying of carboxymethylated CNF suspension. The density and morphology of the aerogels was affected by the consistency of CNF suspension at drying. Aulin et al. (2010) also modified the surface of CNF aerogels using a chemical vapor deposition process. The hydrophobized CNF aerogel can be used as oil absorbent (Cervin et al. 2012; Zhang et al. 2014; Zheng et al. 2014).

2.4 Battery separator

Most commercially available separators in lithium-ion batteries are manufactured from polyolefin, including polypropylene and polyethylene, which are not renewable materials. In addition, one of disadvantages of polyolefin separator is its low thermal stability (Huang 2011). The preparation of eco-friendly separator based on CNF has been reported. Chun et al. (2012) prepared CNF separator membrane for lithium-ion batteries by solvent exchange with isopropanol-water mixture. The CNF separator resulted in a good ionic conductivity and tensile properties, which is comparable to a commercial PP/PE/PP separator. They also reported that the electrochemical performance of CNF separator was comparable to a commercial PP/PE/PP separator.

3. Network Properties of CNF

The network properties of CNF have been evaluated in terms of the suspension rheology. The rheological properties of CNF suspensions are affected by the suspension consistency, regardless of the used preparation method (Pääkkö et al. 2007; Lasseuguette et al. 2008). According to Lasseuguette et al. (2008), the viscosity of a suspension increased linearly with an increase in the suspension consistency at low consistency level (<0.23%). However, the viscosity of a suspension showed a power-law relationship at high consistency level (>0.23%). CNF suspension shows shear-thinning and thixotropic behavior under shear. The storage modulus (G′) increased with the consistency of the suspension. The rheological properties of CNF suspension were also affected by both the suspension consistency and the axial ratio of the fiber (Tatsumi et al. 2002). The yield stress of CNF suspension showed a power-law relationship from 0.5% to 99% of solids content (Ryu 2013).

The rheological properties of CNF suspension may be changed by the degree of electrostatic attraction or repulsion. Numerous studies on control of electrochemical properties of charged particles using polyelectrolyte or salt have been reported, because electrical charge properties can be easily changed by polyelectrolyte or salt addition. Adsorption of cationic polymethacrylate onto the CNF surface changed the rheological properties of the suspension, showing increased storage modulus and viscosity with an increase in polymer dosage (Karppinen et al. 2011). Addition of cationic starch and polyacrylamide also produces a stronger microfibrillated cellulose (MFC) gel

(Vesterinen et al. 2010). Laka and Chernyavskaya (2009) studied the effect of various types of salt on the properties of microcrystalline cellulose (MCC) and microcrystalline chitosan (MCCh) gels. They showed that the lattice formed by a reduction of mutually repulsive forces produces stronger gels. Cellulose hydrogel prepared by integrated acid hydrolysis and mechanical shearing treatment showed aggregation of microfibrils with increasing ionic strength when using sodium chloride (Ono et al. 2004). The chiral nematic property of cellulose nanocrystals was also affected by salt addition (Dong et al. 1996; Araki and Kuga 2001).

The dewatering ability of pulp suspension has a strong relationship to the fiber network structure. The structure of fiber network can be changed by electrochemical property of fiber surface. According to Bhardwaj et al. (2005), the addition of cationic polyelectrolytes made the zeta potential of pulp fibers close to zero and then, the dewatering ability of suspension was improved by flocculation of fibers. In case of CNF, Ryu (2012) added various kinds of polyelectrolytes to CNF suspension and evaluated the dewatering ability of suspension. The high molecular weight of polyelectrolyte showed the better dewatering ability at the zeta potential of near zero. The increased dosage of polyelectrolyte above isoelectric point decreased the dewatering ability of CNF suspension.

4. Pore Properties of Porous Materials

CNF, which has high specific surface areas can be converted to dense film because of the hydrogen bonds between nanofibrils by heat or room temperature drying. However, CNF forms porous structure like aerogels by using a proper drying condition such as freeze drying, solvent exchange drying, and supercritical drying.

Pore properties of dried products such as foam and sheet, especially using CNF, have been evaluated by four kinds of ways. Firstly, apparent porosity can be calculated from the density of the dried product and each component (e.g. cellulose: 1.5 g/cm^3) (Sehaqui et al. 2011a). Secondly, air permeability can be measured, which measures the required time for a certain amount of air to flow through the porous product (Chun et al. 2012). Thirdly, the pore size distribution and average pore size can be obtained by mercury intrusion into the pores as the controlled pressure is applied. The smaller pore size is, the higher pressure of mercury is requires. Lastly, there is BET (Brunauer-Emmett-Teller) method by using an adsorption and desorption of gas. The specific surface area, which is the accessible area per unit weight of material (m^2/g), is obtained from BET measurement.

The structural properties of porous CNF product may be inferred from BET specific surface area because nanofibrils form smaller sized pore structure than pulp fibers in the same volume. Cervin et al. (2012) reported that the freeze dried CNF aerogel showed the porosity from 99.1% to 99.8% and the specific surface area from 11 m^2/g to 42 m^2/g. Aulin et al. (2010)

conducted freeze drying of CNF suspension with the different consistency (0.0031 – 3.13%), resulting in that the density of aerogel increased linearly with an increase in suspension consistency. The maximum porosity of aerogel, 98.2%, was obtained at the lowest consistency of suspension. Sehaqui et al. (2010) investigated the effect of solvent exchange process on the specific surface area of CNF aerogels. When the one-step (with only tert-butanol) and 6-step (with ethanol and tert-butanol) solvent exchange was conducted, the specific surface area of CNF aerogels was 153 m^2/g and 249 m^2/g, respectively. Svensson et al. (2012) reported the ultra-porous structure when the TEMPO-oxidized cellulose was solvent-exchanged.

The pore size distribution and average pore size may be also calculated from the BJH (Barrett-Joymer-Halendar) model (Barrett et al. 1951) analysis after adsorption and desorption of nitrogen gas (Aaltonen and Jauhiainen 2009; Deng et al. 2009; Sehaqui et al. 2011a). The pores are classified to three types according to IUPAC: macropores with pores greater than 50 nm (500 Å) in diameter, mesopores with pores between 2 nm (20 Å) and 50 nm (500 Å) in diameter, and micropores with pores less than 2 nm (20 Å) in diameter (Rouquerol et al. 1994).

5. Filter Media with Nanofibers

Nanofibers are attractive and advantageous to filter applications because they form small size pores and have high specific surface areas (Barhate and Ramakrishna 2007; Guibo et al. 2012). Most studies on filter media using nanofibers and their webs have been aimed at the fibers made of petrochemical polymers. Electrospinning (Fig. 2-1) and melt-blown (Fig. 2-2) methods have been reported to prepare nanofibers web.

Electrospinning is the technology to produce fibers from liquid under high electrical voltage. The production of nanofibers by electrospinning was reported in 1934 for the first time by Formhals's patent (Formhals 1934). When a high voltage is applied to liquid polymer solution, the electrostatic repulsion occurs in the charged liquid droplet, leading to a liquid jet. The nanofibers produced by solvent evaporation from liquid jet are then deposited on collector as web.

Gopal et al. (2006) prepared the nanofiber filter by electrospinning of polyvinylidene fluoride and evaluated the filtration performance. When the particles with 1, 5, 10 μm in diameter were passed through the nanofiber filter, more than 90% of the particles were filtered. Zhang et al. (2010) investigated the effect of layer structure of filter media on filtration performance using an electrospun nano-web with polyacrylonitrile. The nanofilter made of multiple thin layers showed the higher quality factor than one-layered thick filter. Ahn et al. (2006) used the Nylon 6 for electrospinning and investigated the effect of the initial concentration of Nylon 6, electrospinning conditions, thickness

of filter media on the filtration efficiency and pressure drop. The manufactured nanofibers were 80 - 200 nm in width and the nanofilter with Nylon 6 showed better filtration efficiency than a commercial HEPA filter although the pressure drop increased. Barhate et al. (2006) reported that electric field (drawing rate), the rotating speed of collector, and the distance between tip and target during electrospinning of polyacrylonitrile affected the structural properties of web such as pore size distribution. Li et al. (2013) prepared membrane filter with poly(trimethylene terephthalate) by wet-laid method. The mechanical strength increased and the pore size decreased by heat treatment. The filtration efficiency was approximately 99.6% when TiO_2 suspension was passed through the membrane filter.

In melt-blown process, the fine fibers and their web are produced from the thermoplastic polymer by high-velocity hot air (Uppal et al. 2013). The polymer, typically polypropylene, is melted with low viscosity and then passed through a tip of small diameter, forming fine fibers. Although the production rate of nanofibers is better than electrospinning, the diameter of produced fibers has generally a limit from 2 μm to 5 μm (Ward 2005; Dutton 2008). Therefore, struggles have been made to reduce fibers diameter during melt blown process (Ellison et al. 2007; Zhuang et al. 2013).

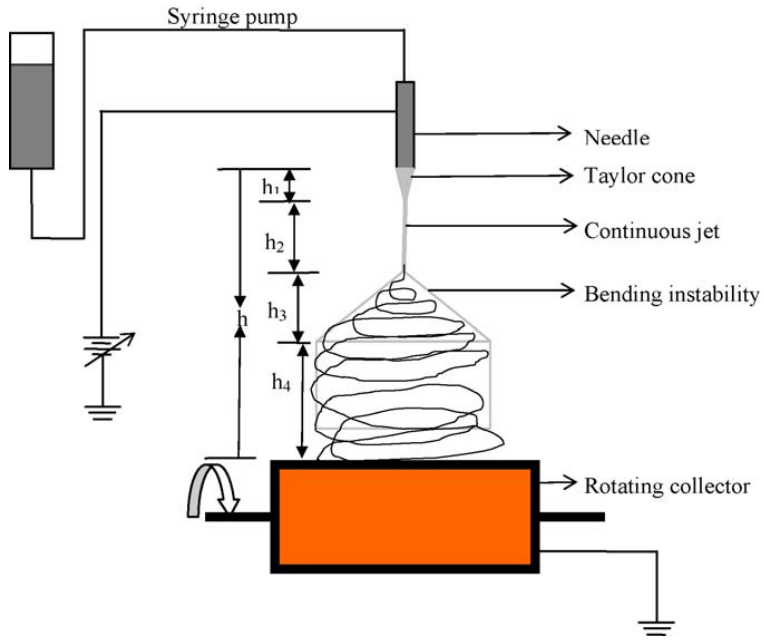

Fig. 2-1. Schematic illustration of electrospinning for nanofiber production (Barhate et al. 2009).

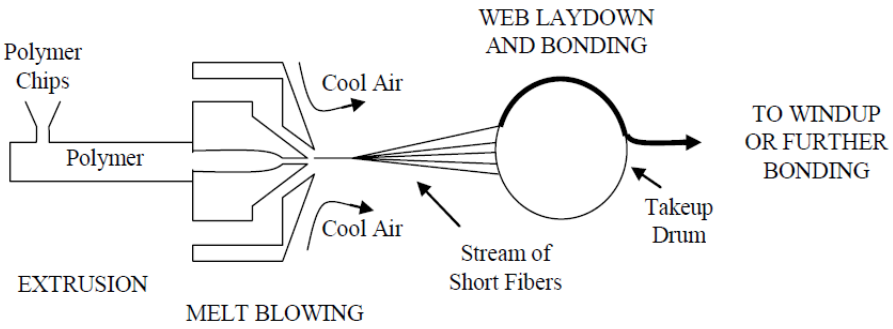

Fig. 2-2. Schematic illustration of melt-blown process (Dutton 2008).

Chapter 3

Structural Characteristics of CNF Sheet

Depending on Preparation Conditions

1. Introduction

CNF suspension can also be converted to sheet form. To create a CNF sheet, it is required to remove water economically before drying. However, because CNF suspension has a lot of water when prepared and has high water holding capacity, it is difficult to remove the water from CNF suspension. Taipale et al. (2010) evaluated the drainage properties of the pulp and MFC mixture using a dynamic drainage analyzer, resulting in drainage time increase with an increase in the amount of added MFC.

The drying process is also important because it affects inter- and intra-bonding of cellulose and structure of the final products. If the pore structure in the CNF sheet can be controlled, the application areas of these porous sheets or foams would be extended to the filtration media, separator, and biocomposites.

Studies on ‘nanopaper’ as a sheet form of cellulose nanofibers have been reported (Henriksson et al. 2008; Chun et al. 2011). However, the main purpose of these studies was the preparation of nanopaper and enhancement of the mechanical properties of nanopaper. Although many papers have dealt with the structure of CNF sheets, it is difficult to find a systematic study on the sheet structure that depends on the preparation conditions of the CNF sheet. Prior to creating valuable product using CNF, it is necessary to understand the structure of the CNF sheet.

In this chapter, it is aimed to investigate the structure of the CNF sheet systematically with different preparation conditions such as the number of grinding passes, initial solids content of a wet CNF sheet, and drying conditions. The mechanical strength of CNF sheets depending on drying conditions was also examined.

2. Materials and Methods

2.1 Preparation of cellulose nanofibrils

Once-dried, commercial eucalyptus bleached kraft pulp was used to prepare the CNF suspension. Prior to grinding, the pulp fibers were beaten to 450 mL Canadian Standard Freeness (CSF) using a laboratory Valley beater. The beaten pulp suspension was passed through a grinder (Fig. 3-1, Super Masscolloider, Masuko Sangyo Co., Ltd, Japan) to produce the CNF suspension. The consistency of the pulp suspension during grinding was 2 wt%. The operation speed and gap distance between the grinder stones were 1500 rpm and -60 μm, respectively. The number of passes through the grinder was controlled from 0 to 20. The CNF suspensions were collected at a different number of passes for further experiments. The 0 pass means just beaten pulp suspension without grinding treatment.

Fig. 3-1. Grinder for preparation of cellulose nanofibrils suspension.

2.2 Preparation of wet CNF sheets

The water from CNF suspension is very difficult to drain by gravity or vacuum and dewatering can take a very long time because of the high water holding capacity and low consistency of CNF suspension. In this study, the removal of a great quantity of water in CNF suspension and the preparation of the CNF sheet were conducted using pressure dewatering equipment (Fig. 3-2 (a)). The dewatering equipment has the container (Φ 70 mm) whose the bottom side is perforated. 400-mesh wire and a filter paper (No. 5C, Advantec MFS Inc.) were put on the bottom inside of the container to retain the CNF during the dewatering process. The 45 g of CNF suspension (2 wt%) was loaded in the container of the dewatering equipment. Then, the CNF suspension was dewatered under 7 bars of pressure.

To investigate the effect of the initial solids content at drying, the solids content of the wet CNF sheet was changed from 2% to 23% by controlling the dewatering time (Fig. 3-3). The four solids contents were selected between 0 to 25 min of drainage time: 10, 15, 20, and 25 min. The solids content of the CNF sheets after dewatering during a certain period was measured by oven drying of the wet sheet. To measure the shrinkage of the CNF sheets before and after drying, the wet sheet was cut to a fixed size using a circular cutter (Fig. 3-2 (b), 32 cm^2 area).

CNF sheets were also prepared by vacuum filtration to investigate the structural properties and mechanical strength of the sheets depending on the drying conditions.

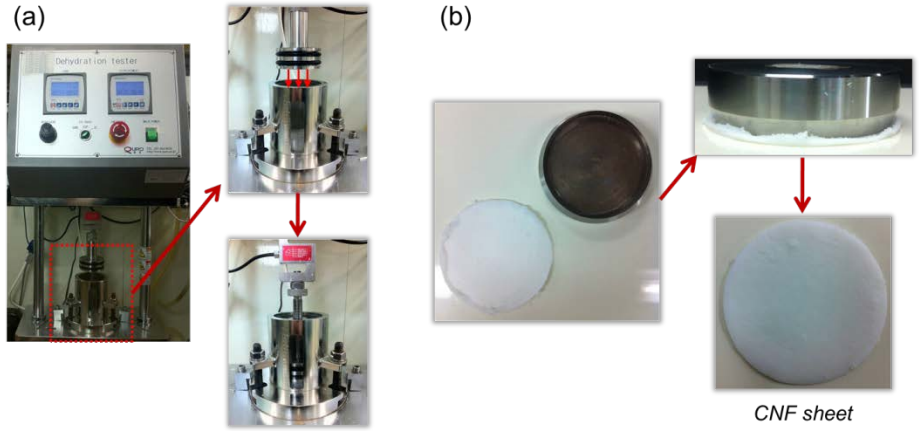

Fig. 3-2. Preparation of CNF sheet using pressure dewatering equipment: (a) dewatering of CNF suspension and (b) cutting of wet sheet using circular cutter.

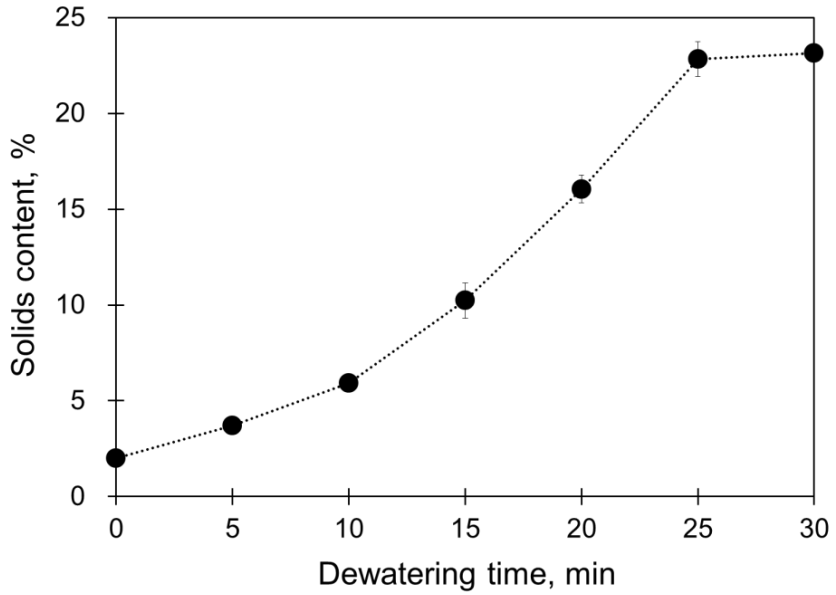

Fig. 3-3. Solids content of 20-passed CNF sheet after pressure dewatering with the dewatering time.

2.3 Drying of wet CNF sheets

Drying of the wet CNF sheets prepared pressure dewatering was carried out through three different drying methods: room temperature drying, freeze drying, and solvent exchange drying. Freeze drying of the CNF sheets was conducted at -81°C for 24 hours. Solvent exchange process was carried out in three steps. The wet CNF sheets were successively immersed in 20, 50, 80, and 100 wt% ethanol solutions in the first step. Then, the wet sheets were immersed in acetone in the second step and in hexane in the final step. The solvent exchanged CNF sheets were kept in a freeze dryer to volatilize the organic solvent.

The wet CNF sheets prepared by vacuum filtration were dried by four different drying methods: hot pressing, freeze drying, solvent exchange drying, and supercritical drying. Hot pressing was conducted at 120°C for 3 min. Supercritical drying was carried out with carbon dioxide at 50°C under 100 bars.

2.4 FE-SEM observation of the CNF and CNF sheets

A field-emission scanning electron microscope (FE-SEM, AURIGA, Carl Zeiss, Germany) was used to examine the morphology of CNF and the micro- or nano-structure of the CNF sheets. All samples were coated with platinum using a BAL-TEC SCD 005 sputter coater for 200 sec at 20 mA. Secondary electron images of the CNF sheets were obtained by a FE-SEM operated at an accelerating voltage of 2 kV.

2.5 Evaluation of shrinkage, density, and porosity of the CNF sheets

The drying shrinkage of the CNF sheets was determined by their volume change (Equation (1)):

$$\text{Shrinkage } (\%) = \frac{V_b - V_a}{V_b} \times 100 \qquad \text{Eq. (1)}$$

where V_b and V_a is the volume of the CNF sheets before and after drying expressed as cm^3, respectively. The volume of the CNF sheets was obtained by the multiplication of thickness and area. The thickness and the diameter of the sheets were measured by a digital vernier caliper. It was difficult to measure the thickness of undried, freeze dried, and solvent exchanged sheets directly due to the collapse of the sheets during measurement. Therefore, both sides of the sheet samples were faced with polyethylene films. Then, the total thickness including CNF sheet and two facing films was measured. The thickness of the film was 0.6 mm, which was subtracted from the total thickness.

The density (ρ) of the CNF-dried sheets was determined from Equation (2), by dividing the dry weight (W) by the volume (V_a) of the sheet.

$$\text{Density } (\rho,\ g/cm^3) = \frac{W}{V_a} \qquad \text{Eq. (2)}$$

The porosity was calculated according to Equation (3) by using the density (ρ) of the CNF sheet and cellulose. The density of cellulose was adapted from an already known value, 1.5 g/cm^3 (Sehaqui et al. 2010).

$$\text{Porosity}\ (\%) = \left(1 - \frac{\rho}{\rho_{cellulose}}\right) \times 100 \qquad \text{Eq. (3)}$$

2.6 Evaluation of specific surface area of the CNF sheets

The specific surface areas of the CNF sheets were determined by nitrogen gas (N_2) adsorption and desorption measurements using the TriStar II 3020 (Micromeritics Instrument Co., USA). The adsorption of gas onto solid material increases with the decrease in temperature and with the increase in pressure (Webb and Orr 1997). The measurement, therefore, is conducted at a cryogenic temperature (N_2 gas: -196°C, its boiling point) by increasing the gas pressure. The samples were dried at 100°C for 72 hours to remove the retained moisture thoroughly before measurement and followed by nitrogen gas adsorption at -196°C. Both adsorption and desorption isotherms were obtained and the specific surface areas of the CNF sheets were determined by the Brunauer-Emmett-Teller (BET) method. The pore size distribution and the average pore size of CNF sheet was obtained from adsorption and desorption isotherm of nitrogen gas according to Barrett-Joyner-Halendar (BJH) model.

2.7 Evaluation of tensile properties of the CNF sheets

The tensile properties of the CNF sheets prepared with different drying conditions were evaluated using a Universal Testing Machine (Instron Co., USA). The width of specimen and the measurement span were 15 mm and 30 mm, respectively. The strain rate during measurement was 5 mm/min.

3. Results and Discussion

3.1 Morphological changes of CNF and CNF sheets

Fig. 3-4 shows the morphology of CNF depending on the degree of nanofibrillation. When the grinding was not conducted (0 pass), the pulp fibers were entangled with each other so large pores were formed between fibers. As the number of passes increased, the shape of pulp fibers disappeared. When the image was magnified and observed, the nanofibrils formed network structure by their entanglement (Fig. 3-5). The width of CNF ranged from 5 nm to 50 nm.

The photographs of CNF sheets with the number of different grinding passes and drying conditions are shown in Fig. 3-6. The dewatering time was 25 min and the number of passes through a grinder was from 0 to 15. When solvent exchange drying and freeze drying were conducted, the shape of the CNF sheets changed minimally. However, in the case of room temperature drying, a significant deformation and shrinkage were observed.

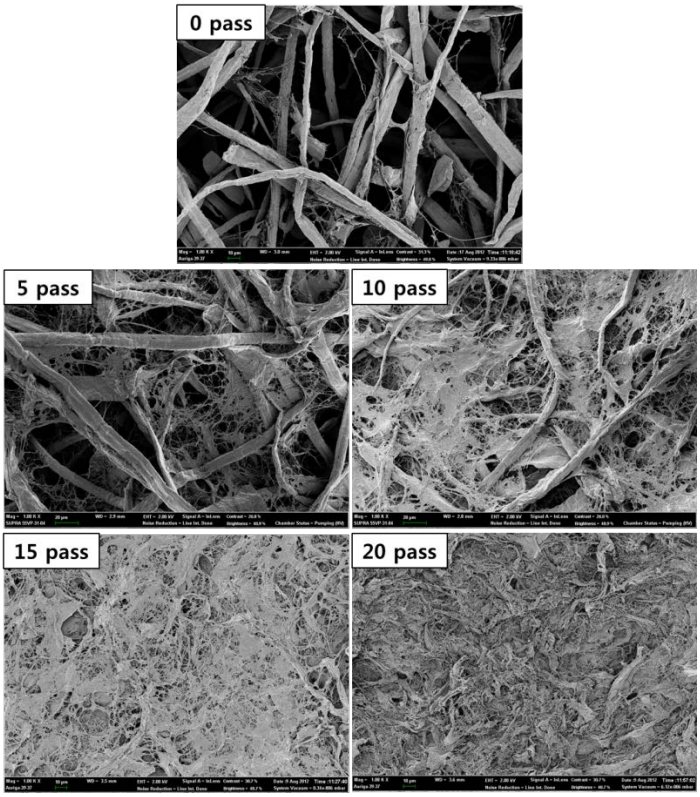

Fig. 3-4. FE-SEM images of CNF with the different number of passes through grinder.

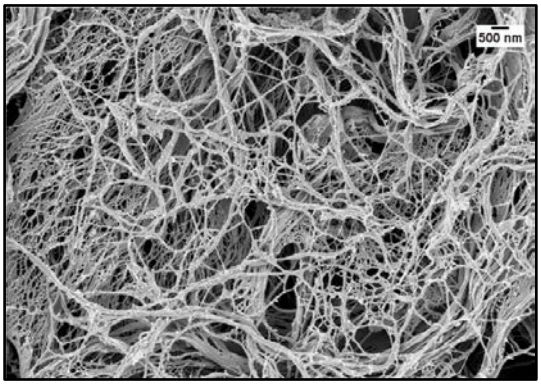

Fig. 3-5. FE-SEM image of 20-passed CNF.

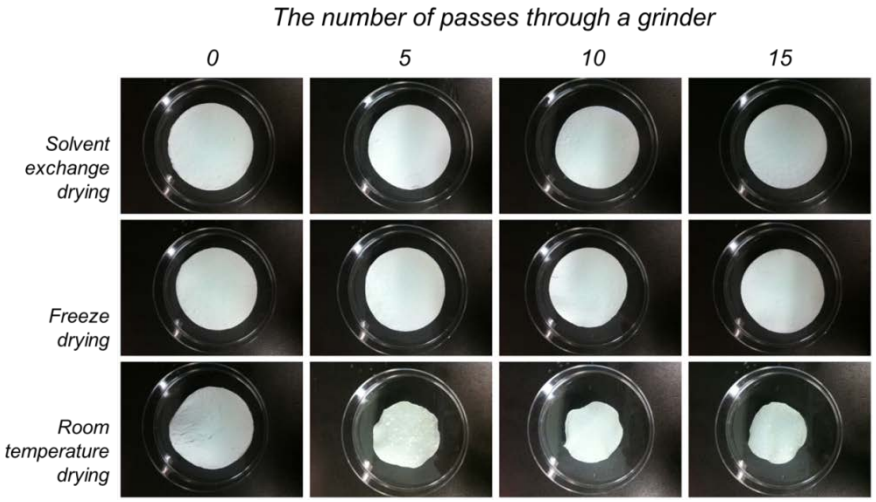

Fig. 3-6. Morphology of CNF sheets depending on the number of grinding passes and drying conditions (initial consistency of the CNF suspension: 2%, dewatering time: 25 min, number of passes through a grinder: 0-15).

3.2 Microstructure of the CNF sheets

The microstructure of the 20-passed CNF sheet prepared by pressure dewatering and the different drying methods was observed by FE-SEM (Fig. 3-7). The initial solids content of the wet CNF sheet and the dewatering time were 23% and 25 min, respectively. The CNF sheet dried with solvent exchange drying showed a network structure formed by each nanofibril (Fig. 3-7 (a)). In the case of freeze drying, the aggregation of nanofibrils occurred, showing the film-like or plate-like structure in Fig. 3-7 (b) (Deng et al. 2009; Peng et al. 2012). The structure was denser than the CNF sheet made by vacuum dewatering, which might be due to a difference in the drainage method (i.e., pressure and vacuum dewatering). The CNF sheet formed by the pressure dewatering method showed greater density than the vacuum dewatering method. When CNF sheets were prepared by the freeze drying method, the pressurizing and vacuum filtered CNF sheets showed 0.36±0.01 g/cm^3 and 0.32±0.01 g/cm^3, respectively. Fig. 3-7 (c) shows that all of the nanofibrils were bonded during room temperature drying.

The effect of the initial solids content at drying on the CNF sheet morphology was evaluated. The FE-SEM picture of the 20-passed CNF sheet dried at solids content of 16% with freeze drying is shown in Fig 3-8. A more bulky structure and larger pores were formed as compared to the CNF sheet dried at an initial solids content of 23% (Fig. 3-7 (b)). This is likely to be because of the removal of the larger ice crystals which was formed during freezing at lower solids content.

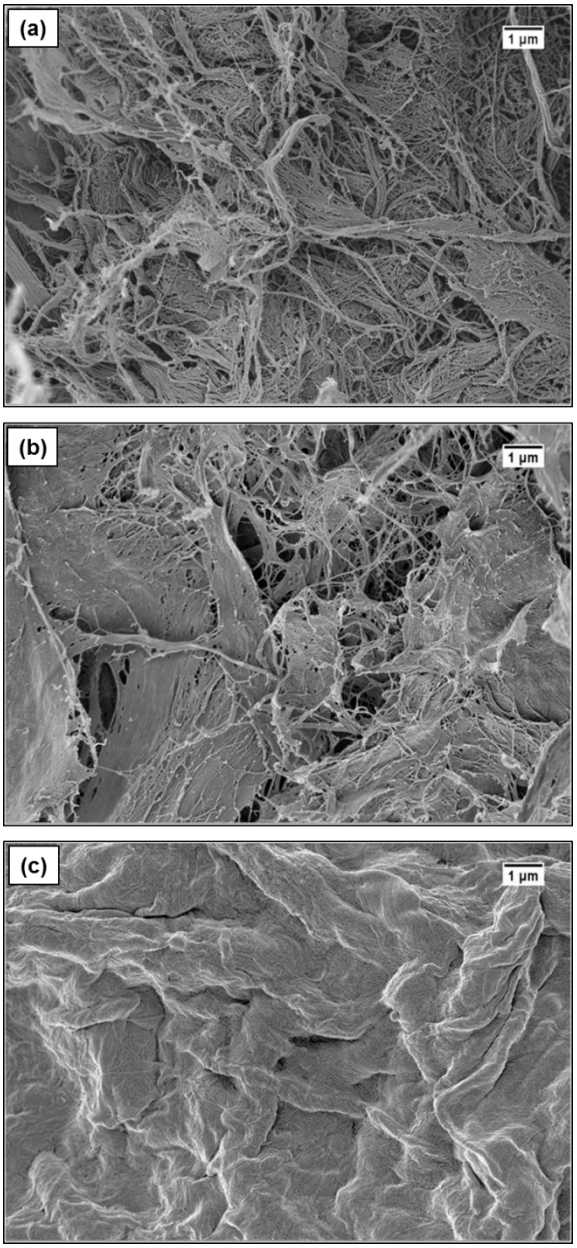

Fig. 3-7. FE-SEM images of 20-passed CNF sheet (initial solids content: 23%) prepared by pressure dewatering and the following drying conditions: (a) solvent exchange drying, (b) freeze drying, and (c) room temperature drying.

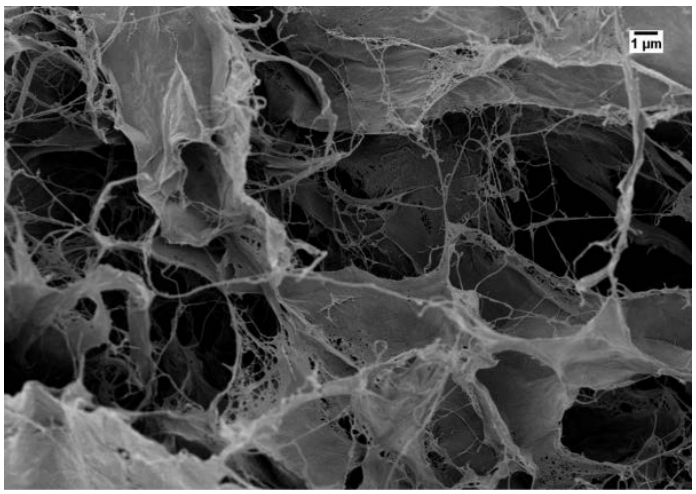

Fig. 3-8. FE-SEM image of the freeze dried CNF sheet from 16% initial solids content (20-passed).

3.3 Effect of the degree of nanofibrillation

The effects of the degree of nanofibrillation on shrinkage, density, and porosity of the CNF sheets are shown in Fig. 3-9. The initial solids content of the wet CNF sheet was 23%. The volume shrinkage of the CNF sheets increased with an increase in the number of passes regardless of the drying conditions. However, the shrinkage did not change after the treatment of 15 passes. Among the drying methods, solvent exchange drying showed the smallest shrinkage for the CNF sheet. The freeze drying method resulted in CNF sheets with a relatively higher shrinkage than the shrinkage for the solvent exchange drying method. The difference in shrinkage between solvent exchange drying and freeze drying may be induced by the bonding degree of nanofibrils represented in Fig 3-7 (a) and (b). When the CNF sheets were dried at room temperature, volume of the sheet shrank more than 80%. The bonding degree between nanofibrils is mainly determined by capillary force, which is related to the surface tension of the liquid. The higher capillary force due to the high surface tension of water (72.75 mN/m at 20°C) gets fibers closer, which contribute to form hydrogen bonds between nanofibrils during room temperature drying. On the other hand, the network of nanofibrils could be formed without inter-bonding because of the lower capillary force of hexane (18.43 mN/m at 20°C) during solvent exchange drying. Although the water was frozen to ice during freeze drying, the bonding was not completely prevented as compared to solvent exchange drying. The CNF sheet had low density and high porosity for the solvent exchange and freeze drying cases. The porosity of the sheets was around 80% for the solvent exchange drying and freeze drying conditions. It has been reported that aerogels made from

CNF suspensions below 2 wt% resulted in the 99.1% to 99.8% porosity with the density of 0.004 g/cm^3 to 0.014 g/cm^3 (Cervin et al. 2012). Pääkkö et al. (2008) also prepared cellulose I nanofiber aerogels, which showed a high porosity of ~98% by freeze drying. Although the width of cellulose nanofibers (approximately 5 nm to 10 nm) in the study of Pääkkö et al. (2008) was a little bit smaller than ours (5 nm to 50 nm), this discrepancy in porosity might be originated from the initial solids content. They prepared CNF sheets at low consistency (2%). Therefore, it was difficult to increase the porosity more than 80% in this study because the wet CNF sheets were prepared under high pressure during dewatering. The dewatering before drying is a necessary process for commercial manufacturing of wet-laid forming process. Therefore, it is indicated that there is a limit to increase the porosity of the CNF sheet in wet-laid forming using pressure dewatering. As shown in Fig. 3-10, volume of the wet CNF sheet decreased with an increase of solids content during pressure dewatering. The volume of the wet CNF sheet at 23% solids content was 3.3 cm^3.

Although the shrinkage was changed with the number of grinding passes, the density and porosity of the CNF sheets were hardly changed with the increase in the number of passes for both solvent exchange and freeze drying conditions. It is expected that the more nanofibrillation continues, the larger quantity of small pores exists in the sheet at a similar density. When drying at room temperature, density of the CNF sheet increased significantly from 0 to 5 passes. Because the thinner and less long fibers exhibits a great tendency to form highly entangled network (Alila et al. 2013), the rapid size reduction by grinding might affect the density and the shrinkage of the CNF sheet. In

addition, it was easy to get closer between nanofibrils by the capillary force induced during drying. These effects caused the film-like structure in the CNF sheets by bonding between nanofibrils as shown in Fig. 3-7 (c). The non-porous material was formed by room temperature drying conditions. The density of the 20-passed sheet was close to a cellulose density of 1.5 g/cm^3.

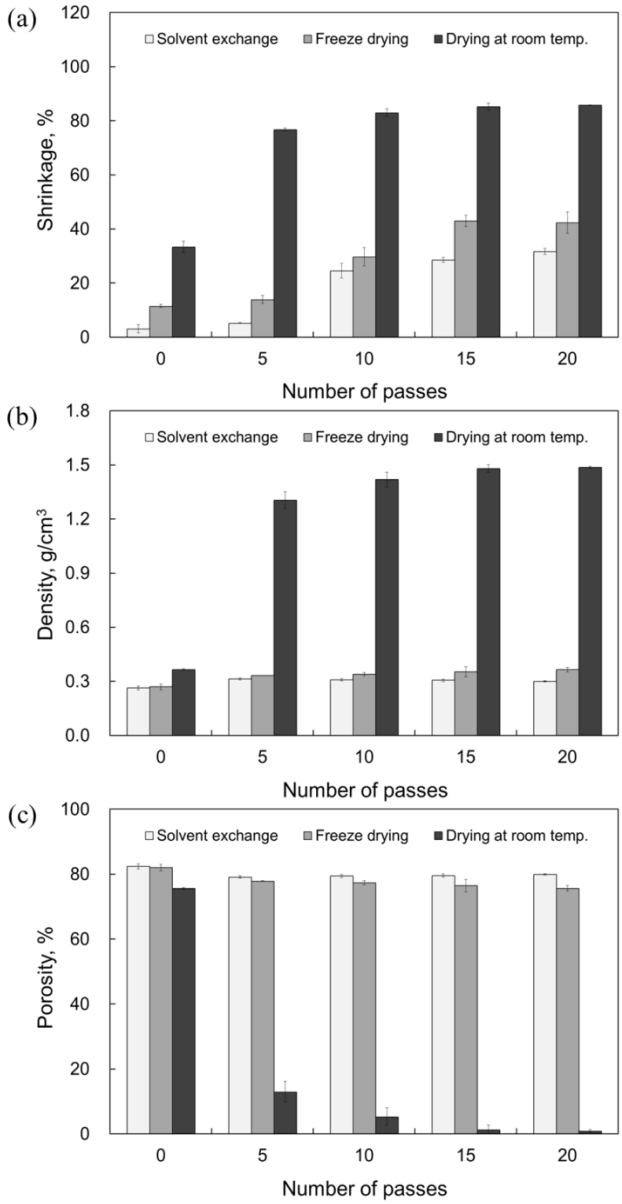

Fig. 3-9. (a) Shrinkage, (b) density, and (c) porosity of the CNF sheet with an increase in the number of grinding passes for the three different drying conditions (initial solids content: 23%).

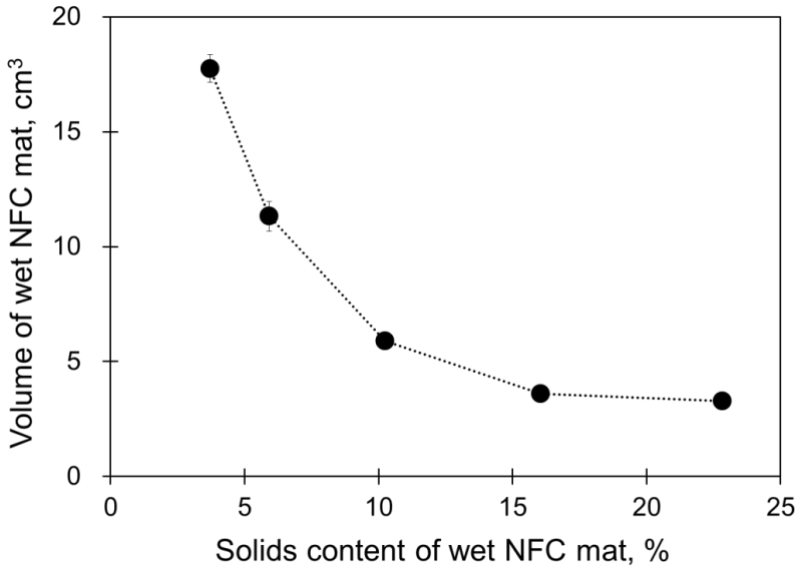

Fig. 3-10. Volume change of the wet CNF sheet depending on the solids content after pressure dewatering.

3.4 Effect of the degree of dewatering

The effect of initial solids content of the wet CNF sheet on the shrinkage, density, and porosity of the dried CNF sheet were investigated (Fig. 3-11). The initial solids content of the wet CNF sheet was controlled by the degree of dewatering. The drying shrinkage of the freeze dried sheet increased with an increase in solids content. Room temperature drying showed a high shrinkage rate of the CNF sheet and there was little effect of the initial solids content. During the freeze drying, the water in the CNF suspension was frozen and the frozen ice was removed slowly in the freeze dryer. Therefore, the deformation of the CNF sheet by drying was smaller than that of room temperature drying. However, the shrinkage rate ranged from 14% to 42% because of the bonds between adjacent nanofibrils. When the initial solids content was below 16%, solvent exchange drying process shrank greatly the wet CNF sheets with solvent. There were large different phase spaces between the nanofibrils of wet CNF sheets with low initial solids content as compared to that with high initial solids content. In the case of solvent exchange drying, the CNF sheets were filled with organic solvent after solvent exchange. Hexane, the last step of solvent exchange drying, was not frozen but just removed in the air. Therefore, the shrinkage rate increased significantly at low initial solids content because the unbonded nanofibrils approached each other and the sheet became more compact.

Density of the CNF sheets was not affected by the initial solids content (>5%) at room temperature drying and solvent exchange drying conditions. On the other hand, the density of freeze dried CNF sheets increased as a

function of the initial solids content. Accordingly, the porosity of the CNF sheets could be changed from 77% to 95% by controlling the initial solids content at freeze drying.

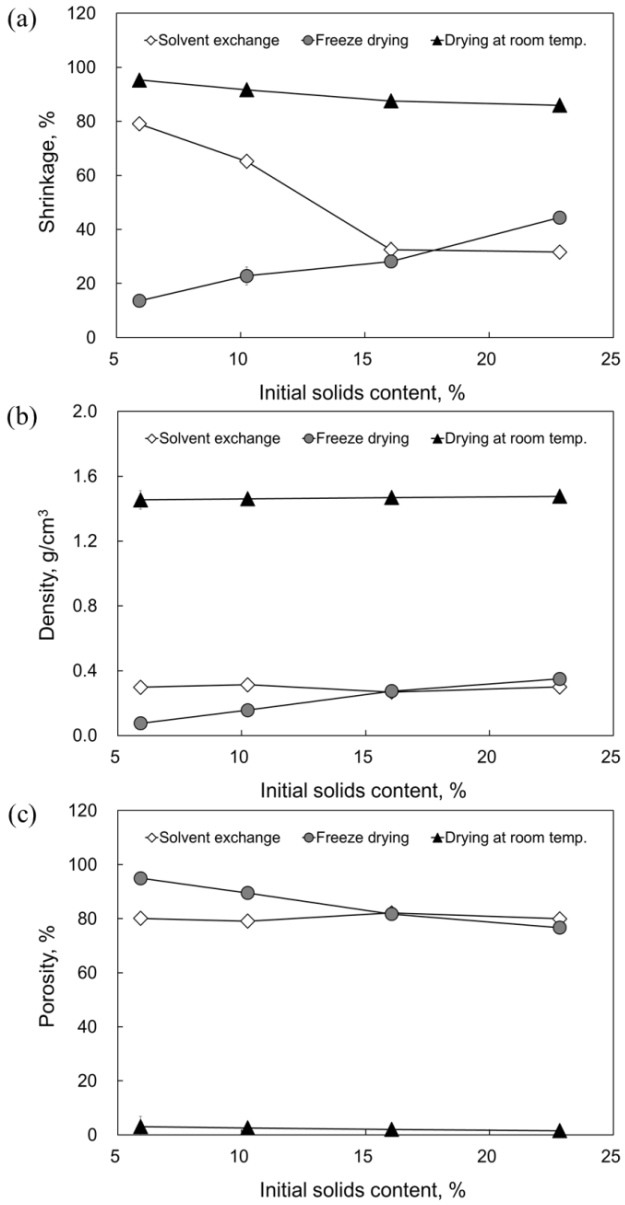

Fig. 3-11. (a) Shrinkage, (b) density, and (c) porosity of the CNF sheet prepared from the different initial solids content (number of grinding passes: 20).

3.5 Effect of drying conditions

The structural properties of CNF sheets prepared vacuum filtration were compared depending on drying conditions (Fig. 3-12). The hot pressed CNF sheet showed the highest density because of the hydrogen bonds during drying. Its apparent porosity was approximately 14%. The density of freeze dried CNF sheet was similar with solvent exchanged CNF sheet. Both freeze dried and solvent exchanged CNF sheets showed a little higher density than the sheets by pressure dewatering at the same drying condition (Fig. 3-9). The CNF sheet dried by supercritical drying showed the highest apparent porosity because of the inhibition of hydrogen bonds during drying. It porosity was approximately 89%.

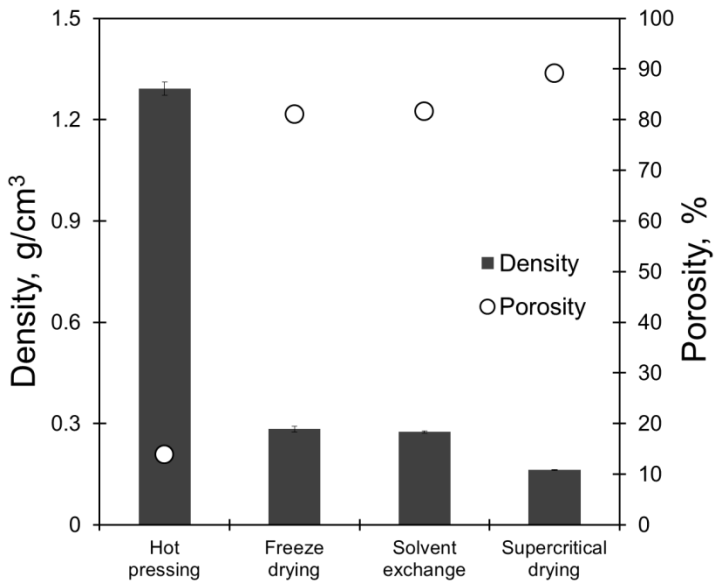

Fig. 3-12. Apparent density and porosity of CNF sheet depending on drying conditions.

3.6 Specific surface area and pore distribution

The specific surface area of the CNF sheets prepared by solvent exchange drying, freeze drying, and room temperature drying was measured by nitrogen gas adsorption (Fig. 3-13). The specific surface area of the CNF sheets increased remarkably with the number of grinding passes under solvent exchange drying conditions. The 0-passed sheet had a specific surface area of 22 m^2/g. In this study, the maximum value of the specific surface area was about 175 m^2/g for the 20-passed CNF sheet. Solvent exchange drying considerably preserves the exposed surface area of CNF. Sehaqui et al. (2011a) investigated the effect of the number of solvent exchange steps on the specific surface area of CNF aerogels. The higher specific surface area, 249 m^2/g, was obtained by a 6-step solvent exchange using both ethanol and tert-butanol, while the CNF aerogel treated with a 1-step solvent exchange using tert-butanol showed a specific surface area of 153 m^2/g. Kuga et al. (2002) reported that the solvent exchange dried bacterial and tunicate cellulose had a high specific surface area of 100 m^2/g to 150 m^2/g due to the preservation of original separated microfibrils compared to freeze drying conditions (30 m^2/g - 40 m^2/g). This indicates that the specific surface area of CNF was dependent on the raw material types and solvent exchange methods.

The specific surface area of the CNF sheets prepared by freeze drying did not change significantly as the number of passes increased. The specific surface area of the 20-passed CNF sheet was around 3.3 m^2/g. Peng et al. (2012) suggested that the aggregation of nanofibrils occurred during the sublimation of the water during freeze drying and a plate-like or ribbon-like

structure was formed. These conditions were also found in the FE-SEM images of the CNF sheet as shown in Fig. 3-7 (b) and Fig. 3-8. This indicates that the aggregation of nanofibrils by hydrogen bonding could not be prevented completely during freeze drying conditions. CNF aerogels prepared from the carboxymethylated and homogenized CNF suspension with a concentration below 3.13 wt% by freeze drying has been reported, which showed a specific surface area of 11 m^2/g to 15 m^2/g (Aulin et al. 2010). Sehaqui et al. (2010) obtained CNF foam having a specific surface area of 14 m^2/g to 42 m^2/g as a function of density by freeze drying. The density range of CNF foams was between 7 kg/m^3 and 79 kg/m^3. In the present study, the 20-passed CNF sheet had a relatively lower specific surface area by the freeze drying method than that of the above mentioned studies because of the higher density of the CNF sheet (300 kg/m^3). The specific surface area of the 0-passed and 20-passed CNF sheet dried at room temperature was below 1 m^2/g. This indicates that most of the nanofibrils were aggregated by hydrogen bonds induced during drying. Consequently, the specific surface area was affected by the preparation method of CNF and porous materials, and drying conditions.

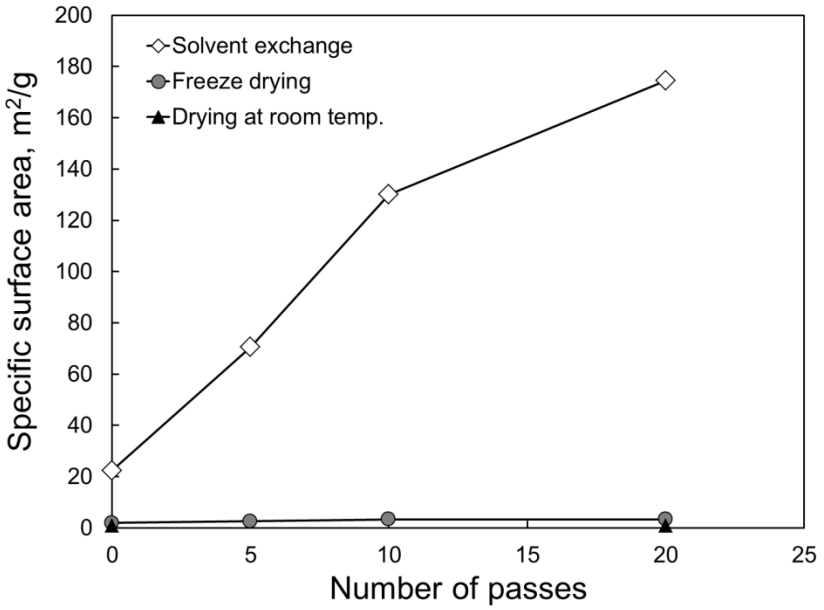

Fig. 3-13. Specific surface area of the CNF sheets with the different number of grinding passes and drying conditions (initial solids content: 23%).

Fig. 3-14 shows the adsorption and desorption isotherms of nitrogen gas for 20-passed CNF sheet. The adsorption and desorption isotherms are classified to 6 types according to IUPAC (Rouquerol et al. 1994). Fig. 3-14 is the ‘type IV’ isotherm, showing the hysteresis loop between adsorption and desorption isotherms. The hysteresis loop occurs because there is a difference between gas condensation and evaporation in pores. The ‘type IV’ isotherm is usually obtained from materials including mesopores or macropores (Webb et al. 1997).

The distribution of pore size of 20-passed CNF sheet was depicted in Fig. 3-15. The BJH adsorption average pore diameter and BJH desorption average pore diameter were 15 nm and 13 nm, respectively. According to IUPAC, it indicates that the 20-passed CNF sheet has mainly mesopores (2 – 50 nm pores in diameter). The porous sheet which has mesopores has a potential to use as a filter media in ultrafiltration that can remove viruses, bacteria, etc.

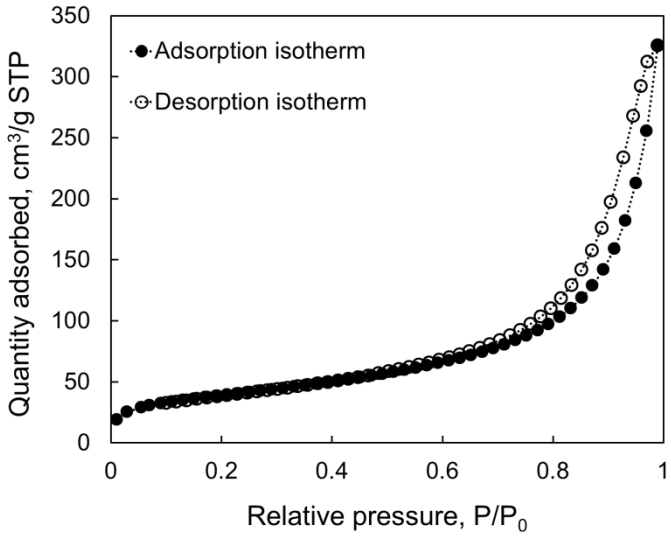

Fig. 3-14. Sorption isotherm of the CNF sheet (20-passed).

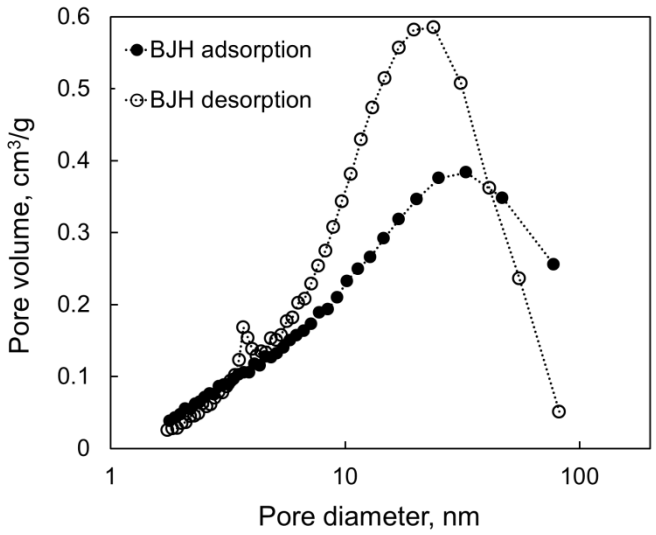

Fig. 3-15. Pore volume of CNF (20-passed) sheet as a function of pore diameter.

3.7 Tensile properties of the CNF sheets

Fig. 3-16 shows the tensile stress at break of commercial printing paper, newsprint, and CNF sheets depending on drying conditions. The hot pressed CNF sheet showed the highest tensile stress, 239 MPa, at break. When the wet CNF sheet was dried by freeze drying method, the tensile stress decreased significantly to 27 MPa. The tensile stress of freeze dried CNF sheet was similar with commercial printing paper and the higher than that of newsprint. As the hydrogen bonds between nanofibrils were inhibited by solvent exchange and supercritical drying, the tensile stress of the CNF sheets decreased continuously. There was a linear relationship between the density of CNF sheet and tensile stress at break depending on drying conditions (Fig. 3-17). The density of CNF sheet was changed by drying condition and then, this affected the tensile stress of CNF sheets.

Although the tensile stress of CNF sheets dried by solvent exchange drying and supercritical drying was the lower than that of commercial printing paper and newsprint, there was a remarkable increase in the case tensile strain at break (Fig. 3-18). The strain at break of supercritical dried CNF sheet was about 18 times higher than that of newsprint. This may be because of the great degree of entanglement between nanofibrils. It is expected that there is no problem with supercritical dried CNF sheet because of the high strain property in spite of the low tensile stress at break.

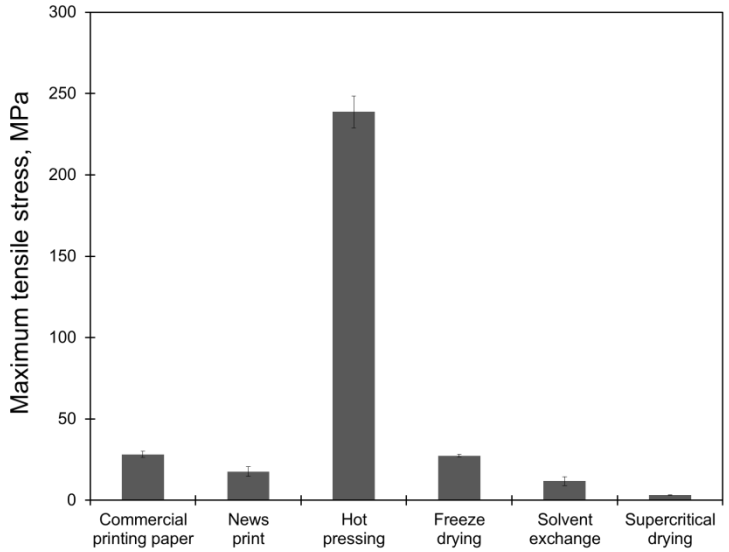

Fig. 3-16. Tensile stress at break of commercial printing paper, newsprint, and CNF sheets depending on drying conditions.

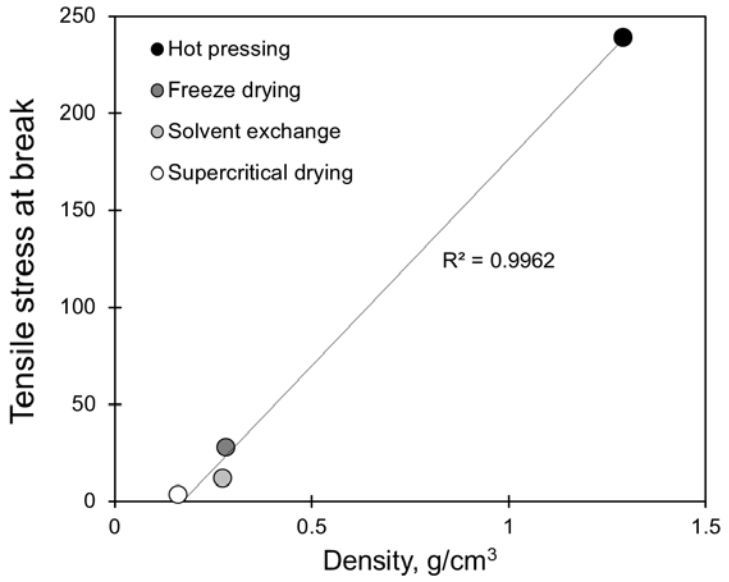

Fig. 3-17. Relationship between tensile stress at break and density of CNF sheets.

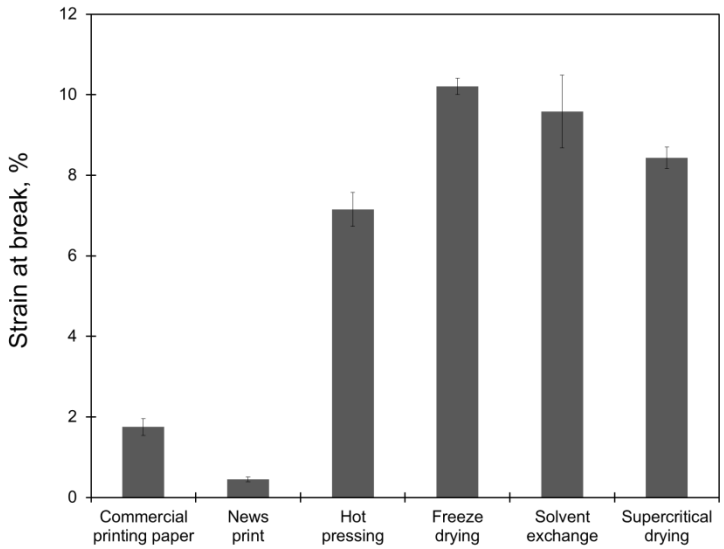

Fig. 3-18. Strain at break of commercial printing paper, newsprint, and CNF sheets depending on drying conditions.

4. Summary

The effect of preparation conditions such as the number of grinding passes, initial solids content, and drying methods on the structural characteristics of CNF sheets was investigated systematically.

The structural change in the CNF sheet was mainly dependent on the drying conditions. The inhibition of hydrogen bonds between nanofibrils could be achieved by solvent exchange drying and supercritical drying conditions. The partial aggregation of nanofibrils occurred during freeze drying, forming a film-like or plate like structure.

The highly porous CNF sheets could be prepared by freeze drying, solvent exchange drying, and supercritical drying conditions, while the drying at room temperature and hot pressing produced very dense material due to significant hydrogen bonds during drying. Although the higher shrinkage occurred as the number of grinding passes increased, the density or porosity hardly changed in the case of solvent exchange and freeze drying conditions.

The specific surface area of the solvent exchanged CNF sheet increased significantly with an increase in the number of grinding passes. The average pore diameter in CNF sheet was calculated from the gas sorption isotherms using BJH model. The value was 13 – 15 nm, indicating the CNF sheet had mesoporous structure. It is expected that pore control might be achieved by understanding the CNF sheet structure, which depends on the preparation conditions. The porous CNF sheet could be utilized as a preformed porous, reinforcing sheet for a biocomposite, filtration media, or battery separator.

Chapter 4

Effect of Chemical Treatment of CNF and Chemical Additives on Properties of Suspension and Sheet

1. Introduction

CNF has negative charge in aqueous suspension, because of chemical components such as hemicellulose remaining after the pulping and bleaching processes (Sood et al. 2010; Olszewska et al. 2011). The charge property of CNF can be controlled by changing the thickness of electrical double layer or surface modification.

As is already well known in colloid and surface chemistry, an electrical double layer consisting of a Stern layer and diffuse layer is formed around a charged colloid particle (Shaw 1992). The zeta potential, which is defined as the potential in shear plane between the particle and the bulk solution (Eklund and Lindström 1991), is measured to study the electrical double layer. The zeta potential is dependent on the pH or concentration and valency of ion in the solution (Kirby and Hasselbrink 2004; Fermin and Riley 2010). Therefore, it is expected that the surface charge property of CNF will change depending on the salt type and salinity, affecting the dispersion or aggregation of the CNF suspension.

Chemical treatments such as carboxymethylation and 2,2,6,6-tetramethylpiperidine-1-oxyl radical (TEMPO)-mediated oxidation can introduce additional carboxyl groups onto the cellulose fiber surface (Wågberg et al. 2008; Isogai et al. 2011), resulting in acceleration of fiber delamination to cellulose fibrils with more negative surface charge; For example, TEMPO-mediated oxidation is used to produce CNF with low energy consumption by introducing the carboxyl group (-COOH) to C-6 of a

glucose unit. Due to this negative charge, the CNF is well dispersed at very low consistency in an aqueous system. However, above a certain consistency (0.125%) CNF form an entangled network structure (Pääkkö et al. 2007).

The rheological properties of CNF suspension are related to the degree of aggregation of the nanofibril network (Tatsumi et al. 2002; Pääkkö et al. 2007; Lasseuguette et al. 2008; Vesterinen et al. 2010; Karppinen et al. 2011). The rheology of CNF suspension can be changed by a colloidal force such as electrostatic attraction or repulsion, leading to flocculation or dispersion.

It is difficult to remove water from CNF suspension because of their high water-holding capacity (Hii et al. 2012). Rapid dewatering of CNF suspension can be beneficial for production of CNF-based products with high efficiency. Taipale et al. (2010) evaluated the drainage properties of pulp and MFC mixture using a dynamic drainage analyzer. Although the amount of MFC added to the pulp fibers was <10% and the total concentration of the mixture was as low as 0.3%, the drainage time increased with an increase in the amount of MFC added. Dewatering was improved by adding NaCl. In addition, drainage of pulp fiber suspension is improved by flocculation as the zeta potential approaches zero with addition of cationic polyelectrolytes (Bhardwaj et al. 2005). Therefore, it is expected that addition of salt positively affects drainage of CNF suspension in terms of charge neutralization.

The morphology and structure of CNF and its sheet form were significantly affected by drying conditions in the previous chapter. This chapter is aimed to investigate the effect of chemical treatment and chemical

additives on the properties of CNF suspension and CNF sheet by adopting three methods as following:

(1) Chemical treatment by carboxymethylation and TEMPO-mediated oxidation
(2) Control of electrical double layer thickness by addition of salt
(3) Change in surface tension of water from CNF suspension by addition of surfactant.

The chemical treatment, carboxymethylation and TEMPO-mediated oxidation, imparts more negative charge to the CNF surface affecting its dispersibility in water. The charge properties, dewatering ability, and structural properties of sheet were evaluated. The flocculation behavior of CNF under different salt conditions using two types of salt, sodium chloride (NaCl) and calcium chloride ($CaCl_2$), was evaluated. Aggregation of nanofibrils by salt addition was characterized by sedimentation behavior, and the effects on the network strength and dewatering ability of the CNF suspension were evaluated. The rheological properties using an oscillatory rheometer and a microrheometer were used to evaluate the network strength of CNF suspension. The structural properties of CNF sheets were also evaluated. The cationic surfactant, cetyltrimethylammonium bromide (CTAB), was used. The surface tension of water, dewatering ability, and the CNF sheet properties were investigated.

2. Materials and Methods

2.1 Pulp and chemicals

Eucalyptus bleached kraft pulp was used as starting material to produce CNF.

For carboxymethylation of pulp fibers, chloroacetic acid ($ClCH_2COOH$, 99.0%, Sigma-aldrich), acetic acid (CH_3COOH, 99.5%, Samchun Chemicals), ethanol (CH_3CH_2OH, 99.9%, Duksan Reagents), isopropanol ($CH_3CHOHCH_3$, 99.5%, Duksan Reagents), methanol (CH_3OH, 99.8%, Duksan Reagents), sodium hydrogen carbonate ($NaHCO_3$, 99.0%, Junsei Chemical) were used.

For TEMPO-mediated oxidation, chemicals such as 2,2,6,6-tetramethylpiperidin-1-oxyl radical (TEMPO, 98.0%, Sigma-aldrich), sodium bromide (NaBr, 99.0%, Samchun Chemicals), sodium hypochlorite (NaClO, 12.0%, Duksan Reagents), sodium hydroxide (1 M NaOH, Duksan Reagents), and hydrogen chloride (1 M HCl, Duksan Reagents) were used.

Two types of salt, namely sodium chloride (NaCl, Samchun Chemicals Co. Ltd., Korea) and calcium chloride ($CaCl_2$, Showa Chemical Co. Ltd., Japan), were used. Salt solutions with different concentrations from 0.01 to 3 M were prepared.

Cationic surfactant, cetyltrimethylammonium bromide (CTAB, Sigma-aldrich Co. Ltd., Korea), was solubilized in deionized water to 0.5%.

2.2 Chemical treatment of CNF

2.2.1 Carboxymethylation as pre-treatment

Pulp suspension was beaten to 450 mL CSF by using Valley beater. The pulp fibers (100 g, oven-dried weight) were solvent exchanged three times with 2000 mL of ethanol by vacuum filtration. Chloroacetic acid (10 g) was dissolved in the solvent mixed with isopropanol (2000 mL) and methanol (500 mL) and then, the solvent exchanged pulp fibers were added to the solvent mixture. After stirring for 30 min, the mixture of isopropanol (300 mL) and NaOH (16 g) was added. The reaction was carried out at 65°C for 60 min. After termination of reaction, the pulp fibers were washed with deionized water (20 L). The acetic acid was added for neutralization and then, the washing with deionized water (10 L) was conducted again. The carboxymethylated fibers were soaked in $NaHCO_3$ solution for Na^+ form and washed with deionized water finally.

2.2.1.1 Preparation of CNF suspension

Carboxymethylated or untreated pulp suspension was passed through a grinder (Super Masscolloider, Masuko Sangyo Co., Ltd, Japan) to produce CNF suspension. The gap distance between stones and rotation speed were -80 μm and 1500 rpm, respectively. Fig. 4-1 shows the morphology of CNF suspensions with 2% consistency. The gel-like and translucent CNF hydrogel was obtained by grinding of carboxymethylated cellulose fibers (Fig. 4-1 (b)).

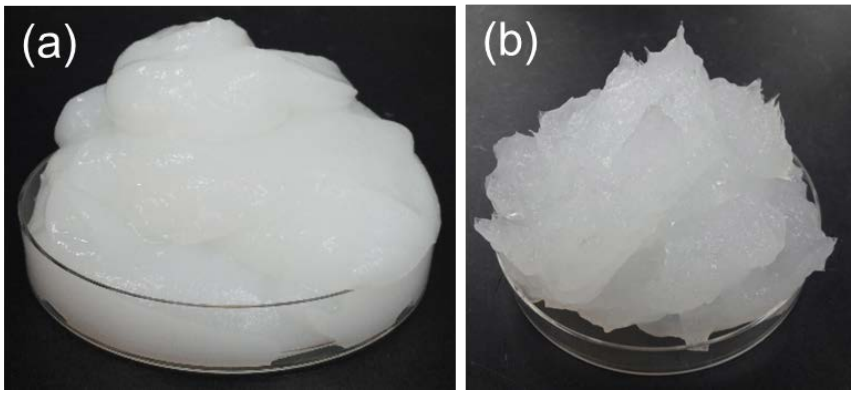

Fig. 4-1. Photographs of (a) untreated CNF and (b) carboxymethylated CNF.

2.2.1.2 Evaluation of carboxyl group content

The degree of substitution of carboxymethyl group (-CH_2COOH) was evaluated by using a FT-IR spectrophotometer (Nicolet 6700, Thermo Scientific, USA). The pulp fibers and CNF suspensions were freeze dried and then, were subjected to ball milling before analysis. Scan number, resolution, and wave number range during measurements were 32, 8, 650 cm^{-1} – 4000 cm^{-1}, respectively. Conductometric titration method was also used for quantitative analysis of carboxyl group (-COOH). The carboxylate content was calculated as following equation.

$$\text{Carboxylate content} = \frac{C_{NaOH} \times V_{NaOH}}{w} \qquad \text{Eq. (1)}$$

where, C_{NaOH}, V_{NaOH}, and w are the concentration of NaOH solution, the volume of NaOH solution, and the oven-dry weight of sample, respectively.

2.2.1.3 Evaluation of dewatering ability of CNF suspension

The dewatering ability of carboxymethylated and untreated CNF suspension was evaluated by using pressure dewatering equipment. The drainage of CNF suspension (0.9 g oven-dried weight) was conducted under a pressure of 7 bars.

2.2.1.4 Preparation and characterization of film and sheet

Film and sheet were prepared with carboxymethylated CNF. To prepare film, CNF suspension with consistency of 0.25% in petri dish was dried at 50°C after deaeration under vacuum condition. In case of sheet preparation, the CNF suspension (0.2 g dry weight) with 0.1% consistency was vacuum filtered after sonication for 1 min and then, the wet sheet was freeze dried. The grammage of sheet was 40 g/m^2. The light transmission and opacity of film and sheet were evaluated by Elrepho (L&W Co., Sweden). The apparent density and porosity of sheet were calculated by using its dry weight (w), volume (V_a), and density of sheet (ρ) and cellulose (1.5 g/cm^3).

$$\text{Density } (\rho,\ \text{g/cm}^3) = \frac{W}{V_a} \qquad \text{Eq. (2)}$$

$$\text{Porosity } (\%) = \left(1 - \frac{\rho}{\rho_{cellulose}}\right) \times 100 \qquad \text{Eq. (3)}$$

2.2.2 TEMPO-mediated oxidation as post-treatment

TEMPO-mediated oxidation using TEMPO/NaBr/NaClO system was conducted according to the conditions of Table 4-1 to substitute the carboxyl group on CNF. In Exp. 1, the reaction time was varied from 0.5 hr to 4 hr and the amount of oxidizing agent (NaClO) was fixed at 5 mmol/g CNF. In Exp. 2, the addition amount of NaClO was varied from 5 mmol/g CNF to 25 mmol/g CNF and the reaction time was 4 hr.

Table 4-1. TEMPO-mediated oxidation conditions of CNF

	Exp. 1	Exp. 2
TEMPO, mmol/g CNF	0.1	
NaBr, mmol/g CNF	1	
NaClO, mmol/g CNF	5	5, 10, 15, 20, 25
Reaction time, hr	0.5, 1, 2, 3, 4	4
pH	10	
Temperature	Room temperature	

TEMPO-mediated oxidation was carried out according to the flow diagram as shown in Fig. 4-2. First of all, TEMPO and NaBr were added to a diluted CNF suspension (1%) and were completely dissolved by stirring. The pH of CNF suspension was adjusted to 10. Oxidation of CNF was initiated by adding NaClO solution of pH 10. NaOH (0.5 M) solution was added continuously in order to maintain the pH until the end of reaction. The oxidation was terminated by adding HCl to pH 7. The oxidized CNF

suspension was washed with deionized water. Mechanical treatment was conducted by using a house blender for 20 min and sonicator for 5 min. The centrifugation was carried out at 5500 G for 15 min. The TEMPO-oxidized cellulose nanofiber (TOCN) from supernatant was collected after 4th centrifugation. The consistency of sedimented CNF after centrifugation was adjusted to 1% and used after sonication for 5 min.

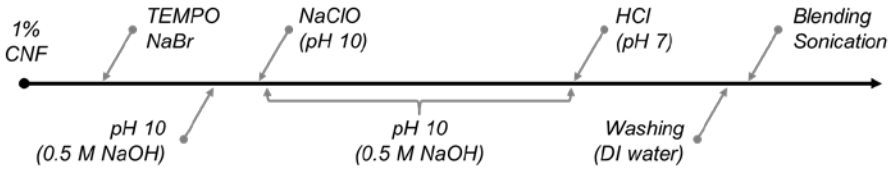

Fig. 4-2. Flow diagram of the TEMPO-mediated oxidation process.

2.2.2.1 Measurement of charge property

The zeta potential of TEMPO-oxidized CNF was evaluated by zetasizer (Nano ZS, Malvern Instrument, Ltd, UK). The charge demand of TEMPO-oxidized CNF was measured by PCD-03 (Mütek Co.).

2.2.2.2 Preparation and characterization of film and sheet

Film and sheet TEMPO-oxidized CNF were prepared and characterized according to 2.2.1.4 in Chapter 4.

2.3 Salt addition on CNF suspension

2.3.1 Preparation of CNF suspension and addition of salt

Beaten pulp suspension (450 mL CSF) was passed 20 times through a grinder (Super Masscolloider, Masuko Sangyo Co., Ltd., Japan) to prepare the CNF suspension. The pulp consistency during grinding was 2 wt%. CNF suspension (2%) was diluted to 1.5% by adding salt solution with different concentrations or deionized water.

2.3.2 Measurement of conductivity and zeta potential of CNF suspension

The conductivity of salt-added CNF suspensions was measured using a conductivity meter (Orion 3 star, Thermo Scientific Inc.). The zeta potential of CNF was evaluated using a Zetasizer (Nano ZS, Malvern Instruments, Ltd) at 25˚C.

2.3.3 Evaluation of flocculation behavior of CNF

The flocculation behavior of CNF due to charge neutralization under different salt conditions was evaluated by observing the sedimentation of very dilute (0.01%) CNF suspension depending on time.

The dispersion instability of the aqueous CNF suspension by flocculation was evaluated using a Turbiscan Ageing Station (Fig. 4-3, Formulaction Inc., France). The light transmittance through a sample vial was measured using a

near-infrared (λ_{air} = 880 nm) light source under room temperature conditions. The total analysis duration and analysis interval were 30 and 1 min, respectively. The change in light transmission was obtained as a result (Fig. 4-4).

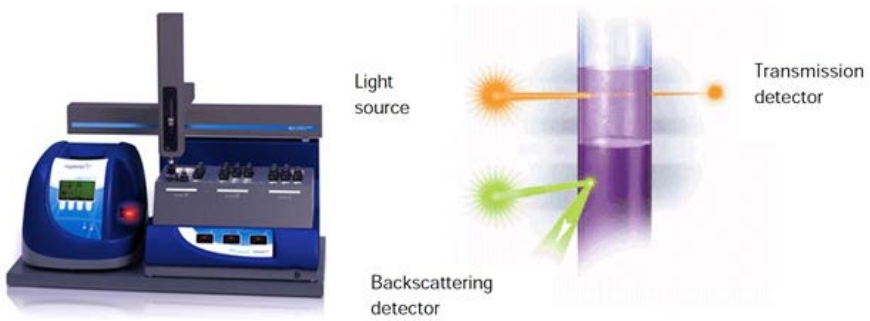

Fig. 4-3. Turbiscan Ageing Station and its measurement principle.

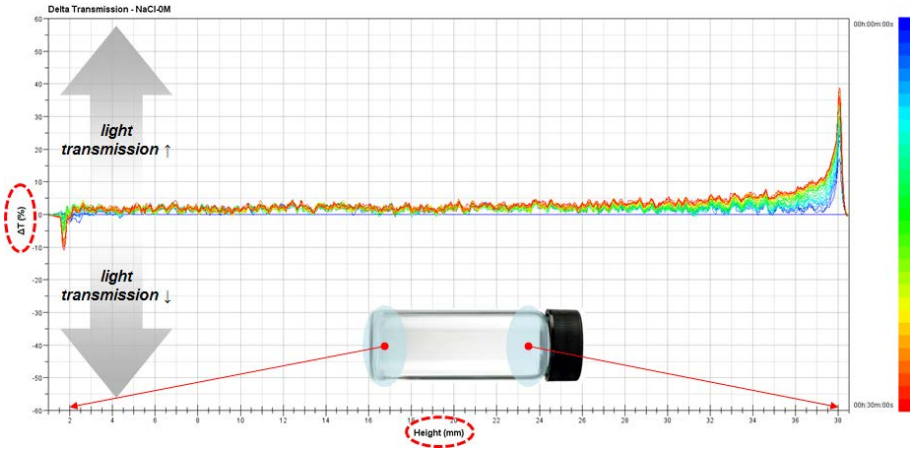

Fig. 4-4. Light transmission obtained from Turbiscan Ageing Station.

2.3.4 Measurement of rheological properties

The rheological properties of CNF suspensions were evaluated using an oscillatory rheometer (ARES, advanced rheometric expansion system, TA Instruments, USA) in a dynamic strain sweep mode. The strain was varied from 0.1 to 100% with the frequency fixed at 1 Hz. Parallel plates (25 mm diameter) were used with a gap size between them of 1 mm. The measurement was conducted at 25.5±0.5°C. The viscosity, storage modulus, and stress curves as a function of the strain change were obtained, and the critical strain was determined. The yield stress was calculated by multiplying the critical strain and the storage modulus at the critical strain (Youn and Lee 2002).

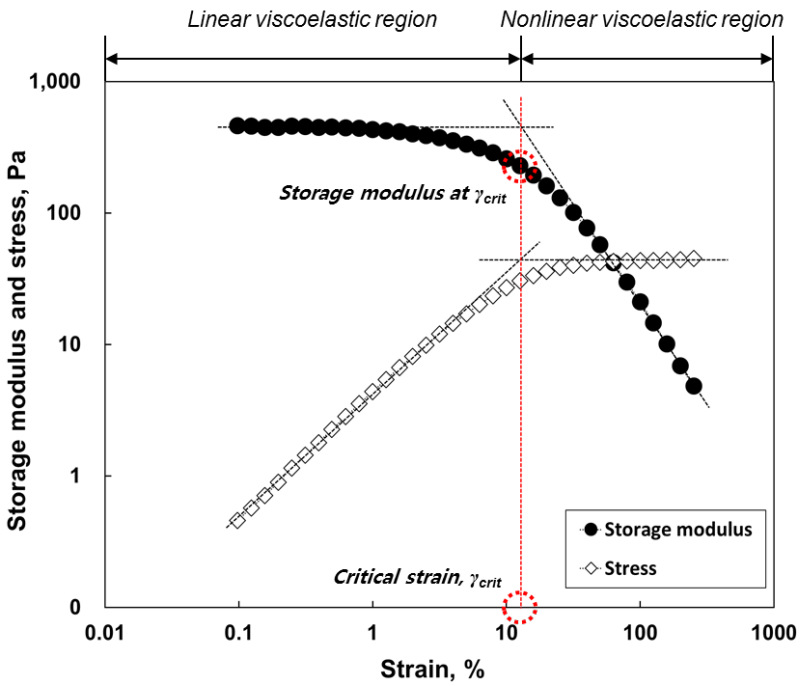

Fig. 4-5. Determination of yield stress of CNF suspension.

The rheology of the CNF suspension was also examined using a microrheometer (Fig. 4-6, Rheolaser MASTER^{TM}, Formulaction Inc., France) based on a dynamic light scattering technique called diffusing wave spectroscopy (DWS). When the illuminated laser is scattered into the viscoelastic material, an interference image called “speckle” is obtained. The mean square displacement (MSD) of CNF was measured from the light intensity fluctuations in speckle images. From the MSD, viscoelastic properties of the CNF suspension such as the elasticity index (EI) and solid liquid balance (SLB) were calculated.

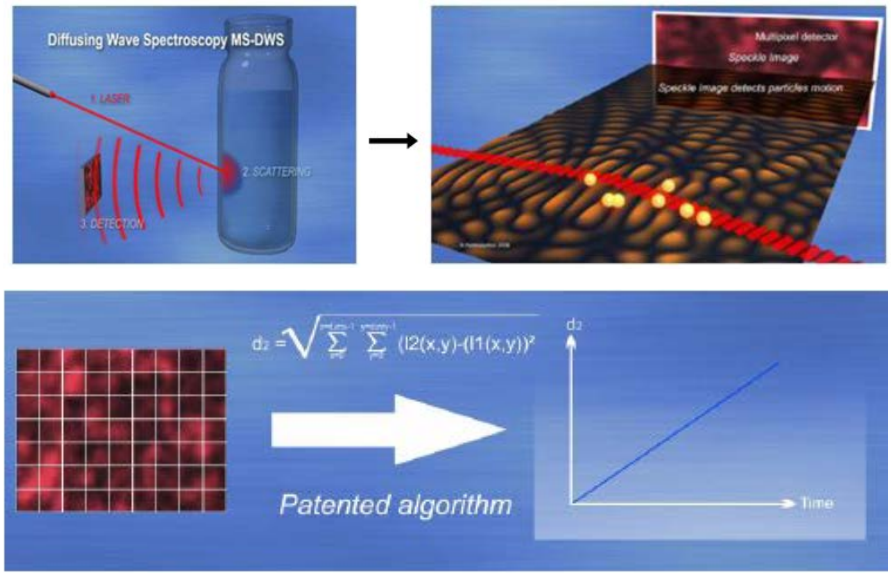

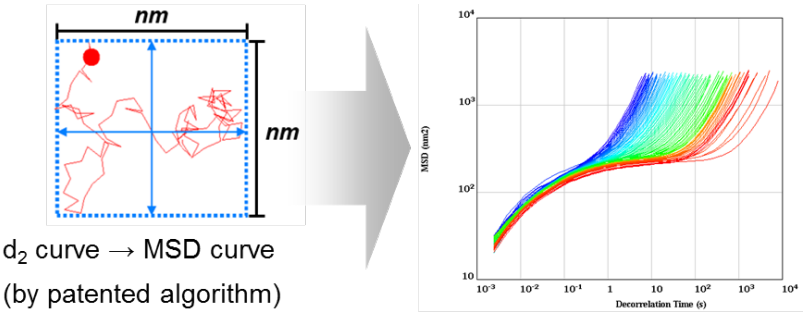

d_2 curve → MSD curve
(by patented algorithm)

Fig. 4-6. Principle of Rhoelaser MASTER^{TM} for measuring of rheological properties.

2.3.5 Evaluation of dewatering ability of CNF suspension

The dewatering ability of CNF suspension was evaluated using pressure dewatering equipment. CNF suspension (1.5%, 60 g) was loaded into the container. Dewatering of CNF suspension was carried out at pressure of 7 bars. Water was removed downward from the container through the filter paper and mesh wire. The removed water was collected and simultaneously weighed using a balance to evaluate the drained water content as a function of dewatering time. The percentage of the amount of drained water against the initial water content in the CNF suspension is expressed as the drained water (%).

2.3.6 Preparation of CNF sheet and evaluation of its properties

To prepare CNF sheet, the CNF suspension was diluted to 0.5% with deionized water and vacuum filtered. The dry weight of salt-added CNF was 0.7 g. The vacuum filtered wet sheet was dried with freeze dryer at -81°C. The apparent density and porosity of CNF sheet was evaluated according to 2.2.1.4 in Chapter 4.

2.4 Surfactant addition on CNF suspension

2.4.1 Addition of surfactant

Surfactant (CTAB) solution was added to the CNF suspension (0, 0.1, 0.5, 1.0, 2.0, 5.0% on oven-dried weight of CNF). The final consistency of CNF suspension was adjusted to 1.5%.

2.4.2 Evaluation of surface tension of water

The static surface tension of water with surfactant of different concentrations was measured using a static surface tensiometer (K12 processer tensiometer, Krüss) at room temperature. The plate method was used.

2.4.3 Evaluation of dewatering ability of CNF suspension

The dewatering ability of surfactant-added CNF suspension was evaluated according to 2.2.5 in Chapter 4.

2.4.4 Preparation of CNF sheet and evaluation of its properties

The apparent density and porosity of CNF sheet was evaluated according to 2.2.1.4 in Chapter 4. The dry weight of surfactant-added CNF for sheet forming was 0.7 g. The specific surface area of surfactant-added CNF sheet was analyzed by BET gas adsorption and desorption method.

2.4.5. Tensile properties of CNF sheet

The tensile properties of CNF sheet depending on the surfactant content was evaluated using a UTM (Universal Testing Machine, Instron, Corporation, USA). The width of sample and the measurement span were 15 mm and 40 mm, respectively. The strain rate during measurement was 0.5 mm/min. The elastic modulus, tensile stress and strain at break were obtained from a stress-strain curve.

3. Results and Discussion

3.1 Chemical treatment of CNF

3.1.1 Effect of carboxymethylation

3.1.1.1 Degree of substitution

The degree of carboxyl group on untreated cellulose fiber, a commercial CMC, and carboxymethylated CNF (CM-CNF) was analyzed by using FT-IR spectrophotometer (Fig. 4-7). Commercial CMC is carboxymethylated cellulose purchased from Sigma-aldrich. It is known that the C=O band by carboxyl group generally appears between 1700 and 1730 cm^{-1} (Pavia et al. 1996). This band is shifted to lower frequencies occasionally. The carboxyl group of untreated cellulose fiber appeared near 1650 cm^{-1} as a weak band. This carboxyl group may be derived from hemicelluloses in pulp fibers themselves (Sood et al. 2010). Commercial CMC with a substitution degree of 0.7 showed a strong absorbance near 1590 cm^{-1}. The absorbance of carboxyl group of CM-CNF, which appeared near 1642 cm^{-1}, was lower than that of commercial CMC, but higher than that of untreated cellulose fibers. It is considered that the band appeared between 1400 and 1450 cm^{-1} is methyl group (Saputra et al. 2014).

To evaluate the substitution degree of carboxyl group quantitatively, the conductometric titration was carried out as shown in Fig. 4-8. The conductivity remains essentially unchanged when the neutralization of

carboxylic groups by NaOH during measurement occurs. The carboxylate content was calculated by the amount of NaOH in the linear region. The carboxylate content of untreated CNF and carboxymethylated CNF was 0.05 mmol/g CNF and 0.24 mmol/g CNF, respectively.

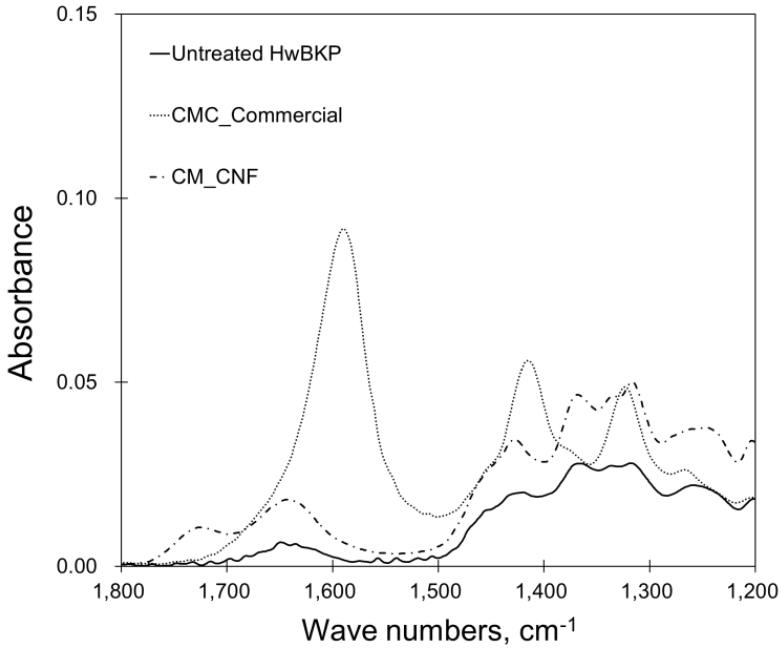

Fig. 4-7. FT-IR spectra of untreated and carboxymethylated cellulose specimens.

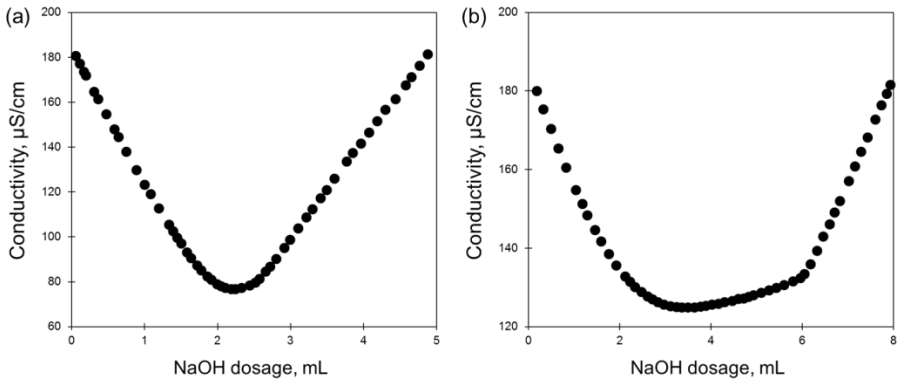

Fig. 4-8. Results on conductometric titration: (a) untreated CNF and (b) carboxymethylated CNF.

3.1.1.2 Dewatering ability and viscosity

The dewatering ability of untreated CNF suspension and carboxymethylated CNF (CM-CNF) suspensions was evaluated by using pressure dewatering equipment (Fig. 4-9). The drained water amount of untreated CNF and CM-CNF suspension for 5, 10, 15, 20 min was compared at the same consistency of 2%. The drained water amount of CM-CNF suspension for 5 min was 2%, whereas untreated CNF suspension showed approximately 20% drained water content. The drained water amount of untreated CNF suspension was increased continuously until 20 min, showing the maximum amount of approximately 58%. The CM-CNF suspension still showed low drained water amount below 10% after 20 min. The drainage of CM-CNF suspension was completed after 105 min. The total drained water amount of untreated CNF and CM-CNF suspension was 59% and 45%, respectively. The CM-CNF suspension showed the higher water holding capacity as well as the lower dewatering rate. This may be because of the good dispersibility and the smaller dimension in width of CM-CNF. As shown in Fig. 4-10, the CM-CNF suspension showed a significantly higher viscosity (1356 cPs) than untreated CNF suspension (215 cPs). This suggests that carboxymethylated nanofibrils are mechanically entangled well and dispersed in water by electrostatic repulsion.

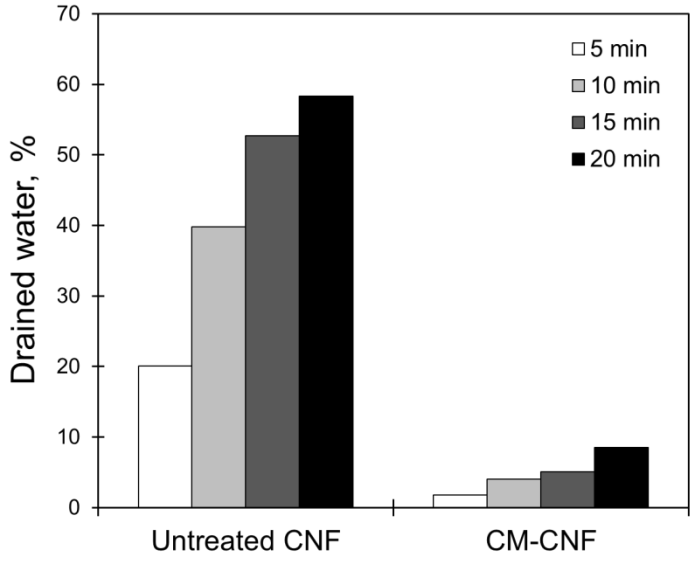

Fig. 4-9. Dewatering ability of untreated and carboxymethylated CNF suspensions.

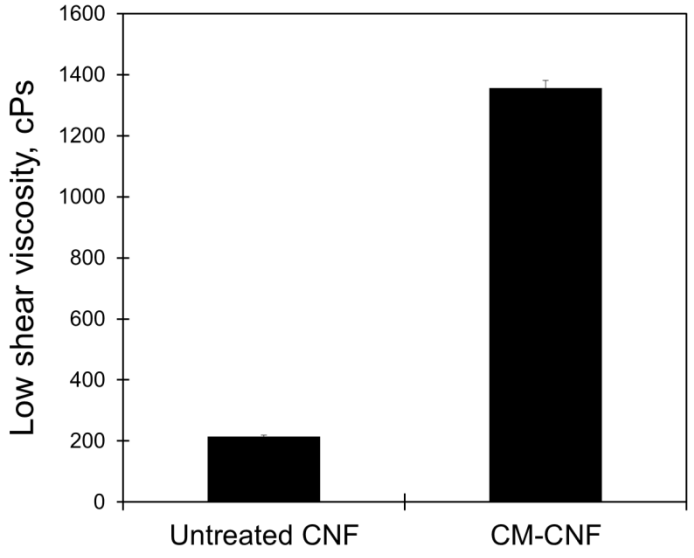

Fig. 4-10. Low shear viscosity of untreated CNF and carboxymethylated CNF suspensions.

3.1.1.3 Characteristics of film and sheet

Film was made of untreated CNF and CM-CNF suspension with 0.25% consistency by drying at 50°C (Fig. 4-11). The size of nanofibrils in width significantly affected the transmittance of CNF film. More transparent film could be produced with CM-CNF, which has width of 13 nm in average. The light transmittance of untreated CNF and CM-CNF film measured by Elrepho (L&W Co., Sweden) was 78.4% and 87.9%, respectively.

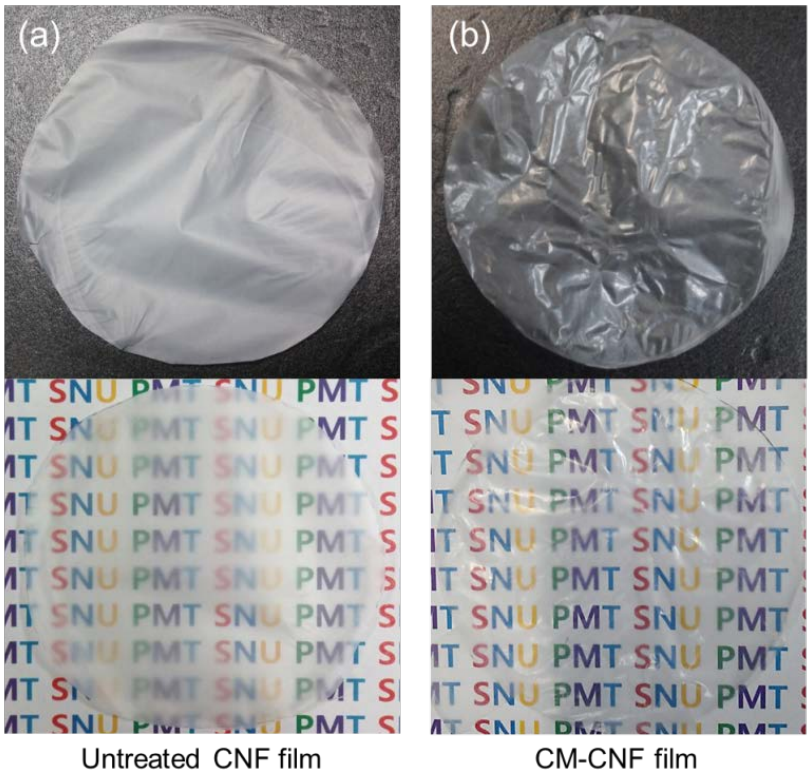

Fig. 4-11. (a) Untreated CNF and (b) carboxymethylated CNF film.

Untreated and carboxymethylated CNF sheets were prepared by vacuum filtration and freeze drying (Fig. 4-12). Even though the same dry weight of CNF was used and freeze drying method was conducted, the translucent sheet was produced with CM-CNF. The density (thickness) of untreated CNF sheet and CM-CNF sheet was 0.25 g/cm^3 (160 μm) and 0.66 g/cm^3 (60 μm), respectively. The preparation of denser sheet with low thickness could be achieved with CM-CNF because it had smaller width and higher specific surface area. When the opacity of sheet was evaluated, the CM-CNF sheet showed opacity of 28.3%, which is one-third of untreated CNF sheet.

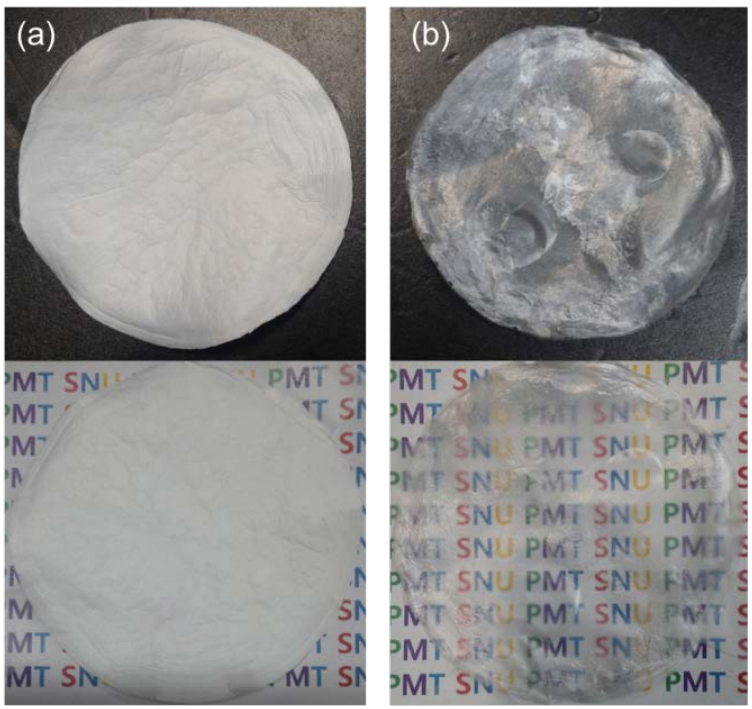

Fig. 4-12. Vacuum filtered and freeze dried sheets made of (a) untreated CNF and (b) carboxymethylated CNF.

3.1.2 Effect of TEMPO-mediated oxidation

3.1.2.1 Charge property

TEMPO-mediated oxidation was conducted on CNF as a post-treatment in order to increase the negative charge onto cellulose surface. Two kinds of fibers were obtained: TOCNs in supernatant which are dispersed well by their electrostatic repulsion and sedimented CNF. The charge property of sedimented CNF was evaluated in terms of zeta potential and charge demand. Fig. 4-13 shows the zeta potential and charge demand of TEMPO-oxidized CNF depending on the oxidation time. The zeta potential and charge demand of untreated CNF were about -36.1 mV and -0.08 meq/g, respectively. The negative charge was increased with an increase in reaction time, resulting in maximum -38.5 mV and -0.138 meq/g at 4 hr. Although the negative charge property of 30 min-oxidized CNF was similar to untreated CNF, it increased rapidly after 1 hr oxidation. From 1 hr to 4 hr, there were no significant changes in zeta potential and charge demand of CNF. The zeta potential and charge demand of CNF depending on the addition amount of oxidizing agent (NaClO) is shown in Fig. 4-14. The negative charge of CNF was increased continuously by increasing the addition amount of NaClO, showing -41.7 mV at 25 mmol/g CNF condition. The TOCNs obtained from supernatant showed the zeta potential of -46.8 mV. The change in charge demand of CNF depending on the addition amount of NaClO was very similar to that in zeta potential. The maximum charge demand of CNF at 25 mmol/g CNF condition was -0.222 meq/g.

The surface charge property of CNF was controlled by carboxymethylation and TEMPO-mediated oxidation. In TEMPO-mediated oxidation, the change in amount of oxidizing agent was more effective to increase negative charge onto fibers than that in reaction time.

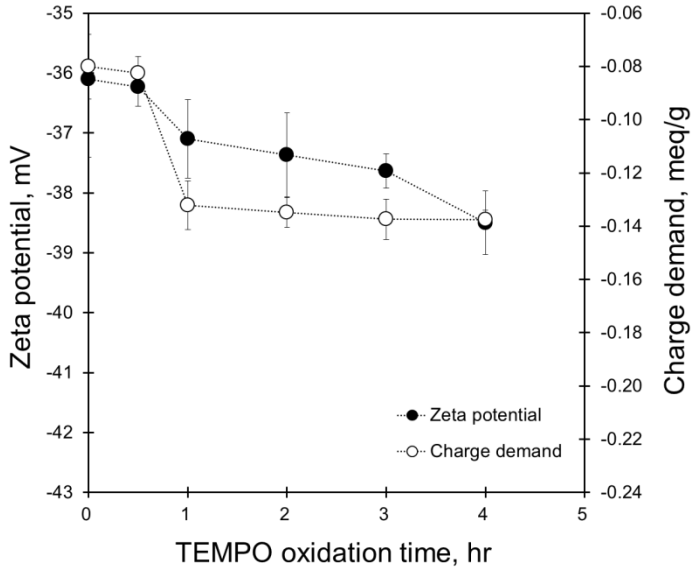

Fig. 4-13. Zeta potential and charge demand of TEMPO-mediated oxidized CNF depending on the oxidation time.

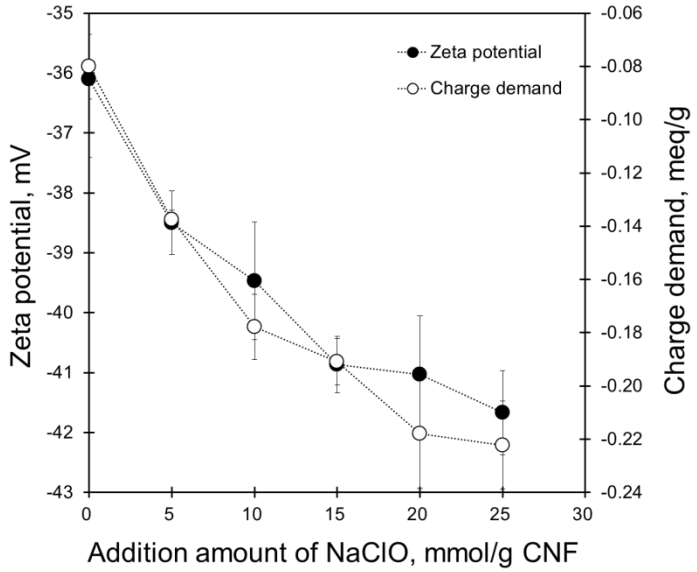

Fig. 4-14. Zeta potential and charge demand of TEMPO-mediated oxidized CNF depending on the addition amount of NaClO.

3.1.2.2 Characteristics of film and sheet

Fig. 4-15 shows the diluted suspensions of TOCN and untreated CNF, and the film made of each suspension. TOCN suspension was more transparent when compared with untreated CNF suspension. Even though it was much diluted (0.03%), the untreated CNF suspension was opaque. It was easy to prepare a transparent film with TOCN because TOCN is well dispersed in water by a strong electrostatic repulsion between nanofibrils and its width is very small. The light transmittance of TOCN film was 89.5%. The highly transparent film without pores is expected to use in packaging due to its excellent barrier property (Fukuzumi et al. 2009).

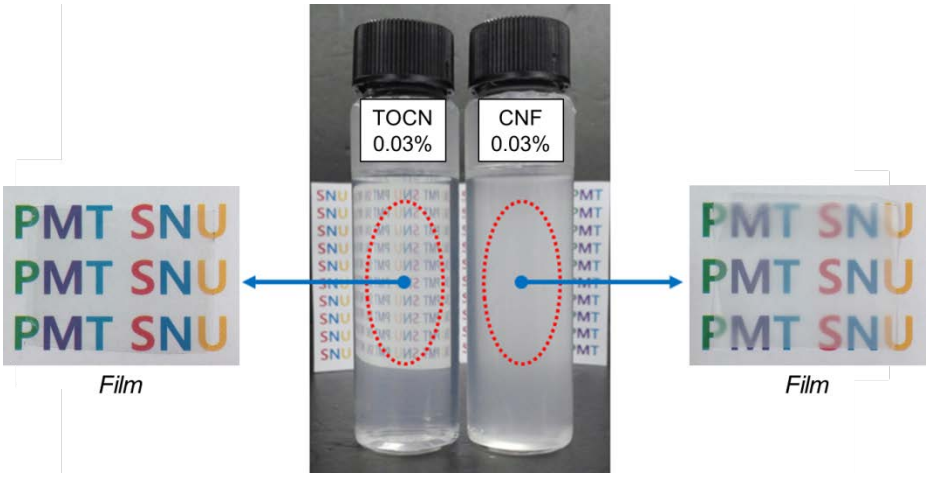

Fig. 4-15. Light transmittance of film made of (a) TOCN and (b) untreated CNF.

Fig. 4-16 shows the freeze dried sheets made of untreated CNF and TEMPO-oxidized sedimented CNF. With an increase in amount of oxidizing agent (NaClO), the sheet became translucent at 25 mmol/g CNF condition. The density and porosity of untreated CNF sheet were 0.23 g/cm^3 and 85%, respectively (Fig. 4-17). When TEMPO-mediated oxidation was conducted with the NaClO amount of 5 mmol/g CNF, the porosity of sheet was decreased to about 81%. With the maximum amount of NaClO (25 mmol/g CNF), the sheet porosity decreased significantly to 56%.

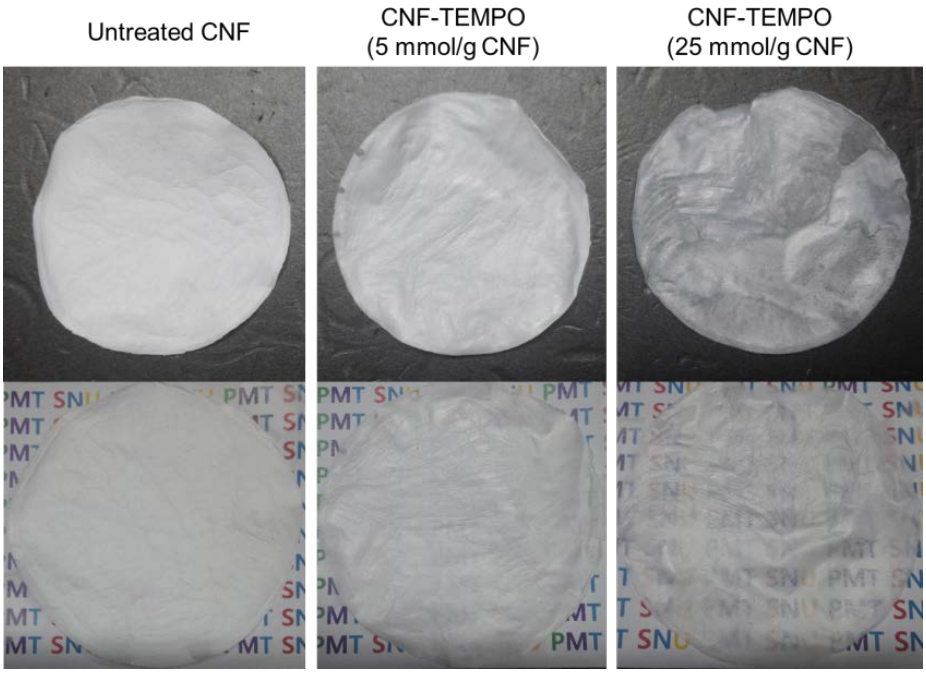

Fig. 4-16. Photographs of TEMPO-mediated oxidized CNF sheets (freeze drying) depending on the addition amount of NaClO.

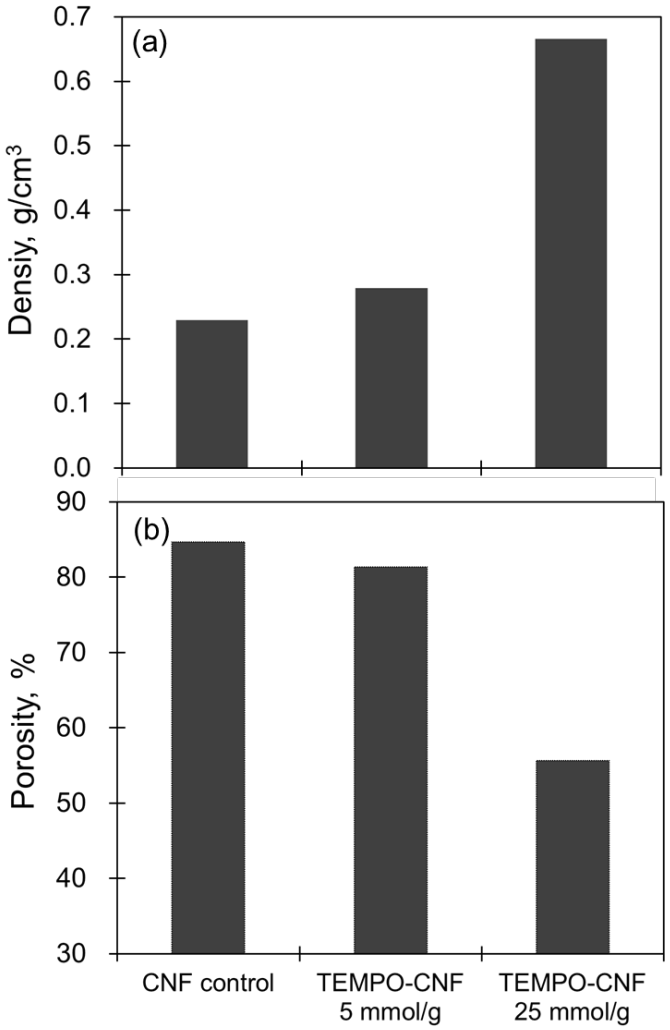

Fig. 4-17. Apparent density and porosity of TEMPO-mediated oxidized CNF sheets.

3.2 Effect of salt addition on the properties of CNF suspension and sheet

3.2.1 Change in charge of CNF with salt

In Fig. 4-18, the zeta potential of CNF in aqueous suspension is plotted against the salt condition. Salt-free CNF (0 M) showed a -43 mV negative charge because of some carboxyl groups derived mainly from hemicelluloses (Sood et al. 2010; Olszewska et al. 2011). As the concentration of the $CaCl_2$ solution was increased, the charge of CNF moved to a positive value, indicating that it was neutralized at 0.5 M. It has already been reported that the sufficient calcium ions (counterions) can cause charge reversal of the charged surface from negative to positive (Kékicheff et al. 1993; Carambassis and Rutland 1999). However, addition of NaCl could not change the charge of CNF to a positive value at the same concentration. The counterions derived from the salt move to the charged surface of the substrate in the colloidal dispersion. Adsorption of counterions (Na^+ or Ca^{2+}) onto the CNF surfaces changed the charge of the CNF. In the case of addition of $CaCl_2$, the charge of the CNF decreased more than the case of addition of NaCl for the same salt concentration because the electrical double layer was more compressed by bivalent ions.

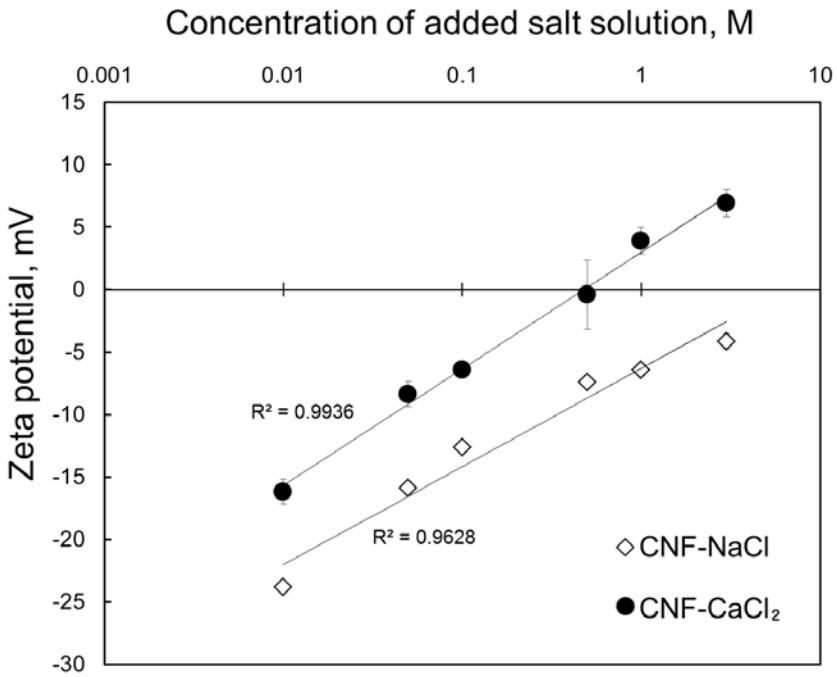

Fig. 4-18. Zeta potential of CNF depending on the type and concentration of salt (zeta potential of CNF without salt addition: -43 mV).

3.2.2 Flocculation behavior of CNF

Fig. 4-19 shows the photographs of highly diluted (0.01%) CNF suspension with the passage of time, depending on the type and concentration of salt. Immediately after shaking the CNF suspension, the salt-free CNF dispersed well in the water because of electrostatic repulsion between nanofibrils with negative charge, appearing like a clear solution. This is an electrostatically stabilized state (Bobacka and Eklund 1999; Fall et al. 2013). However, when salt was added to the CNF suspension, aggregation and sedimentation of nanofibrils were observed because the electrostatic repulsion was weakened by compression of the electrical double layer. In the case of NaCl addition, the flocculation and sedimentation rate increased with increasing salt concentration. Large flocs of nanofibrils were observed at high salt concentrations such as 1 and 3 M. After 25 min, the sedimentation height was maintained similarly regardless of the NaCl concentration. The flocculation behavior of the $CaCl_2$-added CNF was different from that of the NaCl-added CNF suspension. As charge reversion occurred on $CaCl_2$ addition (Fig. 4-18), the sedimentation was high at certain salt concentrations (near neutral charge) within a short duration. However, the final sedimentation height was similar after a long duration (15 min) for all concentrations. This suggests that the network structure of nanofibrils changed depending on the aggregation by charge neutralization under different salt conditions.

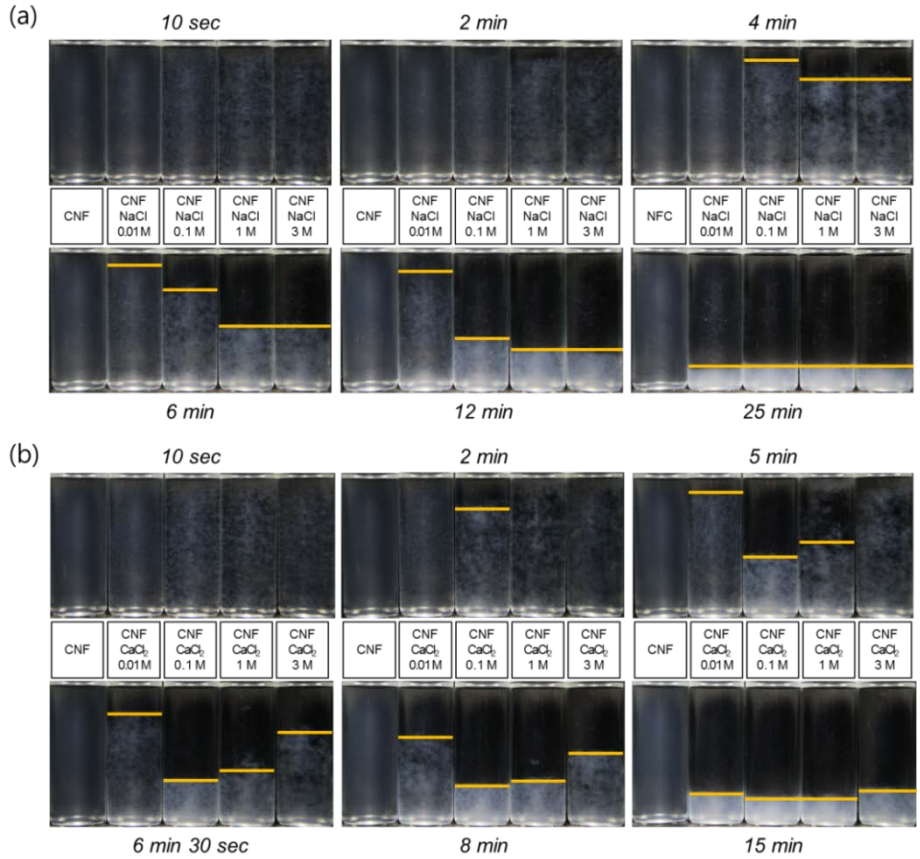

Fig. 4-19. Photographs of CNF suspension depending on the type and concentration of salt and duration: (a) NaCl addition and (b) $CaCl_2$ addition.

The dispersion property of CNF in aqueous media was evaluated by the change in light transmission (Fig. 4-20). The *x*-axis on this graph reflects the height of a vial containing CNF suspension. The left end and right ends of the *x*-axis represent the bottom and top ends of the vial, respectively. Fig. 4-20 (a) shows the delta transmission of light on the CNF suspension without any salt. As the amount of time advances from the bluish to reddish lines, the light transmission changed minimally through the sample vial from bottom to top. Although a minimal amount of change in light transmission was detected at the top part of the vial, the change was negligible. Thus, the CNF suspension without salt was very stable. When the 0.01 M NaCl solution was added (Fig. 4-20 (b)), a significant increase in light transmission at the middle and top position of the vial was detected because of sedimentation with aggregation of nanofibrils, as shown in Fig. 4-19. The light transmission decreased at the lower section of the vial due to sedimentation of the nanofibrils. At higher salt concentration (Fig. 4-20 (c)), the gap between the lines from bluish to greenish became large, indicating that the sedimentation speed of CNF increased. The dispersion of CNF suspension was affected by the salt concentration, which is related to the electrochemical properties of the CNF surface.

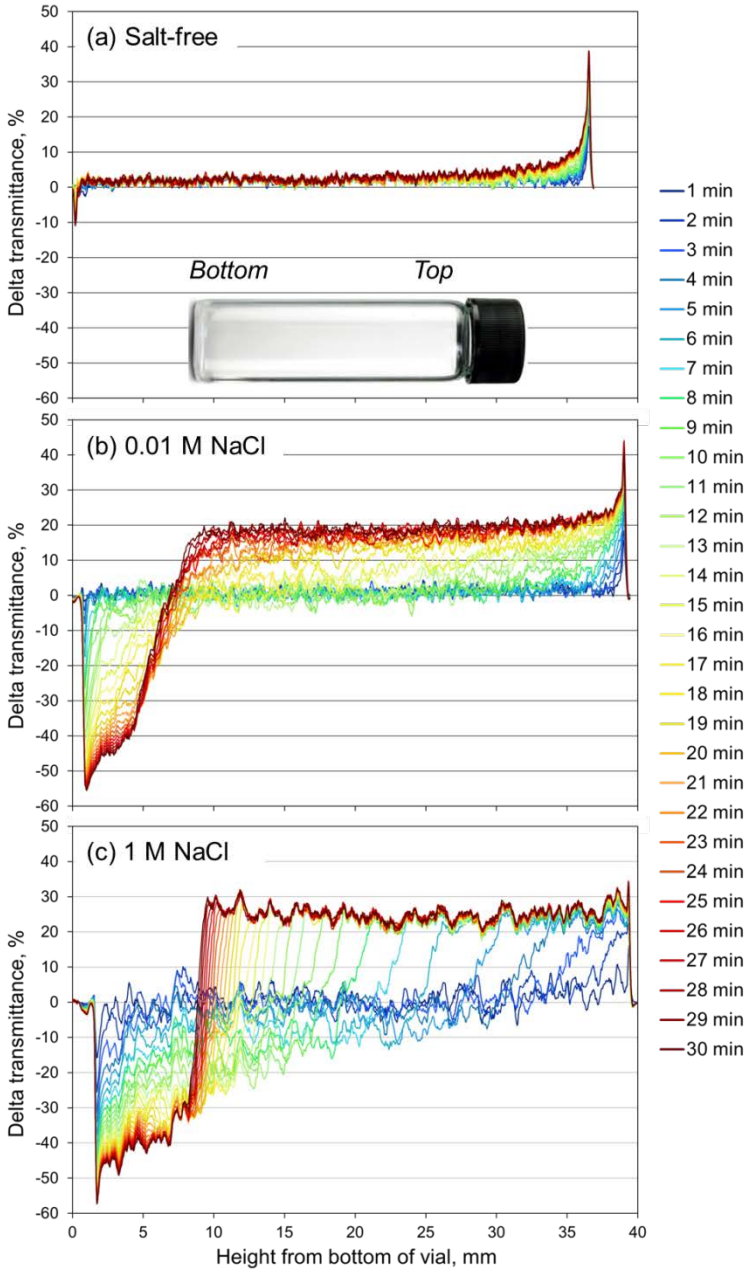

Fig. 4-20. Delta transmission of light on the salt-added CNF suspensions as a function of time: (a) deionized water, (b) 0.01 M NaCl, and (c) 1 M NaCl.

3.2.3 Rheological properties of CNF suspensions

The rheological properties of CNF suspension under different salt conditions were characterized using ARES measurement. Fig. 4-21 shows the viscosity of CNF suspension as a function of strain change at constant frequency (1 Hz). For all samples, the viscosity of CNF suspension was maintained at a low strain level. Then, the viscosity decreased with increasing strain above a critical strain, which is typical shear-thinning behavior. At low strain, the viscosity was higher in the salt-added CNF suspensions than in the salt-free CNF suspension (control). The thickness of the electrical double layer on the nanofibrils surface decreased with addition of salt, so they could flocculate. Thus, the reduced repulsive forces between nanofibrils promoted a strong network structure of CNF suspension with higher viscosity (Laka and Chernyavskaya 2009). In addition, the CNF suspension with $CaCl_2$ showed higher viscosity than the CNF suspension with NaCl for the same salt concentration. However, there was no significant difference in viscosity among the salt conditions at high strain level.

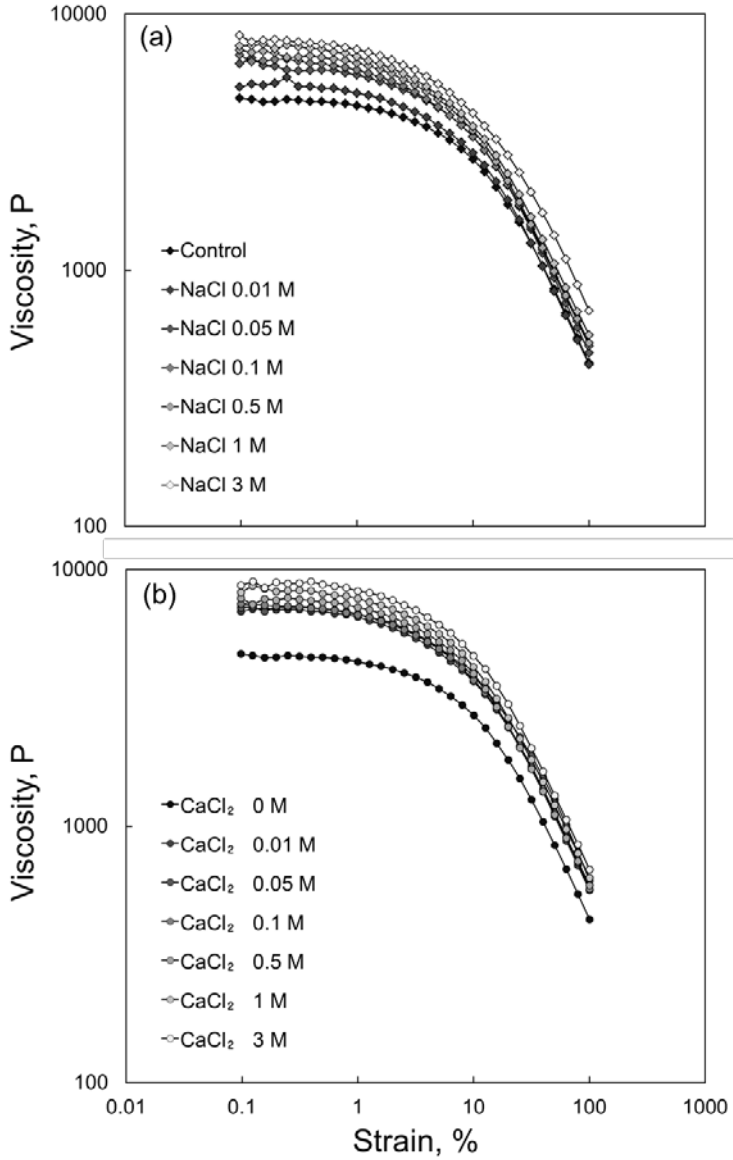

Fig. 4-21. Viscosity of CNF suspension as a function of strain under different salt conditions: (a) NaCl addition and (b) $CaCl_2$ addition.

Fig. 4-22 shows the storage modulus and yield stress of the salt-added CNF suspensions. The dotted lines represent the storage modulus and yield stress of salt-free CNF suspension. The storage modulus of CNF suspensions at 1% strain is plotted to compare the effect of salt conditions at the same strain. The selected strain point was in the plateau region of the storage modulus. Although there is controversy about the resulting yield stress value as a true material property depending on the measurement methods (Derakhshandeh et al. 2010), measurement of yield stress is useful to predict the structure of materials as one of the important rheological properties. The yield stress was determined from the storage modulus and critical strain. The nanofibrils form a network structure in suspension by percolation above a certain consistency (Guenet 2000; Ryu 2013), and this structure is broken down with increase of strain. As the strain reaches the yield point, the network structure loses its elastic nature and breakage of the nanofibril network occurs. When the CNF network is stronger, the yield stress and storage modulus are higher. The storage modulus and yield stress of CNF suspensions resulted in the same tendency, which depends on the salt concentration. Both the storage modulus and yield stress of CNF suspensions increased with increase in the salt concentration. This indicates that a stronger network structure of CNF suspension was formed by flocculation due to charge neutralization. A similar result was reported by Saarikoski et al. (2012) in that the storage moduli (G') of MFC suspension increased with an increase of the NaCl concentration via aggregation. The salt type also affected the strength of the nanofibril network. Higher values of the storage modulus and yield stress were obtained on addition of $CaCl_2$ solution at the same concentration. This indicates that salt with bivalent counterions are more effective for producing a strong nanofibril

network structure through greater reduction of the electrostatic repulsion at a low concentration. According to the Laka and Chernyavskaya (2009), the stronger microcrystalline cellulose (MCC) gels were formed when the polyvalent cations were used. The yield stress of MCC gels was similar to each other if the valency of cation was the same. For example, the yield stress of MCC gels with NaCl, KCl, LiCl, $FeCl_3$, and $AlCl_3$ was 18.6, 15.3, 19.0, 60.9, and 65.1 MPa, respectively. The formation of a stronger network by flocculation can be found in the case of CNF suspension with polyelectrolytes. Change on the MFC surface by adsorption of a cationic polymer leads to a strong gel, which is explained by aggregation of fibers due to electrostatic attractive forces (Karppinen et al. 2011). Therefore, the rheological properties of CNF suspension are affected by the association of fibrils and are controlled by the addition of salt or a polymer.

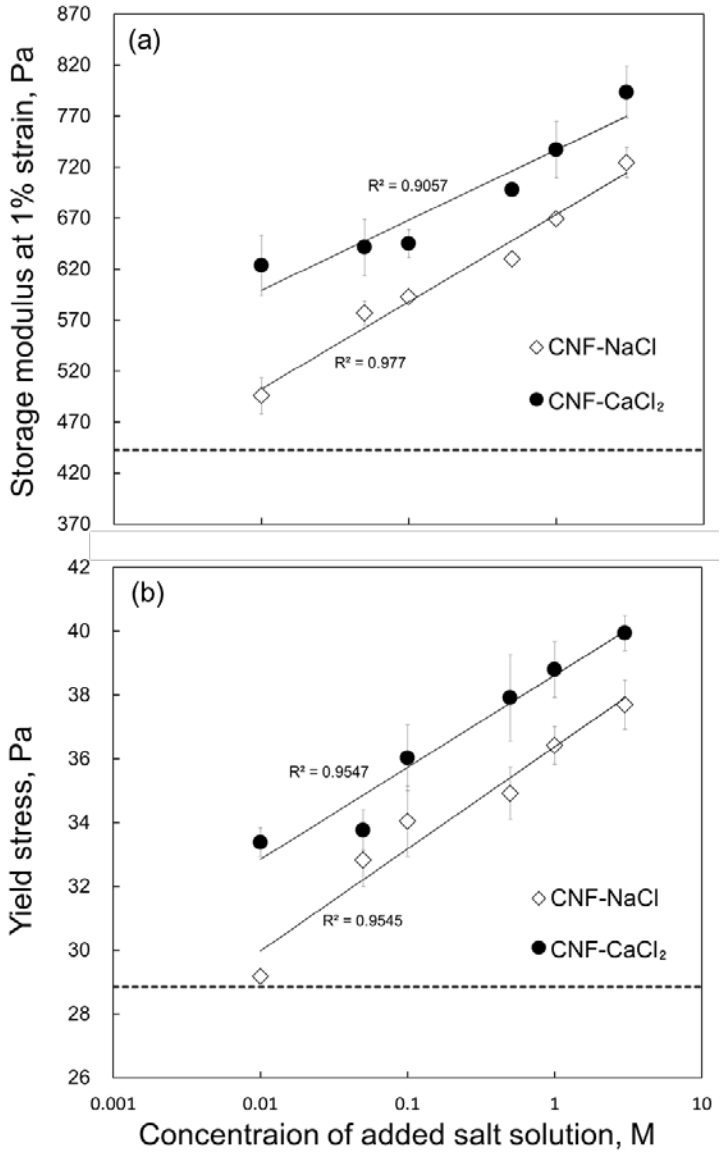

Fig. 4-22. Storage modulus at 1% strain (a) and yield stress (b) of CNF suspensions depending on the type and concentration of salt (dotted line: value of salt-free CNF suspension).

Fig. 4-23 shows example MSD curves obtained by microrheometer for two CNF samples with different viscoelastic characteristics. The EI is calculated automatically from the height of the plateau between 25 and 1500 ms decorrelation time (gray rectangle region) in the MSD curve. The EI ($1/nm^2$) is determined as the reciprocal of the absolute value of the MSD in the plateau region. A lower value MSD in the plateau region (case CNF2) indicates viscoelastic material with stronger structure, thus being difficult to move.

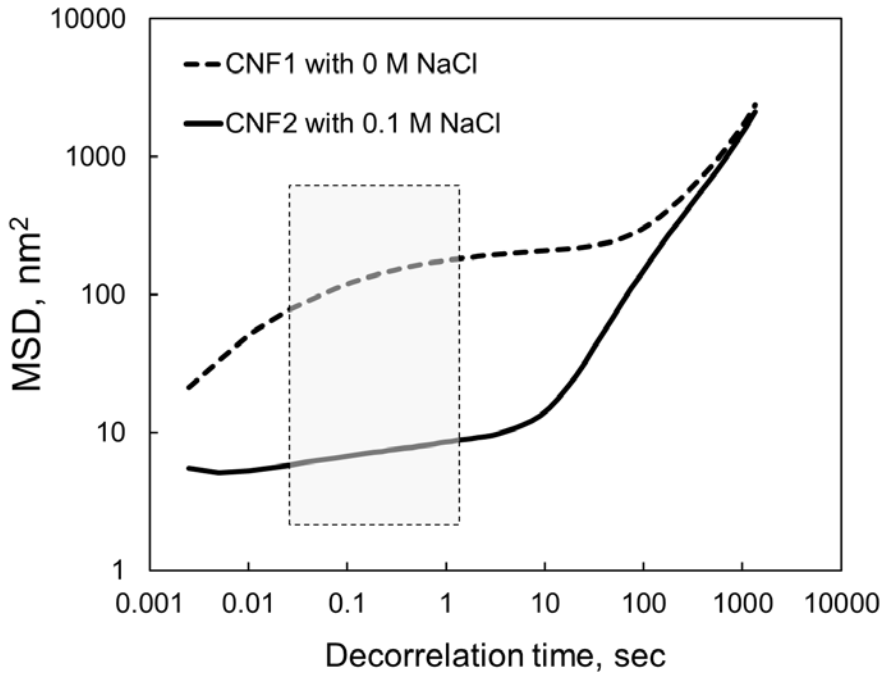

Fig. 4-23. Mean square displacement (MSD) of CNF suspension with decorrelation time in a microrheometer (*gray rectangle* plateau region to calculate the elasticity index and solid liquid balance).

The EI of CNF suspension as obtained from MSD curves is shown in Figs. 4-24 (a) and 4-24 (b). The EI of CNF suspension increased with addition of salt solution. At low salt concentration (0.01 M), $CaCl_2$-added CNF suspension showed a much higher EI compared with NaCl-added CNF suspension. As the salt concentration was increased, the impact of the salt type on the EI weakened. However, a slightly higher value was observed for the $CaCl_2$-added CNF suspensions.

Figs. 4-24 (c) and 4-24 (d) present the SLB, which is the ratio between solid-like and liquid-like characteristics. The SLB is determined by the slope of the MSD at the plateau between 25 and 1500 ms decorrelation time. When the MSD curve slope is lower, the CNF network is more solid like. If the SLB value is below 0.5, the sample is considered to have mainly elastic/solid-like nature. In this study, all the CNF suspensions showed solid-like behavior regardless of the type and concentration of salt, because the SLB value was <0.5. CNF suspension without salt showed solid-like behavior due to the network structure formed by percolation (Guenet 2000; Ryu 2013). The SLB value became lower with increase in the salt concentration and addition of $CaCl_2$, corresponding to an increase of solid-like behavior.

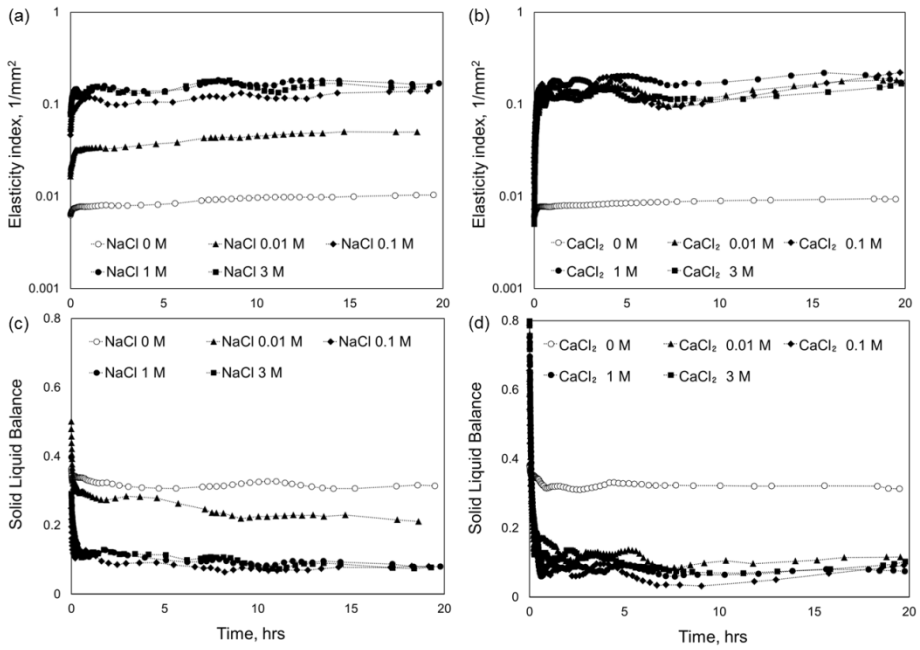

Fig. 4-24. Microrheology of CNF suspensions by salt type and concentration: (a) and (b) elasticity index; (c) and (d) solid liquid balance.

3.2.4 Dewatering ability of CNF suspension

CNF suspensions (1.5%) with different NaCl concentrations were compressed under high pressure in the pressure dewatering equipment. The ratio of the amount of drained water to the initial water content in the CNF suspensions is plotted as a function of dewatering time in Fig. 4-25. In the case of CNF suspension without salt (control), 25 min was needed to remove the water from the CNF suspension using the pressure dewatering equipment. After 25 min, there was no change in the drained water amount. However, with addition of salt, the drainage rate increased significantly. The dewatering of CNF suspension was completed after between 7 to 15 min with addition of NaCl, depending on the concentration.

The amount of water drained from CNF suspensions in 5 min is plotted in terms of the type and concentration of salt in Fig. 4-26. Even though a low concentration (0.01 M) of salt solution was added, the dewatering ability of the CNF suspension increased significantly. Addition of $CaCl_2$ solution with bivalent cations was more effective for dewatering at the same salt concentration and time compared with addition of NaCl. With addition of NaCl solution, the drained water amount during the same time increased continuously with increase in the NaCl concentration until 0.5 M. However, no change was observed between 0.5 M and 3 M. On the other hand, in the case of addition of $CaCl_2$, the drained water content decreased again above the 0.5 M condition. This dewatering ability is related to the degree of aggregation of the CNF. To remove water from the CNF suspension, channels for water to flow through the nanofibril network are necessary. It seemed that

large channels are formed by aggregation of charge-neutralized CNF with addition of salt. That is, lower density areas between flocs can be created as large flocs are formed, developing paths for drainage (Varanasi and Batchelor 2014). However, in the case of addition of 1 or 3 M $CaCl_2$ solution, the drainage channels became smaller due to increase of the electrostatic repulsion, so the dewatering ability became poor.

Fig. 4-27 shows the drained water amount of CNF suspension after 5 min, which depends on the zeta potential of the CNF. The dewatering ability improved near the neutral charge point by the addition of salt. A similar relationship resulted between the drainage and zeta potential for pulp suspension (Bhardwaj et al. 2005). When the zeta potential of pulp fibers was changed from a negative to a near-neutral charge by addition of cationic polyelectrolytes, the drainage of pulp suspension became greater. This indicates that the dewatering ability of suspension can be improved by controlling the zeta potential of the fibers.

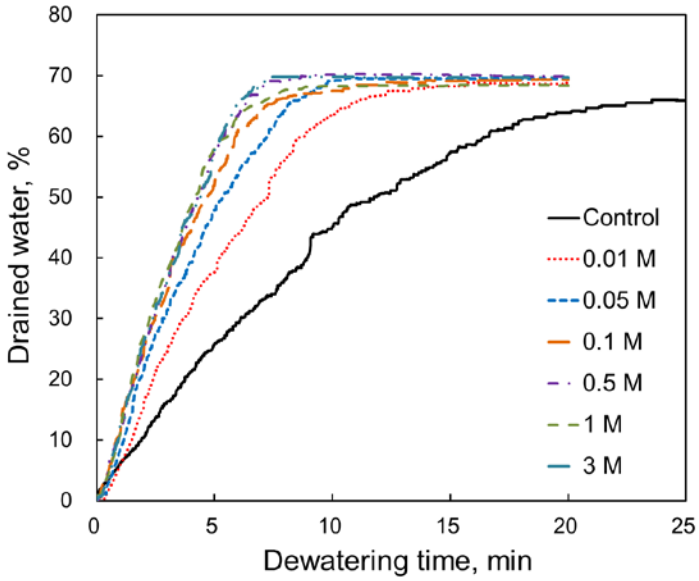

Fig. 4-25. Drained water amount from NaCl-added CNF suspensions with time using pressure dewatering equipment.

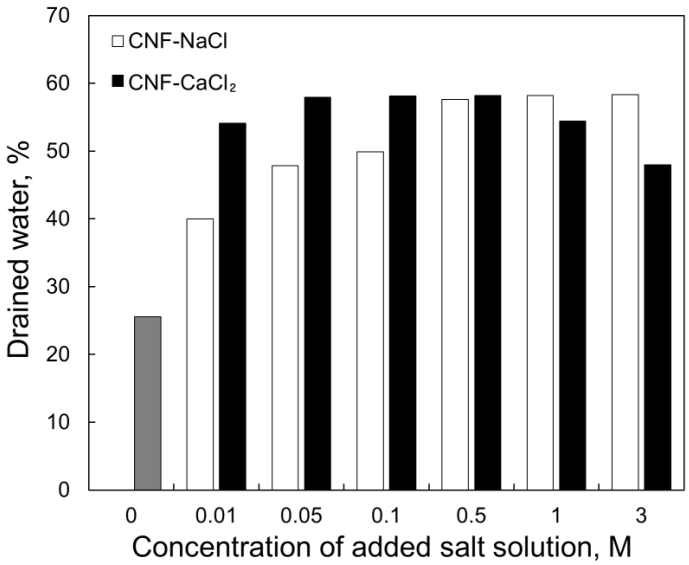

Fig. 4-26. Dewatering ability of CNF suspensions (1.5%) depending on type and concentration of salt (until 5 min).

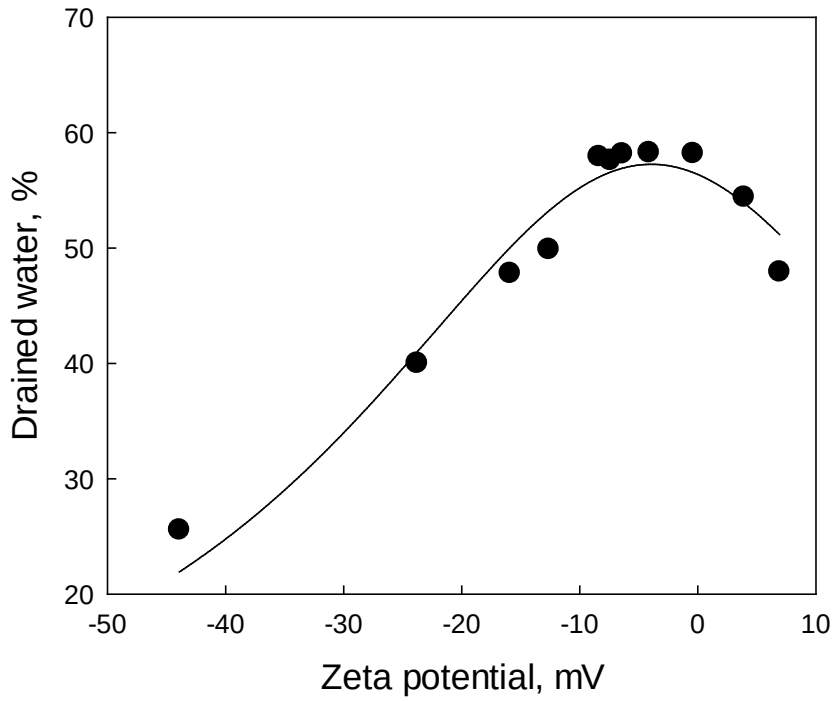

Fig. 4-27. Relationship between zeta potential and drained water amount of CNF suspension with salt.

3.2.5 Structural properties of CNF sheet

The structural properties such as apparent density and porosity of freeze dried CNF sheets were evaluated. Fig. 4-28 and Fig. 4-29 shows the density and porosity of CNF sheet depending on type and concentration of salt added. The vacuum filtered, freeze dried CNF sheet without salt addition showed a density of 0.32 g/cm^3 and its corresponding porosity was 79%. When the sheet was prepared from the suspension with 0.01 M salt, the more porous sheet, which has 83% - 85% porosity, could be obtained. However, it was difficult to find a relationship between flocculation degree and structural properties depending on salt conditions. The density and porosity of sheets were little changed from 0.01 M to 1 M for both NaCl and $CaCl_2$ addition, whereas the flocculation behavior of nanfibrils in water was significantly affected by salt conditions. The removal of salt during sheet forming by dewatering is postulated as the cause. When the concentration of added $CaCl_2$ solution was 3 M, the porosity of CNF sheet decreased significantly to 68%. In contrast, the CNF sheet with the addition of 3M NaCl showed still more porous structure compared with untreated CNF sheet. It is inferred that the excessive flocculation of nanofibrils by high ionic strength, for example with $CaCl_2$ here, made a denser structure by their strong entanglement and packing.

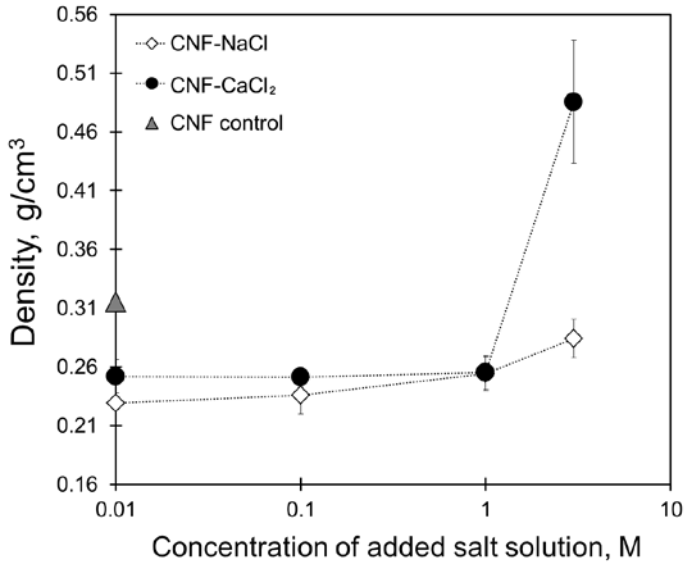

Fig. 4-28. Density of CNF sheets depending on type and concentration of salt.

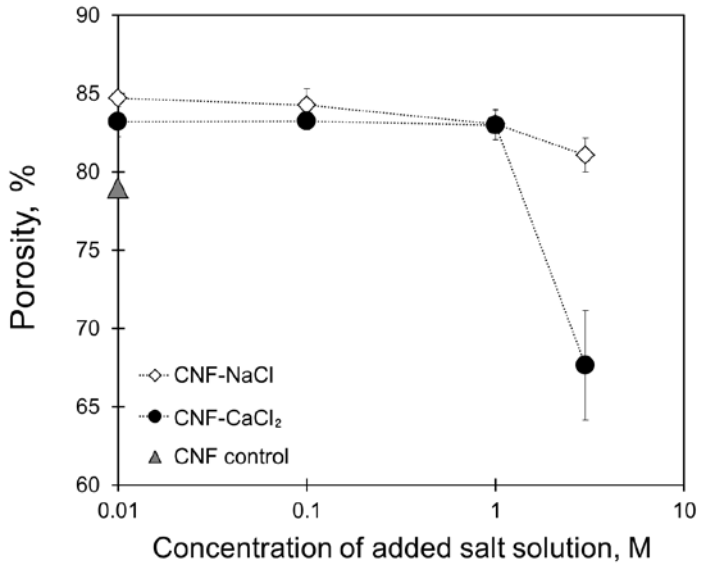

Fig. 4-29. Porosity of CNF sheets depending on type and concentration of salt.

3.3 Effect of surfactant on the properties of CNF suspension and sheet

3.3.1 Dewatering ability of CNF suspension and surface tension of water

Fig. 4-30 shows the dewatering ability of surfactant-added CNF suspension. The *y*-axis is the amount of drained water of CNF suspension depending on the addition amount of CTAB surfactant. The drained water amount for 10 min was increased from 34% to 71% by increasing the addition amount of surfactant from 0% to 5%, especially increased rapidly until 2% addition level. The total drained water amount was also different depending on the addition level of surfactant, showing the continuous increase with an increase in surfactant dosage. The total drained water amount of CNF suspension containing 5% surfactant was approximately 80%, whereas that of untreated CNF suspension was about 73%. The total drained water amount as well as the drainage rate was increased by addition of surfactant because the surfactant decreased the surface tension of water in CNF suspension. The change in static surface tension of water depending on concentration of CTAB surfactant is shown in Fig. 4-31. The vertical dotted line in graph represents the concentration of surfactant in CNF suspension from 0.02% to 5% dosages. The surface tension of pure water was 72.8 mN/m. It decreased rapidly by increasing the concentration of surfactant until 0.001 M (approximately 2% addition level). There was a little difference in surface tension between 2% and 5% addition level. This is thought to correlate significantly with the dewatering result, which the drainage rate became slow from 2% to 5% surfactant dosage. The lowest value of surface tension was 35 mN/m.

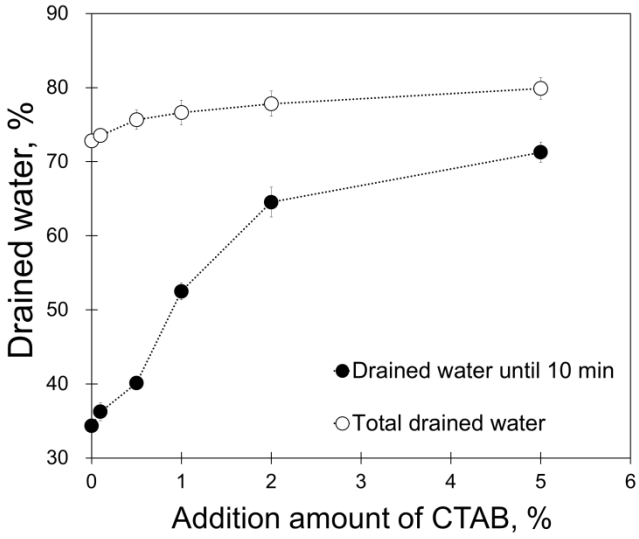

Fig. 4-30. Dewatering ability of CNF suspensions (1.5%) depending on the addition amount of surfactant (CTAB) (until 10 min).

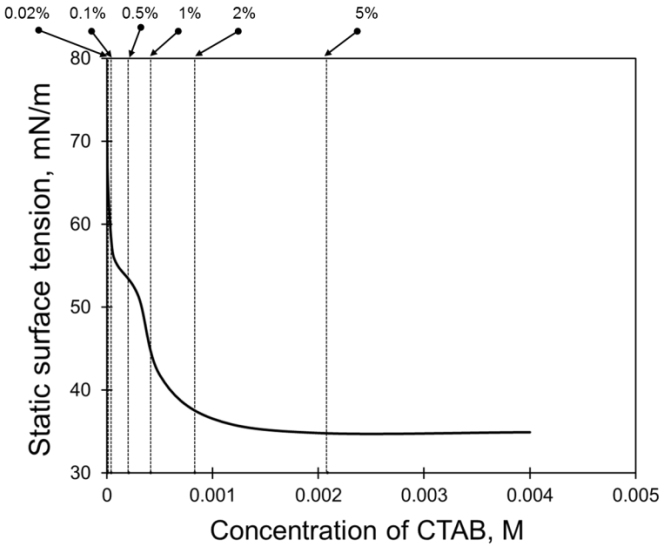

Fig. 4-31. Static surface tension of water depending on the CTAB concentration.

3.3.2 Structural properties of CNF sheet

Fig. 4-32 and Fig. 4-33 show the density and porosity of CNF sheets depending on addition level of CTAB surfactant, respectively. The density of CNF sheet was decreased continuously with an increase in the addition level of surfactant, significantly from 1% to 2% dosage. The highly porous CNF sheet could be produced by addition of surfactant in suspension. The minimum density and maximum porosity of surfactant-added CNF sheet were 0.13 g/cm^3 and 91%, respectively. The change in porosity of CNF sheet may be relevant to surface tension of water. It is considered that the decreased surface tension of water prevented the nanofibrils from shrinkage during drying, resulting in the highly porous sheet. Shrinkage is difficult to occur when the surface tension of water is low because the degree of Campbell effect is weak. The specific surface area of freeze dried CNF sheets depending on the addition level of surfactant was evaluated by BET method (Fig. 4-34). The specific surface area of surfactant-added CNF sheet was lower as compared with untreated CNF sheet despite the sheet porosity was increased. It is inferred that the large pores were formed in CNF sheet by addition of surfactant so the specific surface area was decreased.

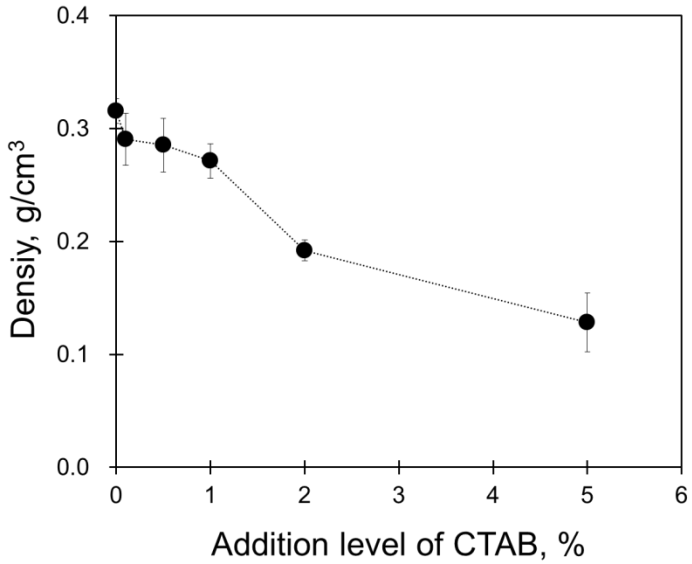

Fig. 4-32. Density of CNF sheets depending on addition level of surfactant.

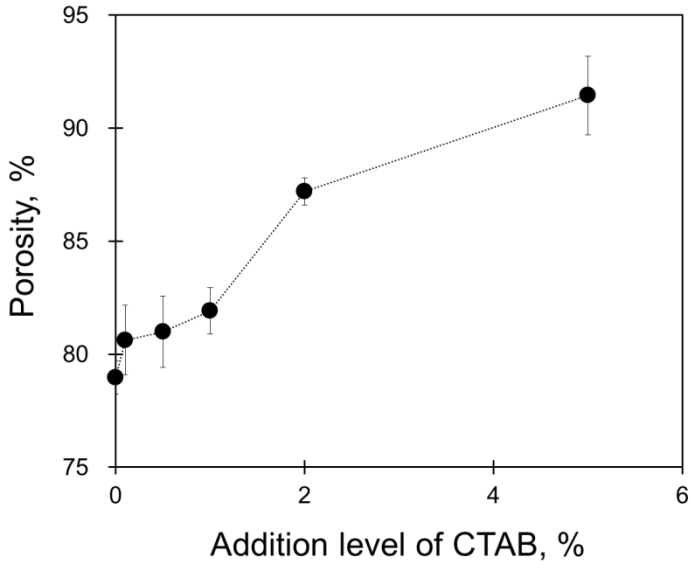

Fig. 4-33. Porosity of CNF sheets depending on addition level of surfactant.

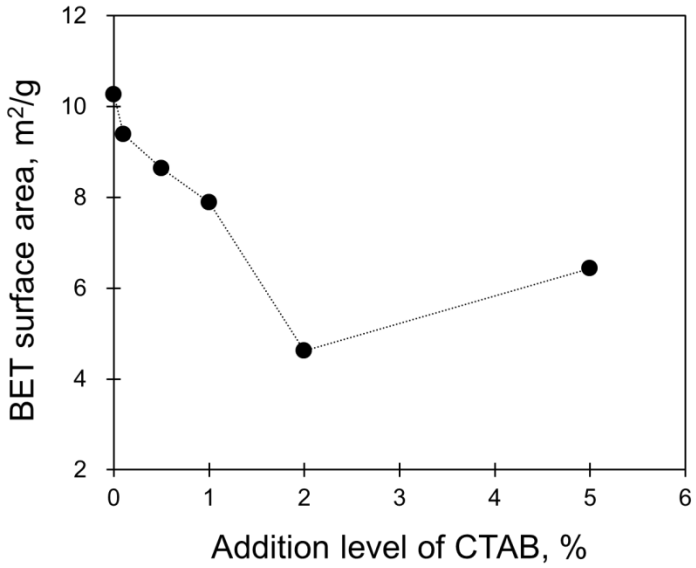

Fig. 4-34. BET specific surface area of CNF sheets depending on addition level of surfactant.

3.3.3 Tensile properties of CNF sheet

The tensile properties of CNF sheet were evaluated. Fig. 4-35 and Fig. 4-36 show the elastic modulus and tensile stress at break of surfactant-added CNF sheet. Both elastic modulus and tensile stress at break showed the similar tendency each other that they were decreased with an increase in addition level of surfactant. This may be because of the density and hydrophobic part of surfactant. As shown in Fig. 4-32, the density of CNF sheet was decreased by the addition of surfactant. The bonding strength between nanofibrils decreased significantly when the addition level of surfactant was 2%.

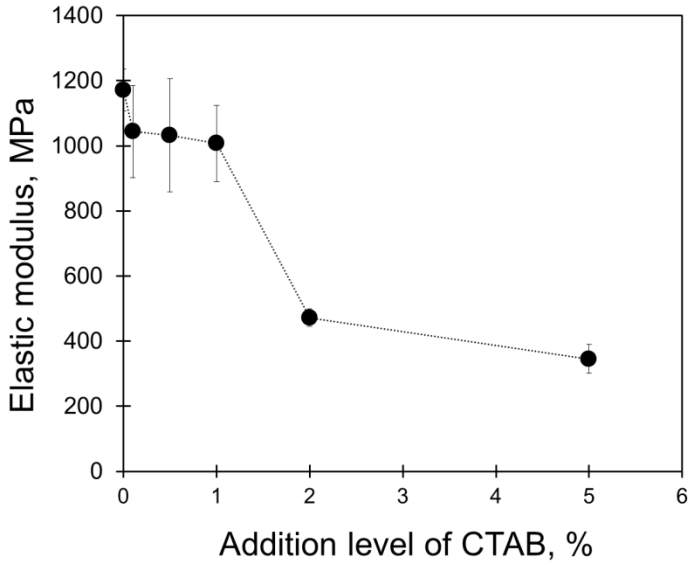

Fig. 4-35. Elastic modulus of CNF sheets depending on addition level of surfactant.

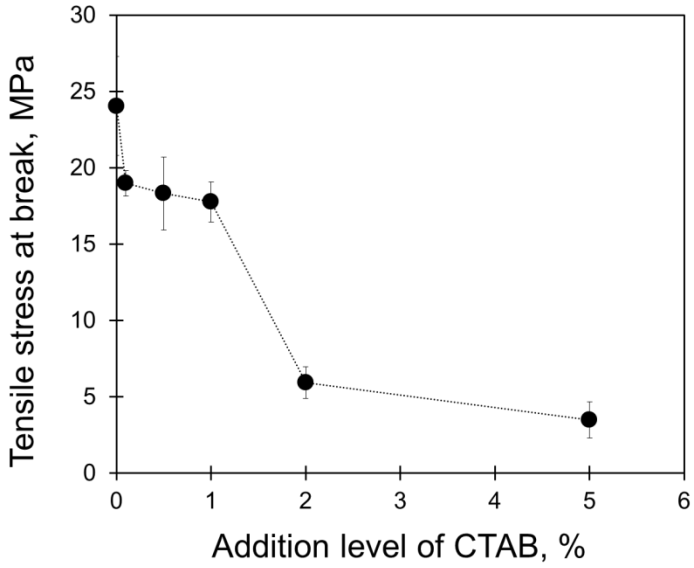

Fig. 4-36. Tensile stress at break of CNF sheets depending on addition level of surfactant.

4. Summary

The surface modification of CNF was conducted by carboxymethylation and TEMPO-mediated oxidation, resulting in the increase in surface negative charge of CNF. The substitution degree of carboxyl group was increased with an increase in reaction time or addition amount of oxidizing agent in TEMPO-mediated oxidation. The dewatering time and viscosity of carboxymethylated CNF suspension was increased because the modified nanofibrils had the smaller size in width and well dispersed in water due to increased electrostatic repulsion than untreated CNF suspension. Transparent film and dense sheet were obtained with carboxymethylated CNF and TEMPO-oxidized CNF. The light transmittance of surface modified CNF film was increased up to approximately 90%. The porosity of CNF sheets ranged from 56% to 85%.

CNF was flocculated by addition of salt, and the impact on the network strength and dewatering ability of the suspension was investigated. Sodium chloride and calcium chloride solutions of different concentrations were used to vary the ionic strength in the CNF suspension. Because of adsorption of cationic electrolyte (Na^+ or Ca^{2+}) and compression of the electrical double layer, aggregation of CNF occurred, resulting in rapid sedimentation of CNF. The flocculation and sedimentation rate were influenced by the type and concentration of salt. When the rheological properties of CNF suspension were measured with an oscillatory rheometer, the storage modulus and yield stress of the CNF suspension increased with an increase in the concentration of the salt solution. Higher yield stress could be achieved when salt with bivalent cations was added. Microrheology measurements based on the

dynamic light scattering technique represent a simple and useful method for investigating the rheological properties of CNF suspension. The microrheology measurements demonstrated a similar tendency in comparison with the oscillatory rheometer. The network structure of the CNF suspension could be changed easily by addition of salt due to aggregation.

The dewatering ability of the CNF suspension was affected by the zeta potential of the CNF when the salt was added. Bivalent cations with higher ionic strength were more effective for drainage of the CNF suspension than monovalent cations. The change in surface tension of water in CNF suspension also influence on the dewatering ability significantly. The total drained water content as well as the drainage rate was increased by adding the surfactant.

The structural properties of freeze dried CNF sheet were affected by flocculation of nanofibilrs and decreased surface tension of water. When the CNF was aggregated a little, the porosity of CNF sheet was increased. However, the excessive flocculation by bivalent ions with high concentration decreased the porosity of CNF sheet. The highly porous sheet could be prepared by decreasing the surface tension of water. The maximum porosity of CNF sheet was approximately 91%. The bonding strength between nanofibrils was decreased by addition of surfactant because of the formed porous structure.

Chapter 5

Applicability of CNF-contained Porous Sheet

1. Introduction

The porous CNF sheet has a potential as filter media, separator of secondary lithium-ion batteries, substrate for biocomposites, etc. In case of filter media, for example, the end use of porous CNF sheet may be changed depending on its pore characteristics.

Most filter media for both air and water filtration have been mainly composed of synthetic fibers such as polypropylene (PP), polyethylene (PE), polyethylene terephthalate (PET) (Lim and Huang 2007; Feng et al. 2014). Synthetic fibers form highly porous webs through both air- and wet-laid processes. Therefore, they are very advantageous as air filter media with a very low pressure drop (Wang et al. 2008). They also show low wettability because of low surface energy (Gotoh and Kikuchi 2005).

To increase filtration efficiency, a great amount of research on the utilization of nanofibers has been conducted. Filter media with nanofibers is efficient to remove substances of very small size because they form small pores and have high specific surface areas (Barhate and Ramakrishna 2007). The high specific surface area of filter media is beneficial to filtration because of improved absorption and retention of small particles (Guibo et al. 2012). Two widely used methods to produce nanofibers for filter media application are electrospinning (Barhate et al. 2006; Bjorge et al. 2009; Zhang et al. 2010) and melt blown (Dutton 2008; Uppal et al. 2013) processes. However, they have several disadvantages, such as the low production rate and low strength of the produced fiber web (Ward 2005). An additional problem with these

plastic-based products is their non-biodegradability, because most of the starting materials are petrochemical polymers (Huang et al. 2003). Large amounts of hazardous vapors are also emitted during the electrospinning process, because organic solvents are required to dissolve the polymer (Podgórski et al. 2006).

In contrast, cellulose is a natural organic polymer mainly obtained from plants. It is an environmentally friendly material because it is biodegradable and its production is sustainable (Klemm et al. 2006). In addition, cellulose-based nanofibers, called cellulose nanofibrils (CNF), can be obtained by the mechanical shearing action of natural pulp fibers (Abe et al. 2007; Zimmermann et al. 2004). CNF is less than 100 nm in width and has a high mechanical strength (Iwamoto et al. 2005; Janardhnan and Sain 2006; López-Rubio et al. 2007) and a high specific surface area. Therefore, the porous substance made of cellulose fibers and CNF has the potential to provide environmentally friendly high-strength products with filtration applications.

The preparation of porous products and the control of their pore characteristics should be preferentially conducted. Because the use of only cellulose pulp fibers forms relatively large pores due to their micro-scale dimensions in width, the utilization of CNF are expected to allow the control of pore characteristics in porous products and the improvement in mechanical properties as well. In the papermaking industry, for example, research on the use of CNF with cellulose pulp fibers has been conducted (Ahola et al. 2008; Eriksen et al. 2008; González et al. 2012). However, these studies have focused on improvements in paper strength. Moreover, the addition level of

CNF was low because of the drainage problem (Taipale et al. 2010).

The main objectives of this chapter are to prepare porous sheets with CNF and to investigate the sheet characteristics for the applicability. Porous sheets were prepared by mixing natural pulp fibers or synthetic fiber with CNF. Commercial hardwood and softwood bleached kraft pulp were used as an eco-friendly raw material. Polyethylene terephthalate (PET) was also selected as a representative synthetic fiber. It was attempted to change the pore structure in the sheet using CNF and varying its mixing ratio. To make the sheet uniformly and rapidly, the wet-laid forming method using a handsheet former was adapted. The porous sheets with the different fiber types and the CNF mixing ratio were dried by cylinder and freeze dryer. The changes in the pore structure, mechanical strength, and filtration performance of porous sheets were evaluated. The solvent exchange and supercritical drying were also used to prepare porous sheets. The effects of sheet grammage and layer structure on structural properties, mechanical properties, and filtration performance were investigated.

2. Materials and Methods

2.1 Materials

A commercial HEPA filter media (80±0.3 g/m^2) without pleating was supplied from CLEAN TECH KOREA Co., Ltd. The thickness and density of the HEPA filter were 316±2.7 μm and 0.25±0.001 g/cm^3, respectively. Three types of fibers, commercial hardwood and softwood bleached kraft pulps (HwBKP and SwBKP) as natural pulp fibers and polyethylene terephthalate (PET) as a synthetic fiber, were the main fibers used to prepare porous sheets. HwBKP and SwBKP were beaten to 450 mL CSF (Canadian Standard Freeness) and 700 mL CSF using a laboratory beater. According to measurements using Kajaani FiberLab (Metso Automation Inc., Finland), the average length-weighted fiber lengths (fiber width) of the SwBKP fibers and the HwBKP fibers were 2.14 mm (29 μm) and 0.54 mm (15 μm), respectively. PET fibers, cut to a constant length of 3 mm, were supplied by Huvis Co., Korea. The width of the PET fibers was 9.9±1.3 μm according to image analysis using the Image-Pro Plus software. The PET fibers were treated with nonionic surfactant to disperse well in the water. PET fibers were disintegrated in deionized water a using laboratory disintegrator to a consistency of 2%. To prepare the cellulose nanofibrils (CNF), commercial hardwood bleached kraft pulp was used. The 2% beaten hardwood pulp suspension was passed repeatedly through a grinder (Super Masscolloider, Masuko Sangyo Co., Ltd, Japan). Cationic polyacrylamide (+1.5±0.1 meq/g) with a Mw of 2,000,000 g/mol (CPAM, Percol 63, BASF) was used for the retention of cellulose nanofibrils during sheet forming. CPAM (0.5%) solution was prepared with deionized water.

2.2 Sheet forming conditions

2.2.1 Cylinder and freeze dried sheets

The final consistency of four types of suspensions (SwBKP, HwBKP, PET, and CNF) was adjusted to 0.5% with deionized water. Each main fiber suspension of SwBKP, HwBKP, or PET was mixed with CNF suspension with a different mixing ratio. The mixing ratio of CNF suspension was varied from 0% to 50%. With increases in the CNF ratio, the mixing ratio of other fibers decreased from 100% to 50%. The mixed fiber suspension was stirred at 550 rpm for 1 min, and then 0.5wt% of CPAM was added based on the oven dried CNF weight. After the addition of CPAM, the suspension was stirred for 1 min at 800 rpm. Porous sheets were prepared using a laboratory rectangular handsheet former. In the case of pulp/CNF suspension, a 200-mesh wire was used because of the slow dewatering. When the PET was mixed with CNF, a 400-mesh wire was inserted in the handsheet former. After stirring and dewatering of the mixed suspension, the wet sheet formed onto the wire was couched. The wet sheet between blotting papers was pressed for 2 min under 3.5 bar and dried using a cylinder dryer or freeze dryer. The temperature during cylinder drying was 120°C. Freeze drying was conducted at -81°C and 5 mTorr. The grammage of dried sheets was adjusted to a similar level, 36±1 g/m^2. After drying the sheets, the CNF content of sheet was calculated according to Equation (1).

$$\text{CNF content of sheet, \%} = \frac{W_s - (W_f \times R_f)}{W_s} \times 100 \qquad \text{Eq. (1)}$$

where, W_s is the weight of dry sheet, and W_f and R_f are the dry weight and the retention rate of the main fibers (PET or SwBKP or HwBKP), respectively. The retention rate of the main fibers was determined through a preliminary retention test carried out with a 100% main fiber suspension using a handsheet former equipped with a certain mesh wire (200-mesh wire for natural pulp fibers, 400-mesh wire for PET fibers).

2.2.2 Solvent exchange and supercritical dried sheets

The porous sheets were also prepared with the different grammage and layer composition (1-layered and 2-layered structure) by using two drying methods: solvent exchange drying and supercritical drying. The grammage was controlled by varying the fibers content. When preparing 1-layered sheet, the CNF and SwBKP suspension were mixed each other with the ratio of 1:1 on the total fibers weight. The mixed suspension was diluted to 0.2% with deionized water, and then was sonicated for 1 min. The wet sheet was prepared by vacuum filtration. In the case of 2-layered sheet, the bottom layer and top layer were SwBKP layer and CNF layer, respectively. The weight ratio of each layer on total sheet weight was the same. Thus, the total grammage was the same with 1-layered sheet. The wet sheets were dried by solvent exchange or supercritical drying. The solvent exchange drying was conducted by dipping the porous sheets in solvents (ethanol, acetone, and hexane). The supercritical drying was carried out with carbon dioxide (CO_2) gas at 50°C under 100 bars.

2.3 Structural properties of sheet

The apparent density (ρ) of the dried sheet was calculated using its dry weight and volume. The volume of the sheet was obtained by multiplying the area by the thickness, which was measured with a micrometer (L&W Co., Sweden). The apparent porosity of the sheet was determined from Equation (2) by adapting the density of cellulose (1.5 g/cm^3 for CNF and pulp fibers) and PET (1.38 g/cm^3).

$$\text{Apparent porosity, \%} = \left(1 - \frac{\rho}{a \cdot \rho_{CNF} + b \cdot \rho_{pulp\ or\ PET}}\right) \times 100 \qquad \text{Eq. (2)}$$

where, *a* and *b* are the weight fractions of actual retained CNF and pulp fibers or PET in the sheet, respectively.

2.4 Pore characteristics of sheet

The air permeability of the sheet was evaluated using a Gurley densometer (Gurley Precision Instruments, Inc., USA). The time required for 300 cc air to flow through the sheet was measured as seconds.

Sheet pore properties were also evaluated by mercury porosimetry using the AutoPore IV 9500 (Micromeritics Instrument Co., USA). This analysis method is based on the mercury intrusion into the pore by applying the controlled pressure to a sheet. The pressure required to intrude mercury into the sheet pores is inversely proportional to the pore size. The theory of

mercury porosimetry is based on a cylindrical pore model. The average pore diameter (D_m) is calculated as following Equations (3) and (4):

$$V = \frac{\pi \cdot D^2 \cdot L}{4} = \frac{A \cdot D}{4} \quad \cdots\cdots \quad A = \pi \cdot D \cdot L \qquad \text{Eq. (3)}$$

$$D_m = \frac{4 \cdot V_{total}}{A_{total}} \qquad \text{Eq. (4)}$$

where, V_{total} and A_{total} are the total specific intrusion volume of mercury and the total cumulative area, respectively. The pressure ranged from 0.54 psia to 4.45 psia. The average pore diameter was calculated as a result.

2.5 Tensile properties of sheet

The tensile properties of the sheets were evaluated using a Universal Testing Machine (Instron Co., USA). The width of specimen and the measurement span were 15 mm and 50 mm, respectively. The strain rate during measurement was 5 mm/min. The elastic modulus, tensile stress and strain at break were obtained from a stress-strain curve.

2.6 Cross-section observation

The specimen for cross-sectional observation was prepared by grinding and polishing after impregnating the sheet in a mixture of epoxy resin and hardener (25:3 w/w). The bubbles in the mixture were removed under vacuum condition (-0.99 bar) for 8 min and then the sample was dried for over 24 hours. Grinding and polishing with sand-paper and diamond particles were carried out using a LaboPol-5 (Struers). Cross-sectional images of porous sheets were observed with a field-emission scanning electron microscope (FE-SEM, AURIGA, Carl Zeiss, Germany). The specimen was coated with platinum with a sputter coater (BAL-TEC SCD 005). The accelerating voltage during image scanning was 10 – 15 kV. The BSE (back scattering electron) mode was used.

2.7 Filtration performance of porous sheet

The filtration performance, filtration efficiency and pressure drop, of a porous sheet was evaluated by using an Automated filter tester (AFT). In the case of freeze dried sheets, model 8130 (TSI Inc.) equipment was used. The maximum value of measuring efficiency in this equipment is 99.999% (five 9's). Polydisperse NaCl particles with a mean diameter of 0.26 μm were used as a filtration aerosol. A light scattering photometer was used for particle detection. The filtration performance of the solvent exchanged or supercritical dried sheets were evaluated by model 3160 (TSI Inc.) equipment. The measurable value of filtration efficiency is 99.999999% (eight 9's). The monodisperse NaCl particles were used.

3. Results and discussion

3.1. Properties of CNF-contained porous sheets depending on preparation conditions: cylinder and freeze dried sheets

3.1.1 Retained CNF content of sheet

Fig. 5-1 shows the retention of CNF in the dried sheet depending on the mixed fiber type and the addition level of CNF in the mixed suspension. Although the CNF ratio in the mixed suspension varied from 0% to 50% at intervals of 10%, the actual retained amount of CNF in the dried sheet was reduced but had a linear relationship for all fiber combinations. The PET/CNF combination showed a higher retention compared to the SwBKP/CNF combination because a fine mesh wire (400-mesh) was used in the sheet forming process. When the same mesh wire (200-mesh) was used in the pulp/CNF combinations, it was possible to retain a higher amount of CNF when mixed with HwBKP. Hardwood fibers could form a more compact network structure because of their smaller size than softwood fibers. As hardwood fibers, as well as CNF, have high water holding capacities (Hii et al. 2012), the high mixing amount containing greater than 40% of CNF caused drainage problems during the sheet forming process. Therefore, it was difficult to prepare uniform sheets with a CNF amount greater than 26% in the case of HwBKP mixing.

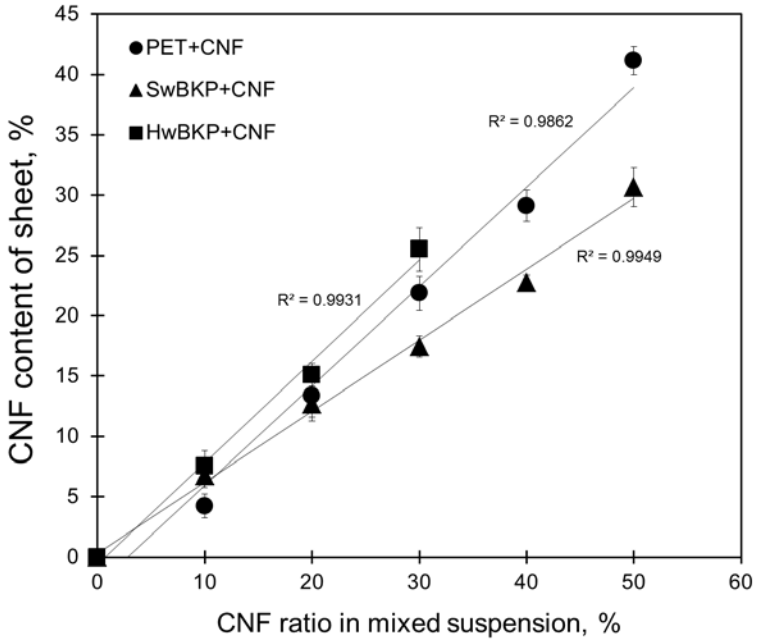

Fig. 5-1. Retained CNF content of the dried sheet.

3.1.2 Thickness of sheets

The thickness of porous sheets with CNF is shown in Fig. 5-2. For all three combinations and both drying conditions, the sheet thickness decreased linearly with an increase in the CNF content. The PET/CNF combination showed the greatest sheet thickness because of the large width of PET fibers. The reduction rate in thickness was also higher with increases in CNF content. There was little difference in thickness between cylinder and freeze drying conditions for the PET/CNF combination with a small amount of CNF. As the CNF ratio increased, freeze dried sheets showed greater thickness compared to cylinder dried sheets. SwBKP/CNF sheets were thicker than HwBKP/CNF sheets because of the large size of softwood fibers. The thickness of the sheets could be controlled from 61 μm to 173 μm by the different mixing combinations and drying conditions.

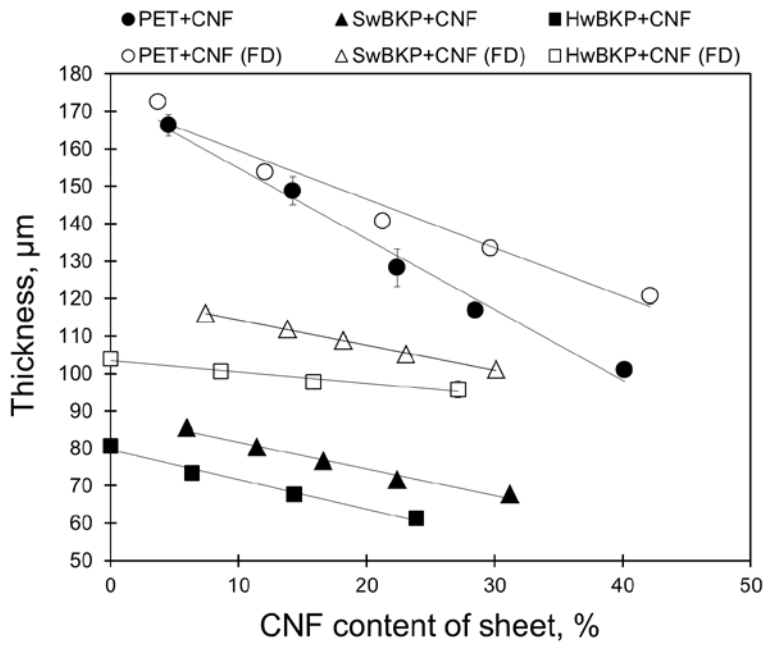

Fig. 5-2. Thickness of sheet made of PET/CNF or pulp/CNF combinations.

3.1.3 Cross-section of sheets

Fig. 5-3 shows the cross-sectional images of freeze dried sheets observed with FE-SEM. Figs. 5-3 (a), (b) and (c) show sheets with PET/CNF, SwBKP/CNF and HwBKP/CNF combinations, respectively. PET fibers with a circle shape and the laminar (nanopaper) structure of nanofibrils were observed. It has been previously reported that freeze drying generates an aggregation of nanofibrils, resulting in a plate-like structure (Deng et al. 2009; Peng et al. 2012). Small and large pores were formed between PET fibers and nanofibrils. The SwBKP/CNF combination resulted in a denser sheet than the PET/CNF combination in Fig. 5-3 (b). The pores were formed between pulp fibers and a nanopaper structure. The HwBKP/CNF combination also showed a porous structure with the pores between hardwood fibers and nanofibrils. Although the CNF content was higher in the PET/CNF sheet than the pulp/CNF sheet, the bulkiest structure was formed in the PET/CNF combination.

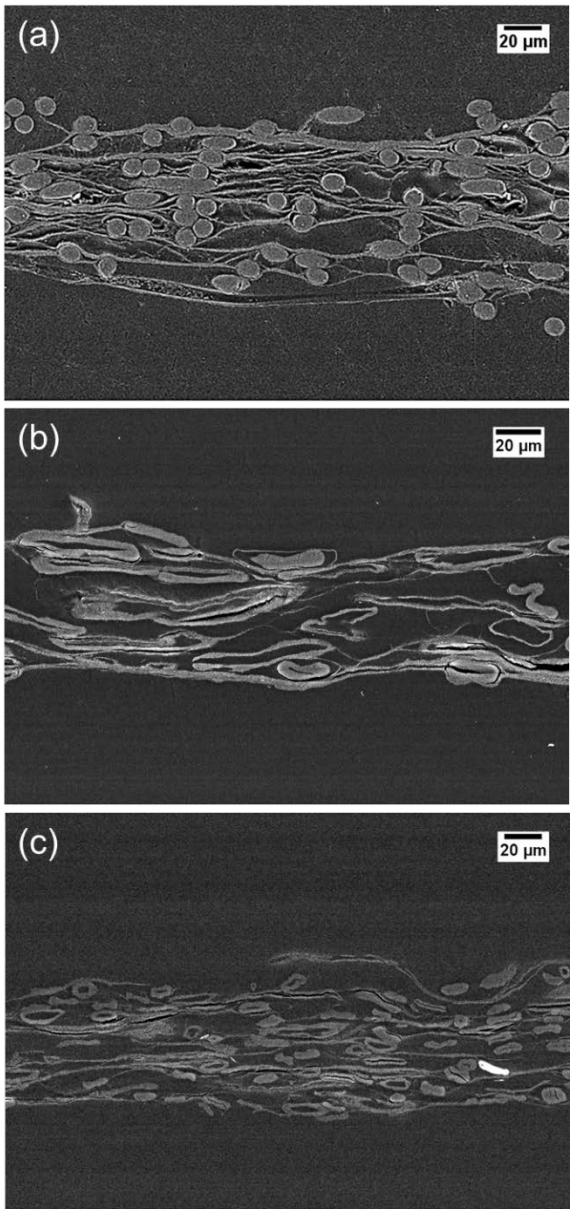

Fig. 5-3. Cross-sectional images of freeze dried sheets with (a) PET/CNF (42.2% CNF), (b) SwBKP/CNF (30.1% CNF), and (c) HwBKP/CNF (27.1% CNF) combinations.

3.1.4 Apparent density and porosity

The apparent porosity of the sheets was plotted against its apparent density in Fig. 5-4. The density of sheets was ranged from 0.21 g/cm^3 to 0.58 g/cm^3 depending on the type of mixed fibers, CNF ratio, and drying conditions. The porosity of sheets decreased linearly with an increase in sheet density, resulting in a change from 61% to 85%. When the CNF in suspension was dried by heat, the capillary effect during drying caused hydrogen bonding and the aggregation of nanofibrils, resulting in a nanopaper sheet with low porosity (Ferrer et al. 2012; Henriksson et al. 2008; Nogi et al. 2009; Sim et al. 2015). Changes in the drying method increased CNF sheet porosity (Sehaqui et al. 2011b; Sim et al. 2015). Although the drying method had a small effect on PET/CNF sheet porosity, sheets with high porosity could be prepared by freeze drying in pulp/CNF combinations. There was an overlapped region of density and porosity between the SwBKP/CNF and HwBKP/CNF combinations despite the difference in mixed fiber dimensions, which may be due to different pore sizes at similar porosities. In the pulp/CNF combinations, the drying condition was the dominant factor underlying sheet porosity.

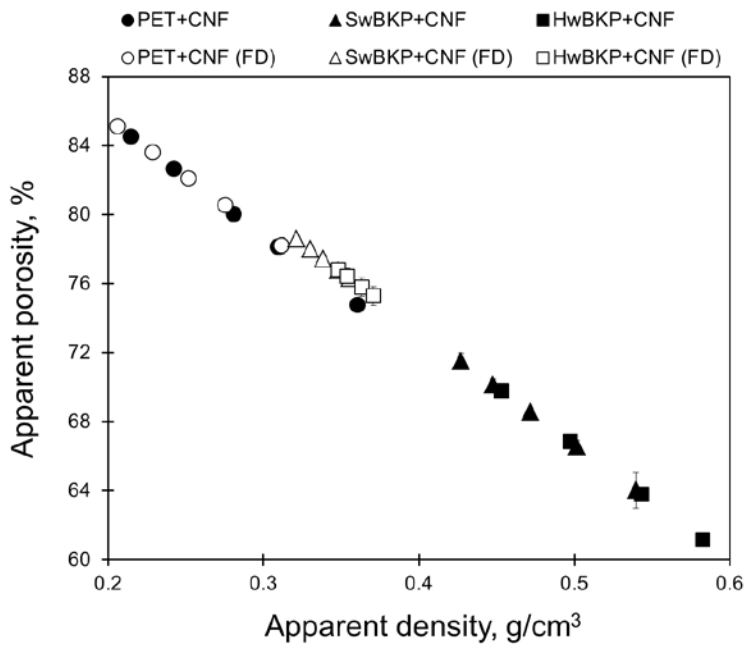

Fig. 5-4. Relationship between apparent density and porosity of sheets.

3.1.5 Air permeability

Fig. 5-5 displays the Gurley air permeability of the sheets depending on the mixing combinations, CNF ratio, and drying conditions. In measurements of air permeability using a Gurley densometer, the y-axis is the required time for 300 cc of air to flow through the sheet. Therefore, a large value means a sheet with low air permeance, that is, high air flow resistance. The air flow resistance increased exponentially with an increase in the CNF ratio for all preparation conditions. The HwBKP/CNF combination showed lower air permeability than SwBKP/CNF combination because of high hydrogen bonding by a large surface area. The pore closure reduces air permeation. The freeze dried pulp/CNF sheets showed a higher air permeability than cylinder dried sheets due to the low degree of hydrogen bonds during drying, whereas the differences between freeze dried and cylinder dried sheets for the PET/CNF combination were relatively small.

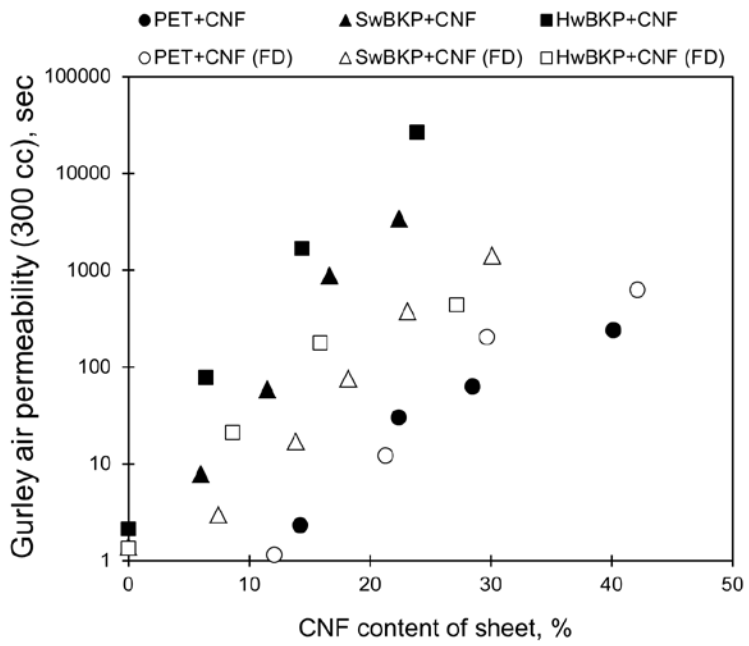

Fig. 5-5. Gurley air permeability of sheets made of PET/CNF or pulp/CNF combination.

3.1.6 Pore size

The average pore size of the sheets was evaluated by the mercury intrusion method. The average pore diameter of the sheets is depicted in Fig. 5-6. When the sheets were dried by freeze drying, all combinations showed an increase in the average pore size with an increase in the porosity (decrease in CNF content). The addition of CNF created small pores between nanofibrils and other fibers during freeze drying, and the small-sized CNF filled the large pores as well. In cylinder drying (Fig. 5-6 (b)), the average pore size of pulp/CNF combinations decreased with an increase in the porosity (decrease in CNF ratio), whereas the average pore size increased in the case of the PET/CNF combination. Cellulose fibers become close to each other by the Campbell effect during heat drying and form hydrogen bonds (Hubbe 2006). This Campbell effect is greater in the case of nanofibrils due to their high specific surface area (Sirviö 2008). It appears that small pores between nanofibrils and pulp fibers as well as between nanofibrils are closed by the Campbell effect, resulting in larger pores. The aggregation of fibers during drying may also create large pores between fibers. In contrast, the small pores were created between PET fibers and nanofibrils because hydrogen bonds were not formed between PET and CNF. Therefore, the average pore size of PET/CNF sheet decreased at the high amount of CNF condition during cylinder drying. The average pore diameter of the sheets could be controlled from 0.6 μm to 36.7 μm mainly depending on the type of mixed fibers and CNF content.

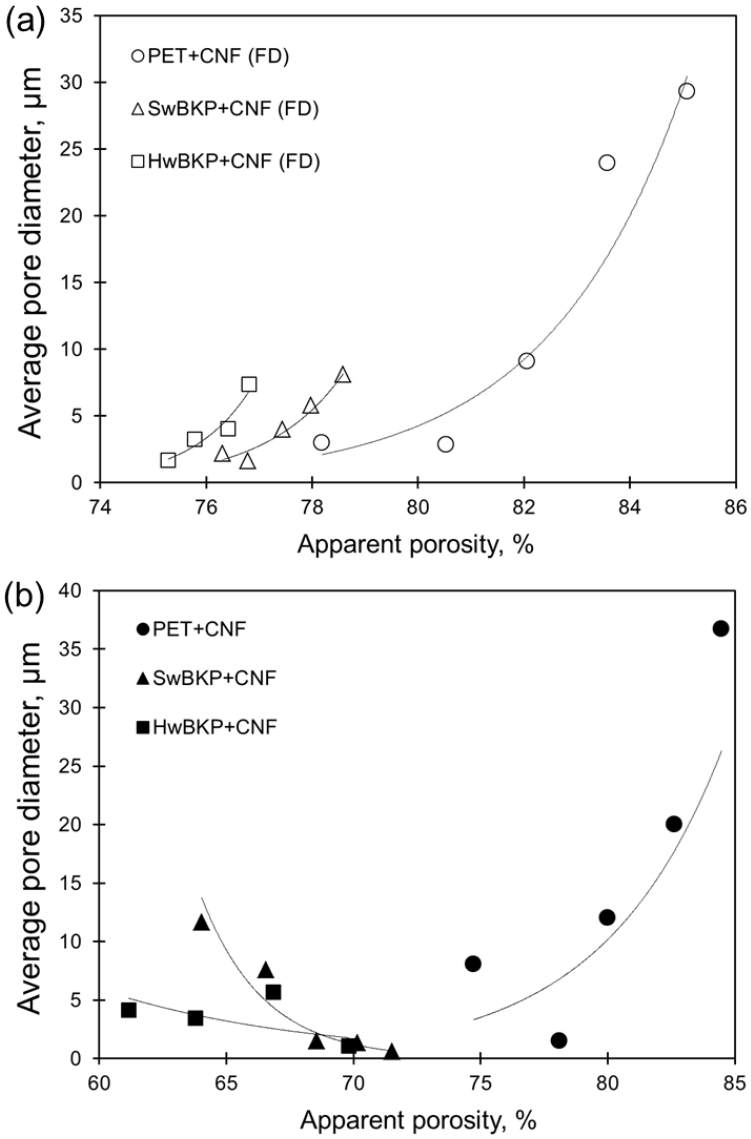

Fig. 5-6. Average pore diameter of (a) freeze dried and (b) cylinder dried sheets made of PET/CNF or pulp/CNF combination.

3.1.7 Tensile properties of sheets

The stress-strain behavior of the cylinder dried sheets with different mixing combinations is shown in Fig. 5-7. The elastic modulus, tensile stress and strain at break tended to increase with the CNF content for all three combinations except for the strain of SwBKP/CNF sheets at high CNF content. It is known that paper made of softwood pulp fiber has a higher tensile strength than paper made from hardwood pulp fiber (Fišerová et al. 2010). However, the sheet made of the HwBKP/CNF combination showed the highest elastic modulus and breaking tensile stress at the same addition amount of CNF in this study. This may be because of poor SwBKP sheet formation, the higher beating degree of hardwood fibers, and larger sites for hydrogen bonds between hardwood fibers and nanofibrils. Eriksen et al. (2008) investigated the effect of microfibrillated cellulose (MFC) addition on the strength of TMP paper, resulting in that 4% addition of MFC increased the tensile strength of sheet up to 34% compared to the sheet without MFC. It has also been reported that handsheets reinforced with 9% CNF showed approximately two-times greater tensile strength than the control (González et al. 2012). In this study, the breaking tensile stress increased up to near 50 MPa with HwBKP/CNF combination, which is approximately 3.3-times greater than in HwBKP sheets (0% CNF). The increase in CNF content had a significant effect on the tensile properties of sheet. The strain at break changed depending on the CNF content for each fiber combination. The strain of PET/CNF and HwBKP/CNF sheets increased continuously with the CNF content, whereas the strain of SwBKP/CNF sheets increased a little and them became constant with the CNF content. At low CNF content, the sheets,

including pulp fibers, showed higher strain than the PET/CNF combination. However, the strain at break of PET/CNF sheets became larger than that of pulp/CNF sheets at high CNF content over the 30% addition level. The maximum value of strain at break of cylinder dried PET/CNF sheets was approximately 7.5%.

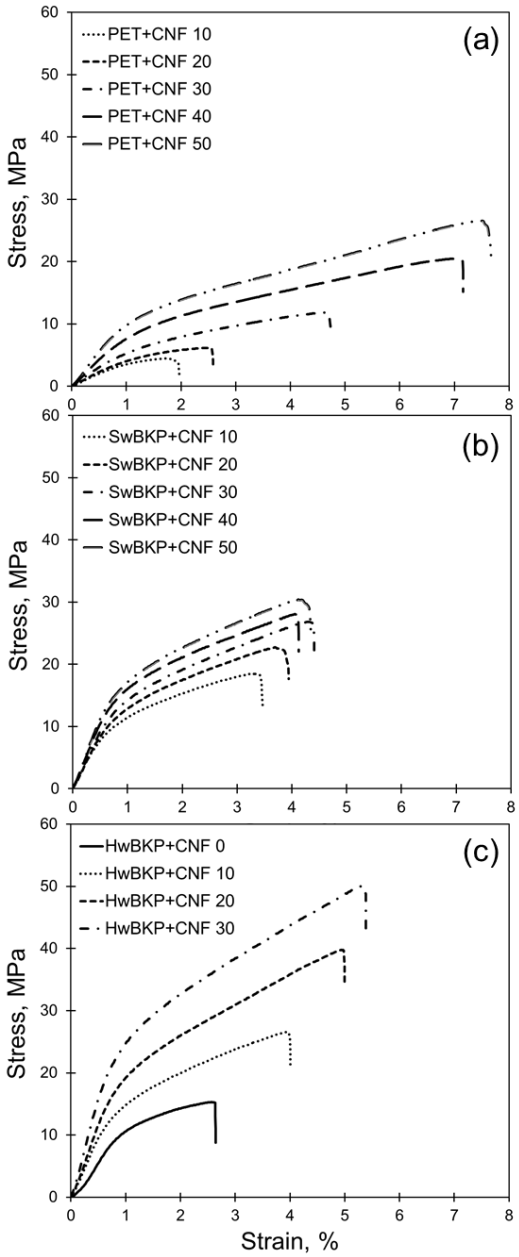

Fig. 5-7. Stress-strain curves of the sheets made of (a) PET/CNF, (b) SwBKP/CNF, and (c) HwBKP/CNF combinations with cylinder drying.

Fig. 5-8 shows the maximum tensile stress and elastic modulus of freeze dried sheets with the addition amount of CNF from 10% to 30%. The tensile stress of freeze dried sheets also increased with CNF content, similar to the cylinder drying condition. However, the freeze dried sheets showed a lower value of tensile stress than the cylinder dried sheets due to the inhibition of hydrogen bonding during drying. The HwBKP/CNF sheets showed the highest tensile stress among the preparation combinations. The elastic modulus of sheets had the same tendency with maximum tensile stress, which was improved by increasing the CNF content. The HwBKP/CNF sheet showed a high elastic modulus despite the small addition level of 10% CNF. The sheets with high mechanical strength such as elastic modulus, tensile stress and strain at break may be prepared by the addition of CNF. The mechanical strength of sheets was also significantly affected by the drying conditions.

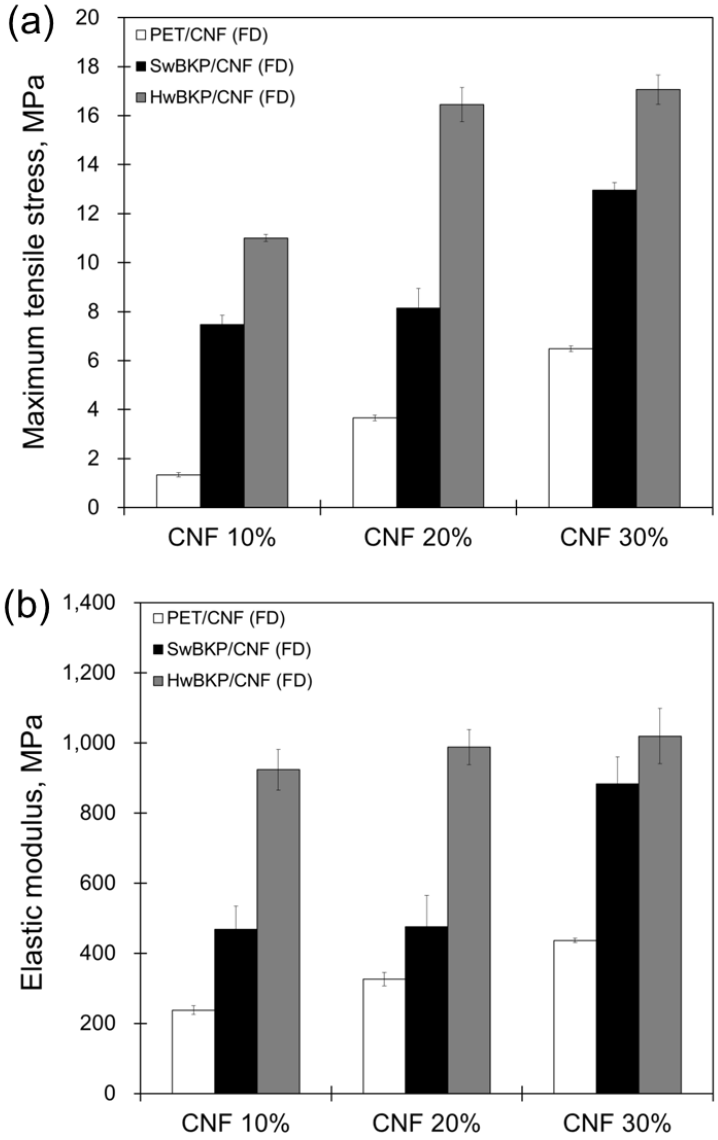

Fig. 5-8. Tensile properties of freeze dried sheets made of PET/CNF, SwBKP/CNF, and HwBKP/CNF combinations: (a) maximum tensile stress and (b) elastic modulus.

3.2 Properties of CNF-contained sheets depending on preparation conditions: solvent exchange and supercritical dried sheets

3.2.1 Structural properties of sheets

The thickness and density of commercial HEPA filter, solvent exchanged, and supercritical dried sheets were evaluated as shown in Fig. 5-9. The thickness of sheet was increased by increasing the sheet grammage for both solvent exchange and supercritical drying conditions. The supercritical dried sheet had the higher thickness compared with solvent exchanged sheet for the same grammage, resulting in the lower sheet density. In contrast to solvent exchanged sheet, the density of supercritical dried sheet was similar regardless of sheet grammage. This indicates that the structure of nanofibril network is maintained after supercritical drying without shrinkage. The thickness and density of sheet was also affected by layer structure. The supercritical dried sheet with 2-layer structure showed the higher thickness and lower density than 1-layered sheet for the same grammage.

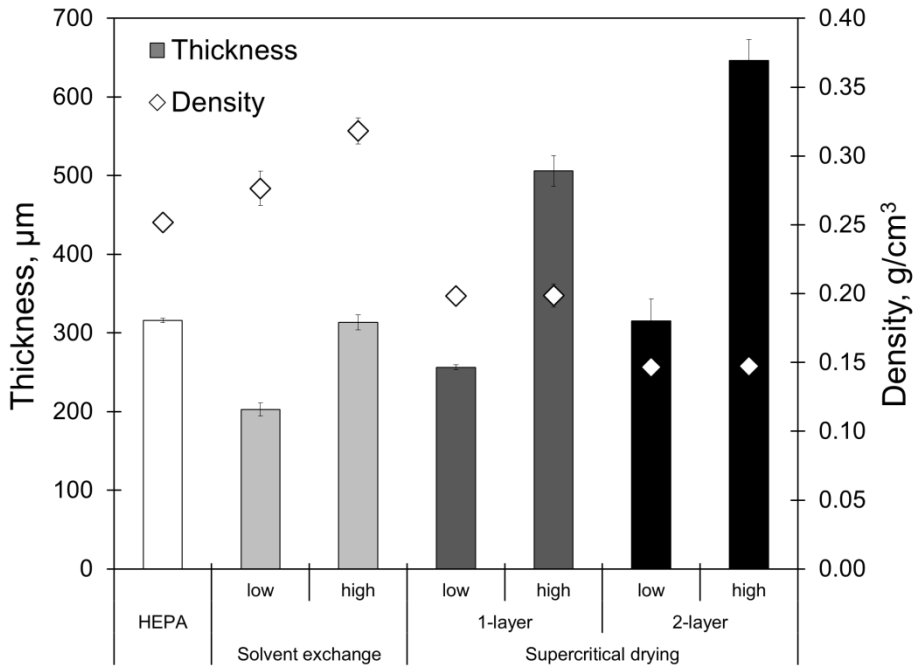

Fig. 5-9. Thickness and density of commercial HEPA filter, solvent exchanged, and supercritical dried sheets.

3.2.2 Tensile properties of sheets

Fig. 5-10 and Fig. 5-11 represent the stress-strain curves of solvent exchanged and supercritical dried sheets, respectively. The mechanical properties such as elastic modulus, stress and strain at break were increased a little by increasing the sheet grammage. For both solvent exchange and supercritical dried sheets, the stress and strain at break were greater significantly compared with commercial HEPA filter, whereas the elastic modulus was lower than HEPA filter. It is considered that the higher elastic modulus of commercial HEPA filter is derived from the binder between fibers. Although the both drying methods (solvent exchange and supercritical drying) inhibited the hydrogen bonds between cellulose nanofibrils, the stress and strain at break were superior to commercial HEPA filter. It may be due to the mechanical entanglement between nanofibrils, which has high aspect ratio. The solvent exchanged sheet showed the higher value of mechanical strength properties when compared to supercritical dried sheet for the same grammage (Fig. 5-12).

The mechanical properties of supercritical dried sheets depending on the grammage and layer structure were depicted in Fig. 5-13. The 2-layered sheet showed the lower mechanical strength than 1-layered sheet, except for strain at break. This may be because the bottom layer (SwBKP layer) contributed little to the sheet strength when supercritical drying was conducted.

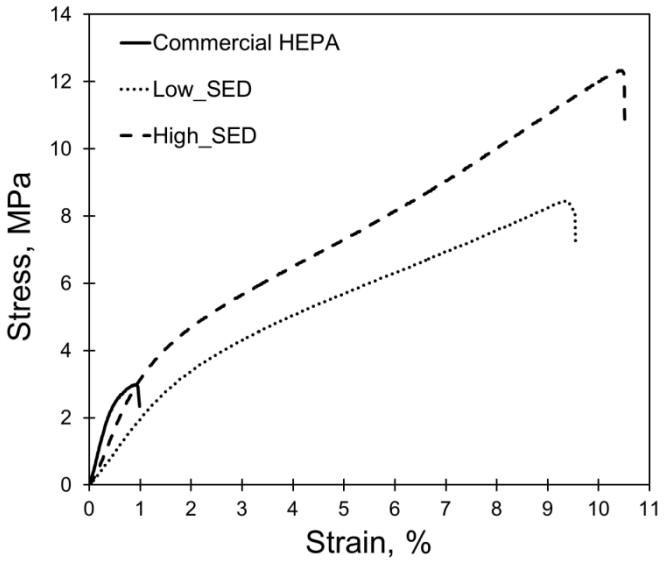

Fig. 5-10. Stress-strain curves of solvent exchange dried porous sheets.

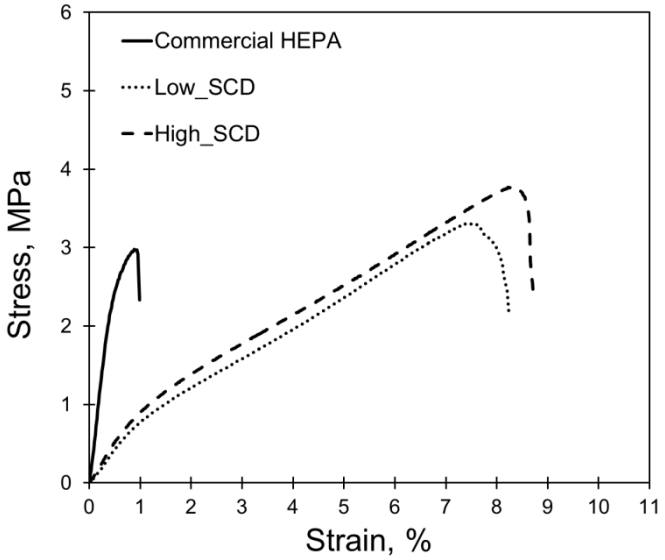

Fig. 5-11. Stress-strain curves of supercritical dried porous sheets.

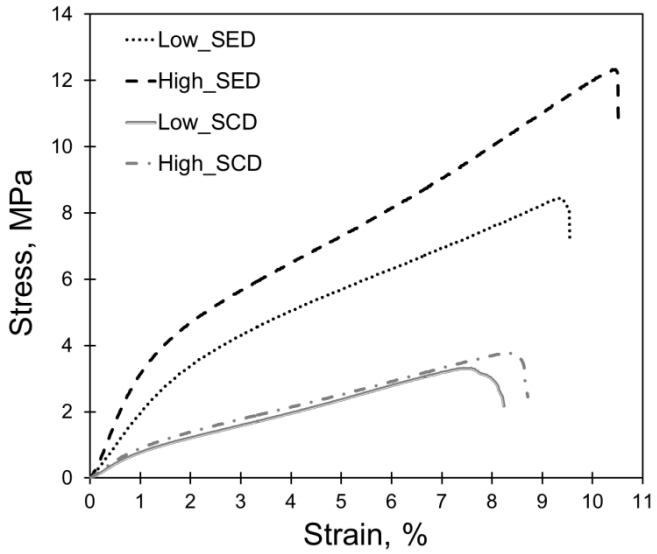

Fig. 5-12. Comparison of tensile properties between solvent exchange dried and .supercritical dried sheets.

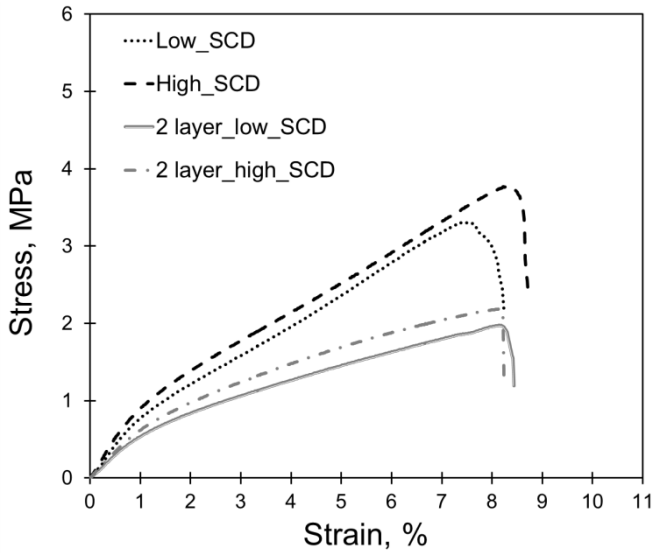

Fig. 5-13. Comparison of tensile properties of supercritical dried sheets depending on the layer composition.

3.3 Filtration performance

3.3.1 Characteristics of HEPA filter

3.3.1.1 Morphological properties

Prior to prepare and characterize the porous sheets by using CNF, the characteristics of a commercial HEPA filter were investigated. The commercial HEPA filter was composed of 3-layered structure (Fig. 5-14). The morphology of each layer of the commercial HEPA filter was observed by FE-SEM. Fig. 5-15 shows the surface images of the top-layer. The width distribution of fibers in top-layer was very broad. According to image analysis using an Image-Pro Plus software, the width of relatively larger fibers ranged from 1.2 μm to 7 μm. The width of nano-sized fiber was 88 nm. The middle-layer of commercial HEPA filter consisted of fibers, which have width ranged from 59 nm to 800 nm (Fig. 5-16). The average of fibers width was 166 nm. In the bottom-layer of commercial HEPA filter, the plate-like structure between fibers was observed (Fig. 5-17). It might be binder to bond fibers together because there was no chemical interaction between synthetic fibers, but only mechanical entanglement. The width of bottom-layer fibers ranged from 88 nm to 3.8 μm and the average valued was 466 nm.

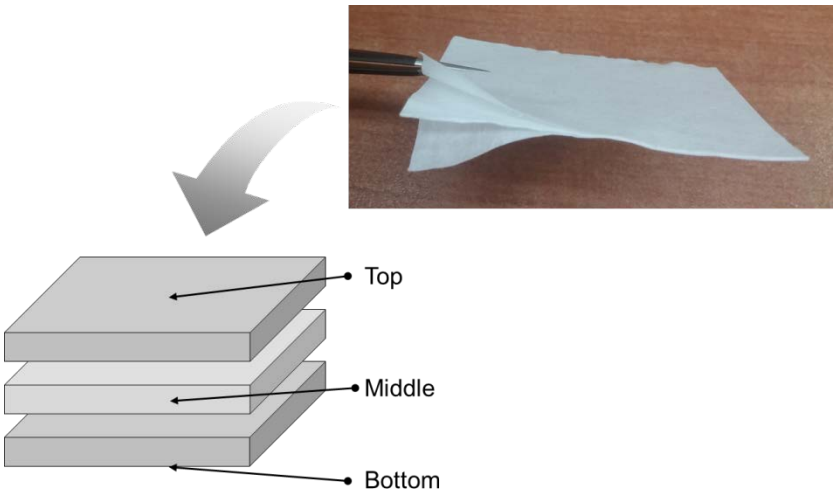

Fig. 5-14. Three layer structure of a commercial HEPA filter media.

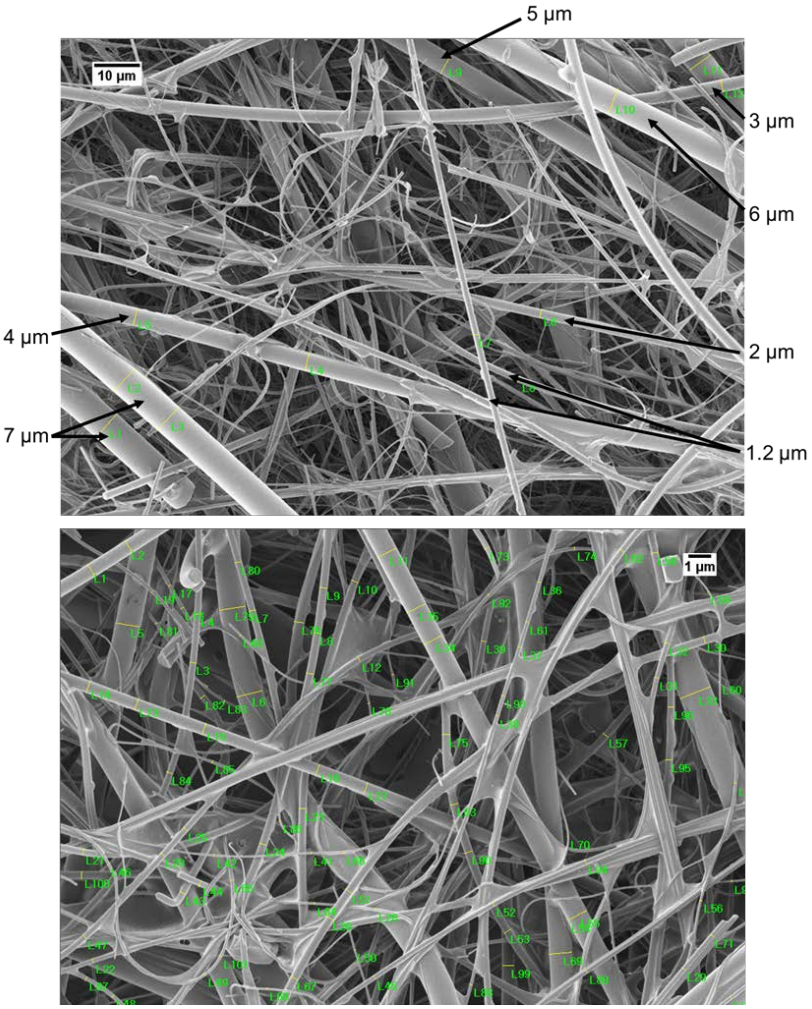

Fig. 5-15. FE-SME images of top-layer of the commercial HEPA filter.

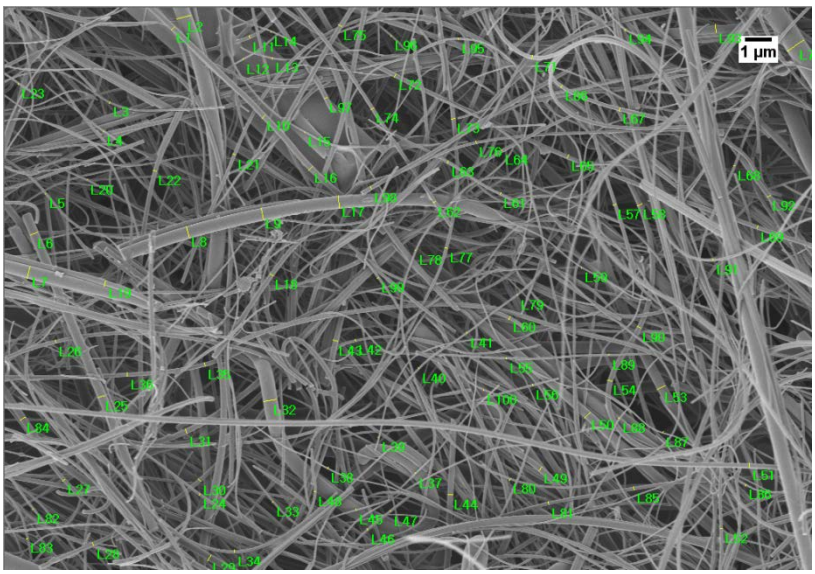

Fig. 5-16. FE-SME images of middle-layer of the commercial HEPA filter.

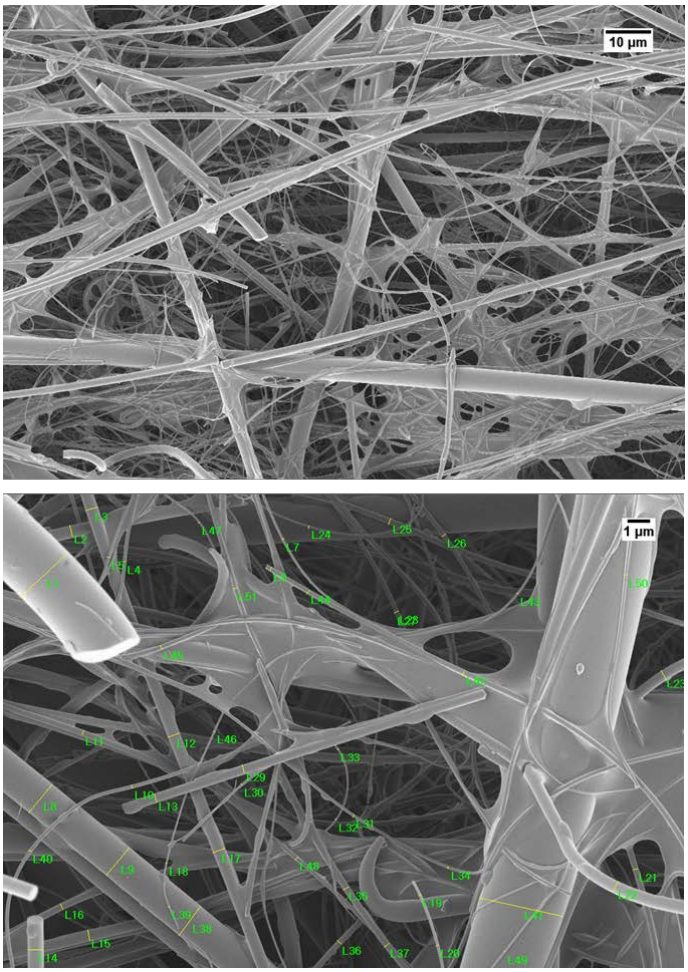

Fig. 5-17. FE-SME images of bottom-layer of the commercial HEPA filter.

3.3.1.2 Filtration performance of HEPA filter

Filtration efficiency and pressure drop of commercial HEPA filter were evaluated as shown in Fig. 5-18. The selected diameter of NaCl particles were 0.05, 0.1, 0.2, 0.25, 0.3, 0.4, 0.5, and 0.6 μm. The filtration efficiency of HEPA filter was decreased with the increase in particle size until 0.2 μm and then, increased again. The most penetrating particle size (MPPS) was 0.2 μm. However, the filtration efficiency for all the particles size was greater than 99.97%.

The three mechanisms for filtration of particles in fibrous media are inertial impaction, interception, and diffusion (Fig. 5-19). Large particles greater than 0.4 μm in diameter are mainly removed by interception and inertial impaction mechanisms, whereas small particles with a diameter less than 0.1 μm are captured in fibrous filters by the mechanism of diffusion due to their Brownian motion. It is known that filtration efficiency changes at a particle diameter of near 0.3 μm (between 0.1 and 0.4 μm) because particles near 0.3 μm are more difficult to capture than any other size (Kowalski et al. 1999). Particles from 0.1 μm to 0.4 μm size are too small to remove by interception and impaction and too large to remove by diffusion.

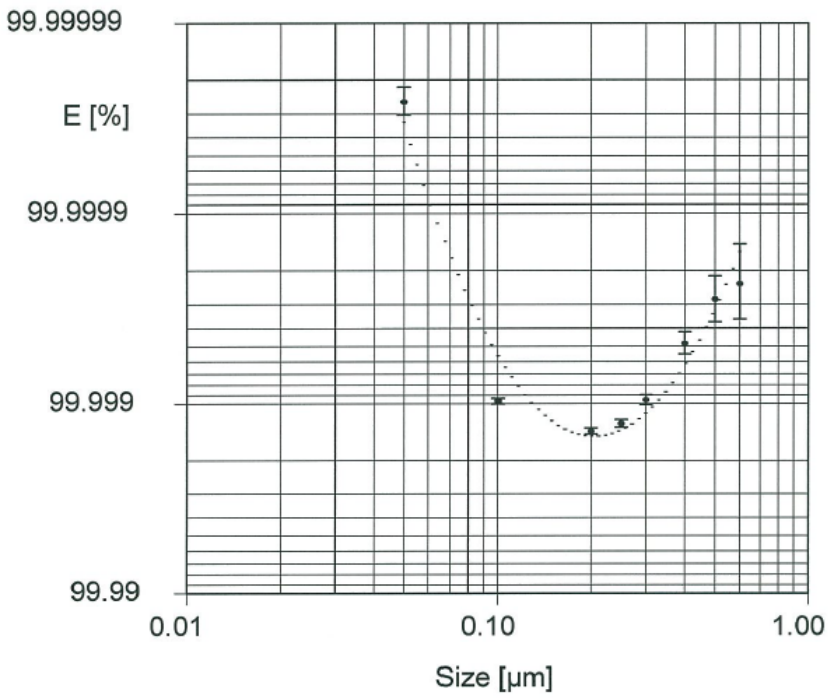

Fig. 5-18. Filtration efficiency of a commercial HEPA filter media at the different size of particles.

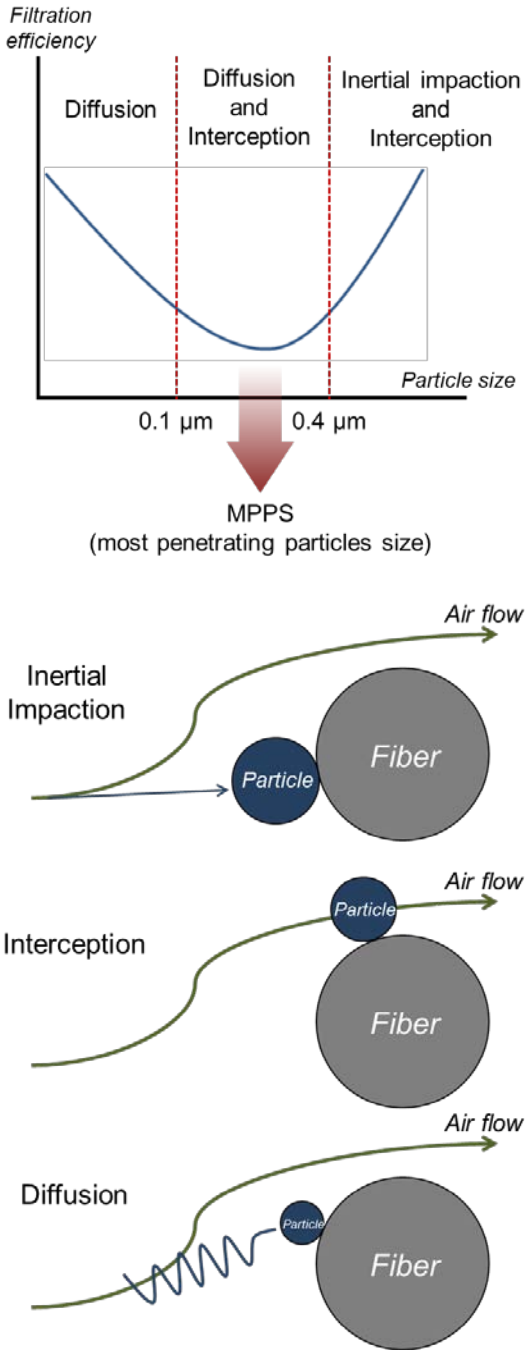

Fig. 5-19. Filtration mechanisms in air filter media.

3.3.1.3 Pore size distribution

The pore size distribution of commercial HEPA filter was evaluated by mercury porosimetry. Fig. 5-20 shows the log differential intrusion of mercury as a function of pore size of 3-ply HEPA filter. The pore size ranged from approximately 5 μm to 90 μm. The average pore size of 3-ply HEPA filter was 19.6 μm. The pore property of 2-ply filter media (middle and bottom layers) without top-layer was also evaluated (Fig. 5-21). The average pore size of 2-ply filter media was the smaller than that of 3-ply filter media, resulting in approximately 14.0 μm. This result has a good relationship to the Figs. 4-4 – 4.6, because the top-layer consisted of relatively larger fibers compared with middle and bottom layers.

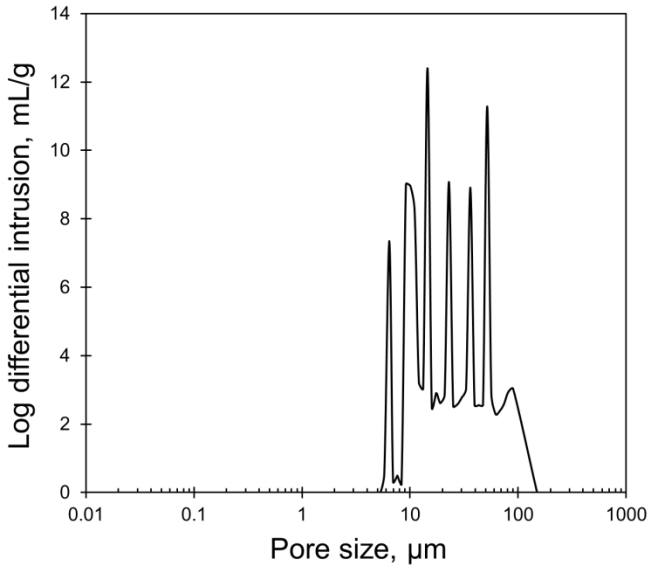

Fig. 5-20. Pore size distribution of a commercial HEPA filter (3-ply).

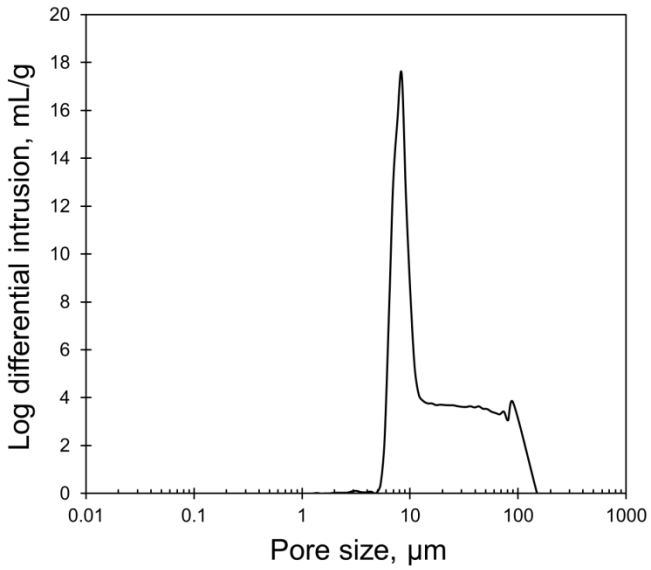

Fig. 5-21. Pore size distribution of a commercial HEPA filter without top layer (2-ply).

3.3.2 Filtration performance of freeze dried sheets

The filtration efficiency of freeze dried sheets was evaluated based on the average pore diameter of sheets (Fig. 5-22). The filtration efficiency decreased with an increase in the average pore diameter for all of mixing combinations. It changed suddenly at an average pore diameter of approximately 3 μm. Although the average pore size of sheet (0.6 – 3 μm) is larger than the average particle size (0.26 μm), high filtration efficiency could be achieved. This may be explained by filtration mechanism of particles in fibrous network structure (Yeh and Liu 1974) as already mentioned. The maximum filtration efficiency of 99.944% could be achieved with HwBKP/CNF combination sheet. It approaches the performance of HEPA (high efficiency particulate air) filters, which have a filtration efficiency of 99.97% for particles with a 0.3 μm size (Ahn et al. 2006). However, the pressure drop increased significantly with a decrease in the average pore diameter (Fig. 5-23). High pressure drops cause a clogging problem of filter media such that the service life of the filter is shortened. As shown in Fig. 5-24, there was a strong relationship between filtration efficiency and pressure drop of cellulose-based filter media. As the filtration efficiency increased, the pressure drop also increased. Therefore, further studies on the reduction in the pressure drop should be conducted to use a CNF-added porous sheet as filter media.

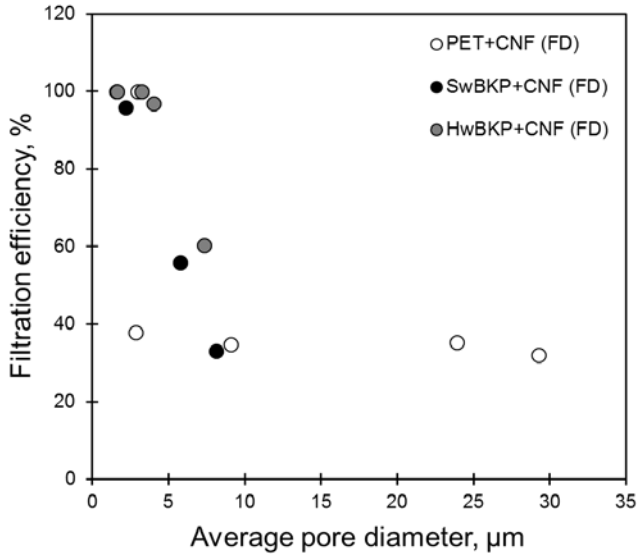

Fig. 5-22. Filtration efficiency of freeze dried porous sheets depending on the average pore diameter.

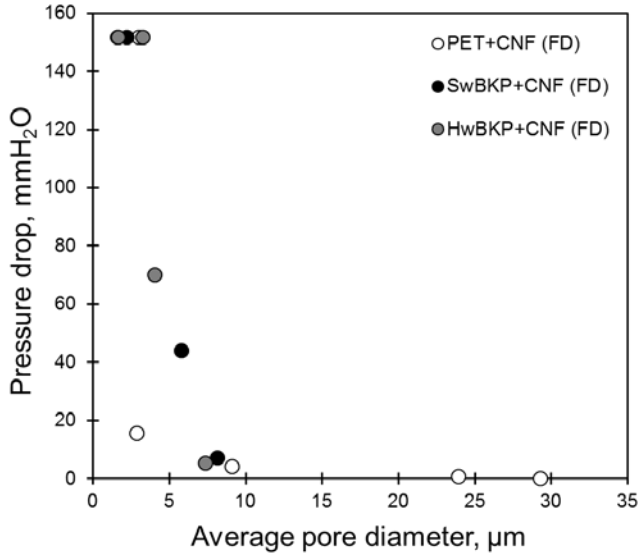

Fig. 5-23. Pressure drop of freeze dried porous sheets depending on the average pore diameter.

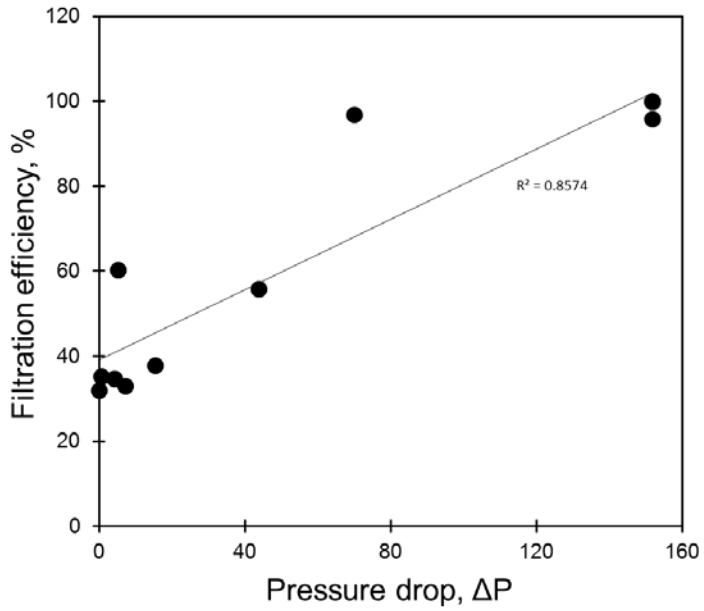

Fig. 5-24. Relationship between filtration efficiency and pressure drop of freeze dried porous sheets.

3.3.3 Filtration performance of solvent exchanged and supercritical dried sheets

The filtration efficiency of commercial HEPA filter, solvent exchanged and supercritical dried sheets were plotted in Fig. 5-25. The solvent exchange dried sheet showed the filtration efficiency of 99.762811%, which is lower than the criterion of HEPA filter (99.97%). When the supercritical drying was conducted, the filtration efficiency of porous sheets was greater than 99.97%. In supercritical dried sheets, the filtration efficiency was increased from 99.988179% to 99.991015% by increasing the sheet grammage. This may be because of the higher capacity to hold particles with high grammage. The 2-layered sheet showed the higher filtration efficiency (99.99514%) when compared to 1-layered sheet (99.991015%). It is considered that the layer with only CNF is efficient to remove particles due to the smaller pores than the layer with mixed fibers of CNF and SwBKP.

Although the solvent exchange and supercritical drying were adopted to inhibit hydrogen bonds and to maintain the structure of nanofibril network, the pressure drop of porous sheet was still high (Fig. 5-26). It may be due to the very small pores formed by nanofibrils (Fig. 5-27).

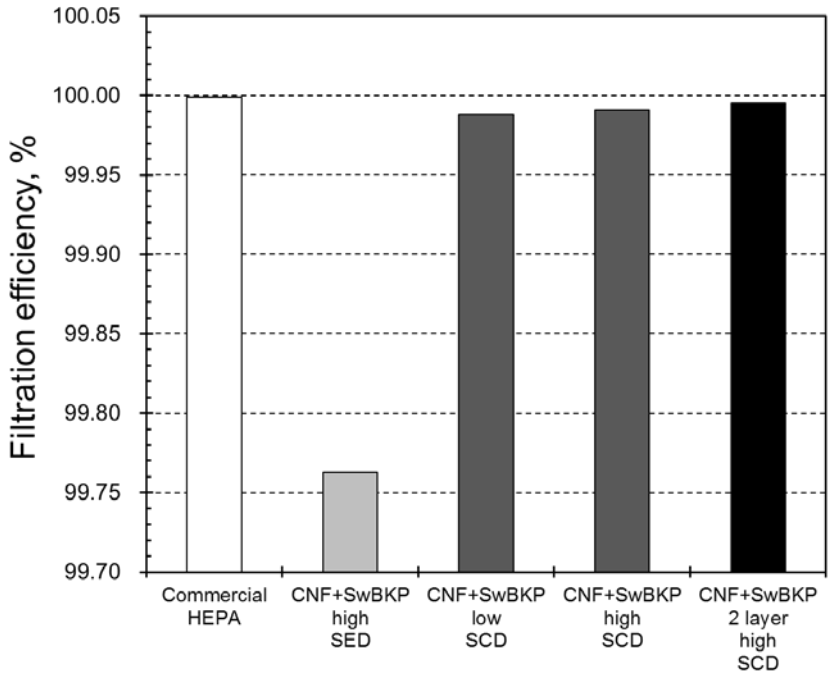

Fig. 5-25. Filtration efficiency of commercial HEPA filter, solvent exchanged, and supercritical dried sheets with the different grammage and layer composition.

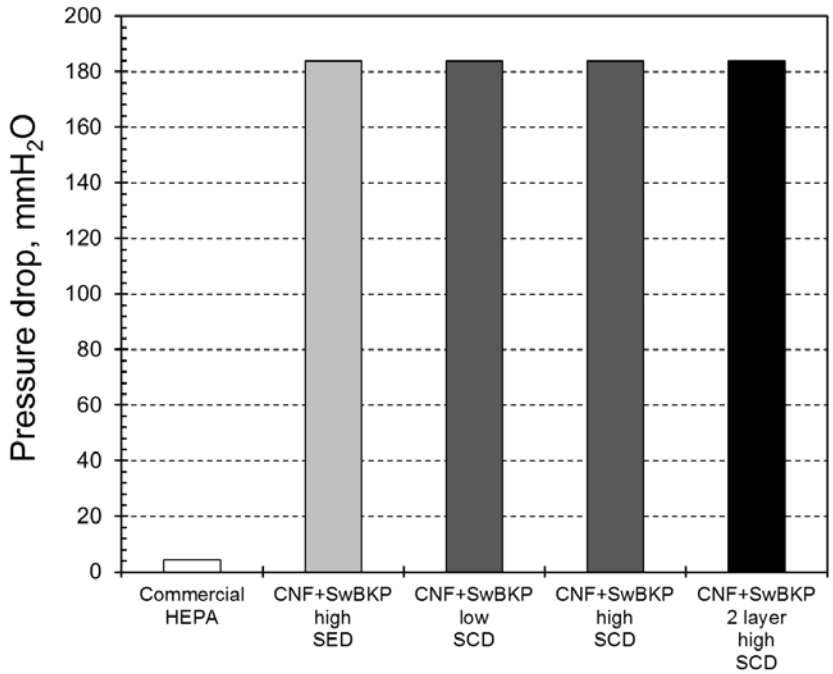

Fig. 5-26. Pressure drop of commercial HEPA filter, solvent exchanged, and supercritical dried sheets with the different grammage and layer composition.

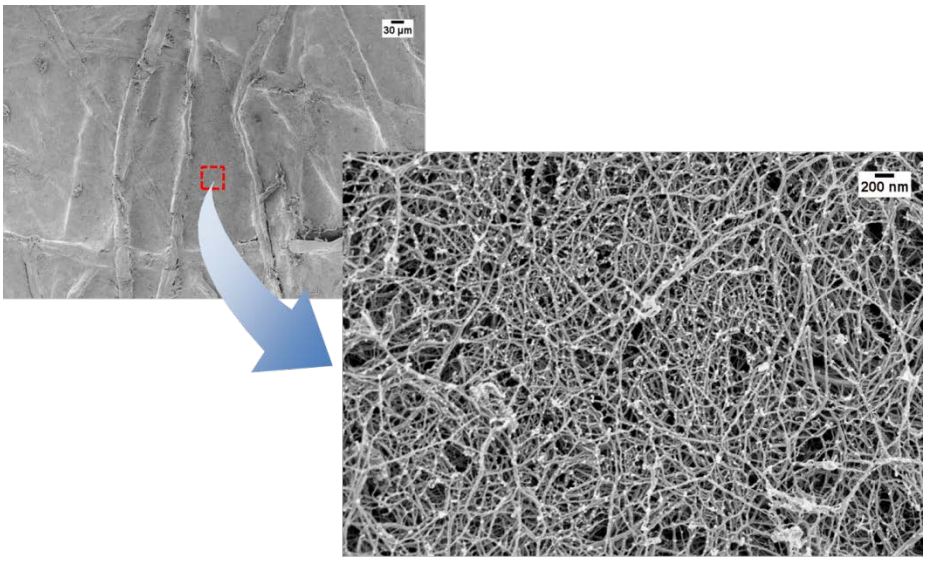

Fig. 5-27. FE-SEM surface images of supercritical dried sheet.

4. Summary

High-strength porous sheets were prepared by the addition of cellulose nanofibrils. The sheets, which consisted of SwBKP/CNF, HwBKP/CNF, PET/CNF combinations, respectively, were made by the wet-laid forming process. The pore properties of the sheets depended on manufacturing conditions such as the type of mixed fibers, CNF mixing ratio, and drying conditions (cylinder and freeze drying). The preparation of bulky sheet structures could be achieved by using fibers with large dimensions and the freeze drying method. The calculated porosity of the sheets changed from 61% to 85% in this study. Air permeability decreased exponentially with an increase in the amount of CNF. The controlled range of average pore diameter in sheets was from 0.6 μm to 36.7 μm. The mechanical strength such as the elastic modulus, tensile stress and strain at break of those sheets that contained CNF was improved for both cylinder and freeze drying conditions. The CNF-contained sheet was also prepared by using solvent exchange and supercritical drying. The highly porous sheet without shrinkage could be prepared by supercritical drying. The solvent exchanged and supercritical dried sheets showed greater stress and strain at break than commercial HEPA filter, even though the elastic modulus was relatively low.

The morphological, structural properties and filtration performance of commercial HEPA filter was investigated. Commercial HEPA filter consisted of multi-ply structure. Each layer of commercial HEPA filter consisted of fibers with different size. The top- and bottom-layer had relatively larger fibers when compared to middle-layer. The minimum width of commercial HEPA filter was approximately 59 nm.

The filtration performance of commercial HEPA filter was evaluated by using an automated filter tester with the different particle size. The most penetrating particle size was appeared between 0.1 μm and 0.4 μm. The filtration efficiency of 0.3 μm particles was 99.999045%. The pressure drop was between 4 mmH_2O and 5 mmH_2O.

The addition of CNF was beneficial in improving the filtration efficiency of particles by increasing the specific area and decreasing the pore size of sheets. In the case of freeze dried sheets, the maximum value of filtration efficiency for porous sheets was 99.944%, even though the pressure drop was high.

The filtration efficiency of CNF-contained sheet greater than 99.97% was achieved by supercritical drying. It was also affected by the grammage and layer structure of sheet. High grammage and multi-layer structure showed the better filtration efficiency. The pressure drop was still high because of the very small-sized pores by nanofibril network.

Further studies should be carried out to reduce the pressure drop for applications using porous sheets with CNF as air filter media. However, it is expected that the CNF porous sheet has a potential for use in water filtration such as microfiltration and ultrafiltration if the surface hydrophobization is accompanied.

Chapter 6

Overall Conclusions

This study was aimed to understand the effect of the physicochemical properties of fiber and suspension, and drying condition on the characteristics of CNF suspension and CNF sheet. To find out key factors for preparing porous CNF sheet, various preparation conditions were adopted. The effect of drying conditions, nanofibrillation, dewatering, chemical treatment, additives, and mixing of other fibers on sheet properties were investigated. Before drying, the properties of CNF suspension such as rheological properties and dewatering ability were evaluated. At last, the applicability of porous CNF sheet as filter media was examined.

To control the hydrogen bonds and nanofibrillation of fibers, the different drying methods, grinding passes, and dewatering time were used. The structural properties such as shrinkage, density, and porosity of CNF sheet was significantly affected by drying conditions. The room temperature drying, hot pressing, freeze drying, solvent exchange drying, and supercritical drying of wet CNF sheets were used to produce the porous CNF sheets. The highly porous CNF sheet was prepared by supercritical drying, solvent exchange drying because most of hydrogen bonds between nanofibrils were inhibited during drying. In the case of freeze drying, the porous sheet could be prepared even though partial hydrogen bonding was caused by ice crystal formed during freezing. The number of grinding passes and initial solids content at drying were also affected the structural properties of CNF sheet. The specific surface area was increased with nanofibrillation. The average pore diameter measured by BJH analysis was approximately 13 nm, which corresponds to mesopores. The sheet with mesopores is expected to use as a filter media for viruses, bacterial, and suspended materials in ultrafiltration.

The electrical charge of CNF was modified by chemical treatment or salt addition and their impacts on suspension properties and dried CNF sheet were investigated. The negative charge of CNF became stronger by carboxymethylation and TEMPO-mediated oxidation. The dispersibility of CNF was improved by electrostatic repulsion between nanofibrils, resulting in the increase in suspension viscosity and dewatering time. The dense sheet as well as optically transparent film was prepared. The density of freeze dried sheet increased with the increase in negative charge of CNF. The ionic strength of CNF suspension was changed by the different salt types and salinity. The flocculation of CNF was induced by salt and its behavior in aqueous suspension and its effect on dried CNF sheet were investigated. The dewatering ability of CNF suspension was improved by the small addition amount of salt. The drained water amount and dewatering time were affected by salt valency and concentration. The zeta potential of CNF was changed by salt addition. The dewatering ability had a strong relationship to zeta potential of CNF. The CNF with neutral charge showed the greatest dewatering ability because of the large channels formed between nanofibrils by their flocculation. The network strength of CNF was analyzed in terms of its rheological properties. The storage modulus and yield stress were increased with the increase in salt concentration. Especially, bivalent cation was more effective in network strength of nanofibrils. The CNF suspension with salt showed more solid-like behavior. The flocculation degree of CNF affected the porosity of CNF sheet. The low degree of flocculation produced the porous sheet, whereas the excessive flocculation made the sheet denser than untreated CNF sheet.

The effect of change in surface tension of suspension on dewatering and pore property of CNF sheet was investigated. The cationic surfactant, CTAB, was added on CNF suspension, resulting in that the dewatering ability was improved by increasing the amount of surfactant. The total drained water amount as well as drainage rate was improved by surfactant. Improvement in dewatering ability can be advantageous for CNF processing and further utilization. The pore property of CNF sheet was affected by decreased surface tension during drying. Highly porous CNF sheet could be prepared, showing the porosity of 91%. The elastic modulus and tensile stress at break was decreased with an increase in surfactant dosage, especially more than 2% addition amount.

Porous sheet with high mechanical strength was prepared by mixing of CNF with pulp fibers or synthetic fibers (PET). The structural properties such as thickness, density, and porosity were affected by types of mixed fibers, CNF ratio, and drying conditions. In case of cylinder and freeze drying, the density and porosity of porous sheet were controlled 0.21 – 0.58 g/cm^3 and 61 – 85%, respectively. The average pore size in porous sheet was varied from 0.6 μm to 36.7 μm. The mechanical strength of porous sheet was significantly improved by addition of CNF. The highly porous sheet was produced by solvent exchange drying and supercritical drying.

The applicability of CNF-contained sheet as an air filter media was examined in terms of filtration efficiency and pressure drop. The high filtration efficiency which is comparable to HEPA filter media was achieved by supercritical drying, whereas the cylinder, freeze, and solvent exchange

dried sheets showed the filtration efficiency below 99.97%. The filtration efficiency of porous sheet was also affected by average pore diameter, grammage, and layer structure. The pressure drop during filtration, however, was high because of the hydrogen bonds or small pores after drying. This problem would be overcome by surface modification like charging and by varying the fiber size in further study. It is expected that the porous sheet with CNF which has nanostructure can be also used as substrate for nanocomposites, membrane, and separator of batteries, etc., but further studies are required for best end-use performance.

References

Aaltonen, O., and Jauhiainen, O., The preparation of lignocellulosic aerogels from ionic liquid solutions, Carbohydr Polym 75: 125-129 (2009).

Abe, K., Iwamoto, S., and Yano, H., Obtaining cellulose nanofibers with a uniform width of 15 nm from wood, Biomacromolecules 8: 3276-3278 (2007).

Ahn, Y.C., Park, S.K., Kim, G.T., Hwang, Y.J., Lee, C.G., Shin, H.S., and Lee, J.K., Development of high efficiency nanofilters made of nanofibers, Current Applied Physics 6: 1030-1035 (2006).

Ahola, S., Österberg, M., and Laine, J., Cellulose nanofibrils – adsorption with poly(amideamine) epichlorohydrin studied by QCM-D and application as a paper strength additive, Cellulose 15: 303-314 (2008).

Alila, S., Besbes, I., Vilar, M.R., Mutjé, P., Boufi, S., Non-woody plants as raw materials for production of microfibrillated cellulose (MFC): A comparative study, Ind Crop Prod 41: 250-259 (2013).

Andresen, M., Johansson, L.S., Tanem, B.S., and Stenius, P., Properties and characterization of hydrophobized microfibrillated cellulose, Cellulose 13: 665-677 (2006).

Araki, J., and Kuga, S., Effect of trace electrolyte on liquid crystal type of cellulose microcrystals, Langmuir 17: 4493-4496 (2001).

Aulin, C., Galstedt, M., and Lindström, T., Oxygen and oil barrier properties of microfibrillated cellulose films and coatings, Cellulose 17: 559-574 (2010a).

Aulin, C., Netrval, J., Wågberg, L., and Lindström, T., Aerogels from nanofibrillated cellulose with tunable oleophobicity, Soft Matter 6: 3298-3305 (2010b).

Aulin, C., Salazar-Alvarez, G., and Lindström, T., High strength, flexible and transparent nanofibrillated cellulose-nanoclay biohybrid films with tunable oxygen and water vapor permeability, Nanoscale 4: 6622-6628 (2012).

Barhate, R.S., Loong, C.K., and Ramakrishna, S., Preparation and characterization of nanofibrous filtering media, Journal of Membrane Science 283: 209-218 (2006).

Barhate, R.S., and Ramakrishna, S., Nanofibrous filtering media: Filtration problems and solutions from tiny materials, Journal of Membrane Science 296: 1-8 (2007).

Barrett, E.P., Joyner, L.G., and Halenda, P.P., The determination of pore volume and area distribution in porous substances. I. Computations from nitrogen isotherms, J Am Chem Soc 73: 373-380 (1951).

Besbes, I., Alila, S. and Boufi, S. Nanofibrillated cellulose from TEMPO-oxidized eucalyptus fibres: effect of the carboxyl content, Carbohydr Polym 84: 975-983 (2011).

Bhardwaj, N.K., Kumar, S., and Bajpai, P.K., Effect of zeta potential on retention and drainage of secondary fibres, Colloids Surf A 260: 245-250 (2005).

Bhattacharya, M., Malinen, M.M., Lauren, P., Lou, Y.-R., Kuisma, S.W., Kanninen, L., Lille, M., Corlu, A., GuGuen-Guillouzo, C., Ikkala, O., Laukkanen, A., Urtti, A., and Yliperttula, M., Nanofibrillar cellulose hydrogel promotes three-dimensional liber cell culture, J Control Release 164: 291-298 (2012).

Bjorge, D., Daels, N., Vrieze, S.D., Dejans, P., Camp, T.V., Audenaert, W., Hogie, J., Westbroek, P., Clerck, K.D., and Hule, S.W.H., Performance assessment of electrospun nanofibers for filter applications, Desalination 249: 942-948 (2009).

Bobacka, V., and Eklund, D., The influence of charge density of cationic starch on dissolved and colloidal material from peroxide bleached thermomechanical pulp, Colloids Surf A 152: 285-291 (1999).

BS EN1822-1, High efficiency air filters (EPA, HEPA and ULPA). Part 1: Classification, parameters examination, marking, (2009).

Bulota, M., Kreitsmann, K., Hughes, M., and Paltakari, J., Acetylated microfibrillated cellulose as a toughening agent in poly(lactic acid), J Appl Polym Sci 126: E448-E457 (2012).

Cai, H., Sharma, S., Liu, W., Mu, W., Liu, W., Zhang, X., and Deng, Y., Aerogel microspheres from natural cellulose nanofibrils and their application as cell culture scaffold, Biomacromolecules 15: 2540-2547 (2014).

Carambassis, A., and Rutland, M.K., Interactions of cellulose surfaces: effect of electrolyte, Langmuir 15: 5584-5590 (1999).

Cervin, N.T., Aulin, C., Larsson, P.T., and Wågberg, L., Ultra porous nanocellulose aerogels as separation medium for mixtures of oil/water liquids, Cellulose 19: 410-410 (2012).

Chun, S.-J., Lee, S.-Y., Doh, G.-H., Lee, S., and Kim, J.H., Preparation of ultrastregnth nanopapers using cellulose nanofibrils, J Ind Eng Chem 17: 521-526 (2011).

Chun, S.-J., Choi, E.-S., Lee, E.-H., Kim, J.H., Lee, S.-Y., and Lee, S.-Y., Eco-friendly cellulose nanofiber paper-derived separator membranes featuring tunable nanoporous network channels for lithium-ion batteries, J Mater Chem 22: 16618-16626 (2012).

Deng, M., Zhou, Q., Du, A., van Kasteren, J., and Wang, Y., Preparation of nanoporous cellulose foams from cellulose-ionic liquid solutions, Mater Latt 63: 1851-1854 (2009).

de Noov, A.E.J., Besemer, A.C., and Vanbekkum, H., Selective oxidation of primary alcohols mediated by nitroxyl radical in aqueous solution – kinetics and mechanism, Tetrahedron 51: 8023-8032 (1995).

Derakhshandeh, B., Hatzikiriakos, S.G., and Bennington, C.P.J., The apparent yield stress of pulp fiber suspensions, J Rheol 54: 1137-1154 (2010).

Dimic-Misic, K., Gane, P.A.C., and Paltakari, J., Micro- and nanofibrillated cellulose as a rheology modifier additive in CMC-containing pigment-coating formulations, Ind Eng Chem Res 52: 16066-16083 (2013).

Dong, X.M., Kimura, T., Revol, J.-F., and Gray, D.G., Effect of ionic strength on the isotropic-chiral nematic phase transition of suspensions of cellulose crystallites, Langmuir 12: 2076-2082 (1996).

Dutton, K.C., Overview and analysis of the meltblown process and parameters, Journal of Textile and Apparel Technology Management 6: 1-24 (2008).

Eklund, D., and Lindström, T., Paper Chemistry: An Introduction, DT Paper Science Publications, Finland, pp 114-118 (1991).

Ellison, C.J., Phatak, A., Giles, D.W., Macosko, C.W., Bates, F.S., Melt blown nanofibers: Fiber diameter distributions and onset of fiber breakup, Polymer 48: 3306-3316 (2007).

Eriksen, Ø., Syverud, K., and Gregersen, Ø., The use of microfibrillated cellulose produced from kraft pulp as strength enhancer in TMP paper, NPPRJ 23: 299-304 (2008).

Fall, A.B., Lindström, S.B., Sprakel, J., and Wågberg, L., A physical cross-linking process of cellulose nanofibril gels with shear-controlled fibril orientation, Soft Matter 9: 1852-1863 (2013).

Feng, Z., Long, Z., and Chen, Q., Assessment of various CFD models for predicting airflow and pressure drop through pleated filter system, Building and Environment 75: 132-141 (2014).

Fermin, D., and Riley, J., Charge in colloidal systems. In: CosgrovenT (ed) Colloid science: principles, methods, and applications, 2nd edn. WILEY, UK, pp 23-44 (2010).

Ferrer, A., Quintana, E., Filpponen, I., Solala, I., Vidal, T., Rodríguez, A., Laine, J., and Rojas, O.J., Effect of residual lignin and heteropolysaccharides in nanofibrillar cellulose and nanopaper from wood fibers, Cellulose 19: 2179-2193 (2012).

Fišerová, M., Giga, J., and Balberčák, J., Relationship between fibre characteristics and tensile strength of hardwood and softwood kraft pulps, Cellulose Chem Technol 44: 249-253 (2010).

Formhals, A., Process and apparatus for preparing artificial threads, U.S. Patent 1975504, Oct. 2, (1934).

Fujisawa, S., Okita, Y., Fukuzumi, H., Saito, T. and Isogai, A. Preparation and characterization of TEMPO-oxidized cellulose nanofibril films with free carboxyl groups, Carbohydr Polym 84: 579-583 (2011).

Fukuzumi, H., Saito, T. and Isogai, A. Influence of TEMPO-oxidized cellulose nanofibril length on film properties, Carbohydr Polym 93: 172-177 (2013).

Fukuzumi, H., Saito, T., Iwata, T., Kumamoto, Y., and Isogai, A., Transparent and high gas barrier films of cellulose nanofibers prepared by TEMPO-mediated oxidation, Biomacromolecules 10: 162-165 (2009).

González, I., Boufi, S., Pèlach, M.A., Alcalà, M., Vilaseca, F., and Mutjé, P., Nanofibrillated cellulose as paper additive in eucalyptus pulps, Bioresources 7: 5167-5180 (2012).

Gopal, R., Kaur, S., Ma, Z., Chan, C., Ramakrishna, S., and Matsuura, T., Electrospun nanofibrous filtration membrane, Journal of Membrane Science 281: 581-586 (2006).

Gotoh, K., and Kikuchi, S., Improvement of wettability and detergency of polymeric materials by excimer UV treatment, Colloid Polym Sci 284: 1356-1360 (2005).

Goussé, C., Chanzy, H., Cerrada, M.L., and Fleury, E., Surface silylation of cellulose microfibrils: preparation and rheological properties, Polymer 45: 1569-1575 (2004).

Guenet, J.M., Structure versus rheological properties in fibrillary thermoreversible gels from polymers and biopolymers, J Rheol 44: 947-960 (2000).

Guibo, Y., Qing, Z., Yahong, Z., Yin, Y., and Yumin, Y., The electrospun polyamide 6 nanofiber membranes used as high efficiency filter materials: filtration potential, thermal treatment, and their continuous production, J Appl Polym Sci 128: 1061-1069 (2012).

Habibi, Y., Lucia, L.A., and Rojas, O.J., Cellulose nanocrystals: chemistry, self-assembly, and applications, Chem Rev 110: 3479-3500 (2010).

Henriksson, M., Henriksson, G., Berglund, L.A., and Lindström, T., An environmentally friendly method for enzyme-assisted preparation of microfibrillated cellulose nanofibers, Eur Polym J 43: 3434-3441 (2007).

Henriksson, M., Berglund, L.A., Isaksson, P., Lindström, T., and Nishino, T., Cellulose nanopaper structure of high toughness, Biomacromolecules 9: 1579-1585 (2008).

Herrick, F.W., Casebier, R.L., Hamilton, J.K., and Sandberg, K.R., Microfibrillated cellulose: morphology and accessibility, J Appl Polym Sci: Appl Polym Symp 37: 797-813 (1983).

Hii, C., Gregersen, Ø.W., Chinga-Carrasco, G., and Eriksen, Ø., The effect of MFC on the pressability and paper properties of TMP and GCC based sheets, Nord Pulp Pap Res J 27: 388-396 (2012).

Ho, T.T.T., Zimmermann, T., Ohs, S., and Caseri, W.R., Composites of cationic nanofibrillated cellulose and layered silicates: water vapor barrier and mechanical properties, ACS Appl Mater Interfaces, 4: 4832-4840 (2012).

Huang, X., Separator technologies for lithium-ion batteries, Cellulose 15: 649-662 (2011).

Huang, Z.M., Zhang, Y.Z., Kotaki, M., and Ramakrishna, S., A review on polymer nanofibers by electrospinning and their applications in nanocomposites, Compos Sci Technol 63: 2223-2253 (2003).

Hubbe, M.A., Bonding between cellulosic fibers in the absence and presence of dry-strength agents – a review, Bioresources 1: 281-318 (2006).

Hubbe, M.A., Rojas, O.J., Lucia, L.A., and Sain, M., Cellulosic nanocomposites: a review, Bioresources 3: 929-980 (2008).

Ifuku, S., Nogi, M., Abe, K., Handa, K., Nakatsubo, F., and Yano, H., Surface modification of bacterial cellulose nanofibers for property enhancement of optically transparent composites: dependence on acetyl-group DS, Biomacromolecules 8: 1973-1978 (2007).

Ifuku, S., and Saimoto, H., Chitin nanofibers: preparation, modifications, and applications, Nanoscale 4: 3308-3318 (2012).

Isogai, A., Saito, T., and Fukuzumi, H., TEMPO-oxidized cellulose nanofibers, Nanoscale 3: 71-85 (2011).

Iwamoto, S., Abe, K., and Yano, H., The effect of hemicelluloses on wood pulp nanofibrillation and nanofiber network characteristics, Biomacromolecules 9: 1022-1026 (2008).

Iwamoto, S., Nakagaito, A.N., Yano, H., and Nogi, M., Optically transparent composites reinforced with plant fiber-based nanofibers, Appl Phys A 81: 1109-1112 (2005).

Iwamoto, S., Nakagaito, A.N., and Yano, H., Nano-fibrillation of pulp fibers for the processing of transparent nanocomposites, Appl Phys A 89: 461-466 (2007).

Iwatake, A., Nogi, M., and Yano, H., Cellulose nanofiber-reinforced polylactic acid, Compos Sci Technol 68: 2103-2106 (2008).

Janardhnan, S., and Sain, M., Isolation of cellulose nanofibrils – an enzymatic approach, Bioresources 1: 176-188 (2006).

Karppinen, A., Vesterinen, A.-H., Saarinen, T., Pietikäinen, P., and Seppälä, J., Effect of cationic polymethacrylates on the rheology and flocculation of microfibrillated cellulose, Cellulose 18: 1381-1390 (2011).

Kékicheff, P., Marcelja, S., Senden, T.J., and Shubin, V.E., Charge reversal seen in electrical double layer interaction of surfaces immersed in 2:1 calcium electrolyte, J Chem Phys 99: 6098-6113 (1993).

Kim, D.Y., Nishiyama, Y., and Kuga, S., Surface acetylation of bacterial cellulose, Cellulose 9: 361-367 (2001).

Kirby, B.J., and Hasselbrink, E.F., Zeta potential of microfluidic substrates: 1. theory, experimental techniques, and effects on separations, Electrophoresis 25: 187-202 (2004).

Klemm, D., Schumann, D., Kramer, F., Hessler, N., Hornung, M., Schmauder, H.P., and Marsch, S., Nanocelluloses as innovative polymers in research and application, Polysaccharides 205: 49-96 (2006).

Klemm, D., Philipp, B., Heinze, T., Heinze, U., and Wagenknecht, W., Comprehensive cellulose chemistry, WILEY-VCH Verlag GmbH, Weinheim, (1998).

Kowalski, W.J., Bahnfleth, W.P., and Whittam, T.S., Filtration of airborne microorganisms: modeling and prediction, ASHRAE Trans 105: 4-17 (1999).

Kuga, S., Kim, D.-Y., Nishiyama, Y., and Brown, R.M., Nanofibrillar carbon from native cellulose, Mol Cryst Liq Cryst 387: 13-19 (2002).

Laka, M., and Chernyavskaya, S., Effect of salts on the formation and properties of microcrystalline cellulose and chitosan gels, Holzforschung 63: 665-669 (2009).

Lasseuguette, E., Roux, D., and Nishiyama, Y., Rheological properties of microfibrillar suspension of TEMPO-oxidized pulp, Cellulose 15: 425-433 (2008).

Lavoine, N., Bras, J., and Desloges, I., Mechanical and barrier properties of cardboard and 3D packaging coated with microfibrillated cellulose, J Appl Polym Sci 131: 40106 (2014).

Li, M., Wang, D., Xiao, R., Sun, G., Zhao, Q. and Li, H., A novel high flux poly(trimethylene terephthalate) nanofiber membrane for microfiltration media, Separation and Purification Technology 116: 199-205 (2013).

Lim, T.T., and Huang, X., Evaluation of hydrophobicity/oleophilicity of kapok and its performance in oily water filtration: Comparison of raw and solvent-treated fibers, Industrial Crops and Products 26: 125-134 (2007).

López-Rubio, A., Lagaron, J.M., Ankerfors, M., Lindström, T., Nordqvist, D., Mattozzi, A., and Hedenqvist, M.S., Enhanced film forming and film properties of amylopectin using micro-fibrillated cellulose, Carbohydr Polym 23: 718-727 (2007).

Nakagaito, A.N., and Yano, H., The effect of morphological changes from pulp fiber towards nano-scale fibrillated cellulose on the mechanical properties of high-strength plant fiber based composites, Appl. Phys. A 78: 547-552 (2004).

Nakagaito, A.N., and Yano, H., Novel high-strength biocomposites based on microfibrillated cellulose having nano-order-unit web-like network structure, Appl Phys A 80: 155-159 (2005).

Nogi, M., Abe, K., Handa, K., Nakatsubo, F., Ifuku, S. and Yano, H., Property enhancement of optically transparent bionanofiber composites by acetylation, Appl Phys Lett 89: 1-3 (2006).

Nogi, M., Iwamoto, S., Nakagaito, A.N., and Yano, H., Optically transparent nanofiber paper, Adv Mater 21: 1595-1598 (2009).

Nogi, M., and Yano, H., Optically transparent nanofiber sheets by deposition of transparent materials: a concept for a roll-to-roll processing, Appl Phys Lett 94: 233117 (2009).

Okahisa, Y., Yoshida, A., Miyaguchi, S., and Yano, H., Optically transparent wood-cellulose nanocomposite as a base substrate for flexible organic light-emitting diode displays, Compos Sci Technol 69: 1958-1961 (2009).

Okita, Y., Saito, T. and Isogai, A. Entire surface oxidation of various cellulose microfibrils by TEMPO-mediated oxidation, Biomacromolecules 11: 1696-1700 (2010).

Olszewska, A., Eronen, P., Johansson, L.-S., Malho, J.-M., Ankerfors, M., Lindström, T., Ruokolainen, J., Laine, J., and Österberg, M., The behaviour of cationic nanofibrillar cellulose in aqueous media, Cellulose 18: 1213-1226 (2011).

Ono, H., Shimaya, Y., Sato, K., and Hongo, T., ^{1}H spin-spin relaxation time of water and rheological properties of cellulose nanofiber dispersion, transparent cellulose hydrogel (TCG), Polym J 36: 684-694 (2004).

Pääkkö, M., Ankerfors, M., Kosonen, H., Nykänen, A., Ahola, S., Österberg, M., Ruokolainen, J., Laine, J., Larsson, P.T., Ikkala, O., and Lindström, T., Enzymatic hydrolysis combined with mechanical shearing and high-pressure homogenization for nanoscale cellulose fibrils and strong gels, Biomacromolecules 8: 1934-1941 (2007).

Pääkkö, M., Vapaavuori, J., Silvennoinen, R., Kosonen, H., Ankerfors, M., Lindström, T., Berglund, L.A., and Ikkala, O., Long and entangled native cellulose I nanofibers allow flexible aerogels and hierarchically porous templates for functionalities, Soft Matter 4: 2492-2499 (2008).

Pavia, D.L., Lampman, G.M., and Kriz, G.S., Introduction to spectroscopy: a guide for students of organic chemistry, 2nd (ed), Saunders College Publishing, (1996).

Peng, Y., Gardner, D.J., and Han, Y., Drying cellulose nanofibrils: in search of a suitable method, Cellulose 19: 91-102 (2012).

Plackett, D.V., Letchford, K., Jackson, J.K., and Burt, H.M., A review of nanocellulose as a novel vehicle for drug delivery, Nord Pulp Pap Res J 29: 105-118 (2014).

Podgórski, A., Balazy, A., and Gradoń, L., Application of nanofibers to improve the filtration efficiency of the most penetrating aerosol particles in fibrous, Chem Eng Sci 61: 6804-6815 (2006).

Rodionova, G., Lenes, M., Eriksen, Ø., and Gregersen, Ø., Surface chemical modification of microfibrillated cellulose: improvement of barrier properties for packaging applications, Cellulose 18: 127-134 (2011).

Rouquerol, J., Avnir, D., Fairbridge, C.W., Everett, D.H., Haynes, J.H., Pernicone, N., Ramsay, J.D.F., Sing, K.S.W., and Unger, K.K., Recommendations for the characterization of porous solids (Technical Report, IUPAC), Pure Appl Chem 66: 1739-1758 (1994).

Ryu, J., Fundamental properties of nanofibrillated cellulose in suspension and mat states, PhD thesis, Seoul National University (2013).

Saarikoski, E., Saarinen, T., Salmela, J., and Seppälä, J., Flocculated flow of microfibrillated cellulose water suspensions: an imaging approach for characterization of rheological behavior, Cellulose 19: 647-659 (2012).

Saito, T., Hirota, M, Tamura, N., Kimura, S., Fukuzumi, H., Heux, L. and Isogai, A., Individualization of nano-sized plant cellulose fibrills by direct surface carboxylation using TEMPO catalyst under neutral conditions, Biomacromolecules 10: 1992-1996 (2009).

Saito, T., and Isogai, A., TEMPO-mediated oxidation of native cellulose. The effect of oxidation conditions on chemical and crystal structure of the water-insoluble fractions, Biomacromolecules 5: 1983-1989 (2004).

Saito, T., Kimura, S., Nishiyama, Y., and Isogai, A., Cellulose nanofibers prepared by TEMPO-mediated oxidation of native cellulose, Biomacromolecules 8: 2485-2491 (2007).

Saito, T., Nishiyama, Y., Putaux, J.-L., Vigon, M. and Isogai, A. Homogeneous suspension of individuallized microfibrils from TEMPO-catalyzed oxidation of native cellulose, Biomacromolecules 7: 1687-1691 (2006).

Saputra, A.H., Qadhayna, L., and Pitaloka, A.B., Synthesis and characterization of carboxymethyl cellulose (CMC) from water hyacinth using ethanol-isobutyl alcohol mixture as the solvents, International Journal of Chemical Engineering and Applications 5: 36-40 (2014).

Sehaqui, H., Salajková, M., Zhou, Q., and Berglund, LA., Mechanical performance tailoring of tough ultra-high porosity foams prepared from cellulose I nanofiber suspensions, Soft Matter 6: 1824-1832 (2010).

Sehaqui, H., Zhou, Q., and Berglund, L.A., High-porosity aerogels of high specific surface area prepared from nanofibrillated cellulose (NFC), Compos Sci Technol 71: 1593-1599 (2011a).

Sehaqui, H., Zhou, Q., Ikkala, O., and Berglund, L.A., Strong and tough cellulose nanopaper with high specific surface area and porosity, Biomacromolecules 12: 3638-3644 (2011b).

Shaw, D.J., Charged interfaces, In: Shaw DJ (ed) Introduction to colloid and surface chemistry. 4th edn. Butterworth Heinemann, UK, pp 174-209 (1992).

Shimaoka, T., Development of transparent cellulose nano fiber film for flexible displays, 2015 TAPPI International Conference on Nanotechnology for Renewable Materials, June 22-25, Atlanta, GA, (2015).

Silva, T.C.F., Habibi, Y., Colodette, J.L., Elder, T. and Lucia, L.A. A fundamental investigation of the microarchitecture and mechanical properties of TEMPO-oxidized nanofibrillated cellulose (NFC)-based aerogels, Cellulose 19: 1945-1956 (2012).

Sim, K., Ryu, J., and Youn, H.J., Structural characteristics of nanofibrillated cellulose mats: Effect of preparation conditions, Fibers and Polymers 16: 294-301 (2015).

Siqueira, G., Bras, J., and Dufresne, A., Cellulosic bionanocomposites: a review of preparation, properties, and applications, Polymers 2: 728-765 (2010).

Siró, I., and Plackett, D., Microfibrillated cellulose and new nanocomposite materials: a review, Cellulose 17: 459-494 (2010).

Sirviö, J., Fibres and bonds. In: Kaarlo N (ed) Paper physics, 2nd edn. Finnish Paper Enginners' Association/Paperi ja Puu Oy, Finland, pp.60-92 (2008).

Sood, Y.V., Tyagi, R., Tyagi, S., Pande, P.C., and Tondon, R., Surface charge of different paper making raw materials and its influence on paper properties, J Sci Ind Res 69: 300-304 (2010).

Spence, K.L., Venditti, R.A., Rojas, O.J., Pawlak, J.J., and Hubbe, M.A., Water vapor barrier properties of coated and filled microfibrillated cellulose composite films, Bioresources 6: 4370-4388 (2011).

Stenstad, P., Andresen, M., Tanem, B.S., and Stenius, P., Chemical surface modifications of microfibrillated cellulose, Cellulose 15: 35-45 (2008).

Sundarrajan, S., Balamurugan, R., Kaur, S., and Ramakrishna, S., Potential of engineered electrospun nanofiber membranes for nanofiltration applications, Drying Technology 31: 163-169 (2013).

Svensson, A., Larsson, T., and Wågberg, L. Formation of dry ultra-porous cellulose structure - Characterisation and initial utilisation, International Paper Physics Conference & 8th International Paper and Coating Chemistry Symposium, June 10-14, Stockholm, Sweden, (2012).

Syverud, K., and Stenius, P., Strength and barrier properties of MFC films, Cellulose 16: 75-85 (2009).

Taipale, T., Österberg, M., Nykänen, A., Ruokolainen, J., and Laine, J., Effect of microfibrillated cellulose and fines on the drainage of kraft pulp suspension and paper strength, Cellulose 17: 1005-1020 (2010).

Tanaka, R., Saito, T. and Isogai, A. Cellulosic nanofibrils prepared from softwood cellulose by TEMPO/NaClO/$NaClO_2$ systems in water at 4.8 or 6.8, International Journal of Biological Macromolecules 51: 228-234 (2012).

Taniguchi, T., and Okamura, K., New films produced from microfibrillated natural fibres, Polym Int 47: 291-294 (1998).

Tatsumi, D., Ishiok, S., and Matsumoto, T., Effect of fiber concentration and axial ratio on the rheological properties of cellulose fiber suspension, J Soc Rheol Jpn 30: 27-32 (2002).

Tingaut, P., Zimmermann, T., and Lopez-Suevos, F., Synthesis and characterization of bionanocomposites with tunable properties from poly(lactic acid) and acetylated microfibrillated cellulose, Biomacromolecules 11: 454-464 (2010).

Turbak, A.F., Snyder, F.W., and Sandberg, K.R., Microfibrillated cellulose, a new cellulose product: properties, uses, and commercial potential, J Appl Polym Sci: Appl Polym Symp 37: 815-827 (1983).

Uppal, R., Bhat, G., Eash, C., and Akato, K., Meltblown nanofiber media for enhanced quality factor, Fibers and Polymers 14: 660-668 (2013).

Varanasi, S., and Batchelor, W., Superior non-woven sheet forming characteristics of low-density cationic polymer-cellulose nanofiber colloids, Cellulose 21: 3541-3550 (2014).

Vesterinen, A., Myllytie, P., Laine, J., and Seppälä, J., The effect of water-soluble polymers on rheology of microfibrillar cellulose suspension and dynamic mechanical properties of paper sheet, J Appl Polym Sci 116: 2990-2997 (2010).

Wågberg, L., Decher, G., Norgren, M., Lindström, T., Ankerfors, M., and Axnäs, K., The build-up of polyelectrolyte multilayers of microfibrillated cellulose and cationic polyelectrolytes, Langmuir 24: 784-795 (2008).

Wang, X., Kim, K., Lee, C., and Kim, J., Prediction of air filter efficiency and pressure drop in air filtration media using a stochastic simulation, Fibers and Polymers 9: 34-38 (2008).

Ward, G., Nanofibers: media at the nanoscale, Filtration & Separation 42(7):22-24 (2005).

Webb, P.A., and Orr, C., Analytical methods in fine particle technology, Micromeritics Instrument Corporation, Norcross, GA, (1997).

Xhanari, K., Syverud, K., Chinga-Carrasco, G., Paso, K., and Stenius, P., Reduction of water wettability of nanofibrillated cellulose by adsorption of cationic surfactants, Cellulose 18: 257-270 (2011).

Yano, H., Sugiyama, J., Nakagaito, A.N., Nogi, M., Matsuura, T., Hikita, M., and Handa, K., Optically transparent composites reinforced with networks of bacterial nanofibers, Adv Mater 17: 153-155 (2005).

Yeh, H.-C., and Liu, B.Y.H., Aerosol filtration by fibrous filters – I. theroretical, J Aerosol Sci 5: 191-204 (1974).

Youn, H.J., and Lee, H.L., An experimental investigation of the effect of pulp types, mechanical treatments and crill contents on fibre network strength, Nord Pulp Pap Res J 17: 187-192 (2002).

Yun, K.M., Hogan, C.J., Matsubayashi, Y., Kawabe, M., Iskandar, F., and Okuyama, K., Nanoparticle filtration by electrospun polymer fibers, Chem Eng Sci 62: 4751-4759 (2007).

Zhang, Q., Welch, J., Park, H., Wu, C.Y., Sigmund, W., and Marijnissen, J.C.M., Improvement in nanofiber filtration by multiple thin layers of nanofiber mats, J Aerosol Sci 41: 230-236 (2010).

Zhang, Z., Sèbe, G., Rentsch, D., Zimmermann, T., and Tingaut, P., Ultralightweight and flexible silylated nanocellulose sponges for the selective removal of oil from water, Chem Mater 26: 2659-2668 (2014).

Zheng, G.Y., Cui, Y., Karabulut, E., Wågberg, L., Zhu, H., and Hu, L., Nanostructured paper for flexible energy and electronic devices, Mrs bulletin 38: 320-325 (2013).

Zheng, Q., Cai, Z., and Gong, S., Green synthesis of polyvinyl alcohol (PVA) – cellulose nanofibril (CNF) hydrid aerogels and their use as superabsorbents, J Mater Chem A 2: 3110-3118 (2014).

Zhuang, X., Cheng, B., Guan, K., Kang, W., Ren, Y., Preparation of polyacrylonitrile nanofibers by solution blowing process, J Eng Fiber Fabr 8(1): 1-6 (2013).

Zimmermann, T., Pöhler, E., and Geiger, T., Cellulose fibrils for polymer reinforcement, Adv Eng Mater 6: 754-761 (2004).

Zugenmaier, P., Crystalline cellulose and cellulose derivatives: characterization and structures, Springer series in wood science, Springer-Verlag, Berlin, Heidelberg, (2008).

초 록

셀룰로오스 나노피브릴 (Cellulose nanofibrils, CNF)은 재생가능하고 생분해성이며, 높은 강도 특성과 비표면적을 나타낸다. 섬유의 폭은 100 nm 미만이고 길이는 수 마이크로미터에 달한다. CNF 현탁액은 다량의 물을 가지고 있기 때문에 고부가가치 물질로서 활용하기 위해서는 탈수와 건조를 통해 현탁액으로부터 물을 제거하는 과정이 필요하다. 탈수 및 건조 과정을 거쳐 CNF를 다공성의 재료로 제조할 수 있으며, 나노 수준에서의 구조적 성질을 이해하고 제어하는 것이 중요하다. 본 연구에서는 CNF를 이용하여 다공성 시트를 제조하고, 섬유 및 현탁액의 물리화학적 성질과 건조 조건이 다공성 CNF 시트의 특성에 미치는 영향을 구명하고자 하였다. 첫째로, 섬유의 나노화 정도, 시트 포밍 조건, 건조 조건이 CNF 시트의 구조적 특성에 미치는 영향을 평가하였다. 둘째로는, 표면 처리 및 첨가제가 CNF 현탁액 및 시트 특성에 미치는 영향을 평가하였다. 마지막으로, 다공성 CNF 시트를 이용하여 공기 필터로서의 적용성을 연구하였다.

초임계건조, 용매치환건조 및 동결건조 방식을 통해 건조 시 수소 결합을 억제함으로써 저밀도, 다공성의 CNF 시트를 제조할 수 있었다. 상온건조 및 열기압착건조는 고밀도의 시트를 제조하는데 용이하였다. CNF 시트의 공극률은 건조 방법뿐만 아니라 나노피브릴화 및 탈수된 정도에 의해서도 영향을 받았다. BET 분석 시 CNF 시트는 메조포어 (mesopores)를 가졌다.

CNF의 표면전하 특성 또는 현탁액의 표면장력을 조절함으로써 CNF의 응집 또는 분산 정도를 변화시켰으며, 이것이 CNF 현탁액과 시트 특성에 미치는 영향을 평가하였다. CNF의 표면전하 특성은 카르복시메틸화 또는 TEMPO 촉매 산화와 같은 화학적 처리 또는 염과 같은 화학 첨가제를 통해 조절하였다. 카르복시메틸화는 CNF 제조 시 전처리로서 실시하였으며, 반투명한 하이드로젤 성상의 CNF가 제조되었다. 정전기적 반발력이 증가함에 따라 현탁액의 점도가 증가하고 탈수성이 감소하였다. 동결건조 시트는 무처리 시트에 비해 고밀화되어 투명성이 증가하였다. TEMPO 촉매 산화는 CNF에 대해 후처리로서 실시하였으며, 산화제 투입량이 증가함에 따라 시트의 밀도가 증가하였다. 염의 종류 및 농도에 따라 전기이중층이 압축되는 정도가 달라지면서 CNF의 응집 거동이 달라졌다. 염에 의해 이온성이 변함에 따라 CNF 현탁액의 점도, 저장탄성계수 및 항복응력이 증가하였고 고체와 같은 거동을 나타냈다. 2가 양이온이 1가 양이온에 비해 적은 양으로도 현탁액의 네트워크 강도 증가 및 탈수성 향상에 더 효과적인 것으로 나타났다. 또한, CNF의 응집된 정도에 따라 시트의 구조적 성질이 영향을 받았다. CNF 현탁액 내 물의 표면장력을 변화시키기 위해 계면활성제를 첨가하였다. 물의 표면장력이 감소함에 따라 현탁액의 총 탈수량 및 탈수 속도가 증가하였고, 건조 시 CNF 시트의 공극률이 증가하였다.

다공성 CNF 시트의 공기 필터로서의 적용성을 탐색하기 위해 천연 펄프 섬유 또는 PET 섬유를 CNF와 혼합함으로써 고강도 다공성 시트를 제조하고 특성을 평가하였다. 다공성 시트의 밀도 및

공극률은 혼합된 섬유의 성상 및 건조 조건에 의해 영향을 받았다. CNF 첨가를 통해 시트의 강도 특성을 크게 향상시킬 수 있었다. 다공성 시트의 필터링 성능을 평가한 결과, 초임계건조를 통해 99.97% 이상의 필터링 효율을 달성할 수 있었다. 차압 문제는 표면 처리 및 섬유 크기 조절을 통해 해결될 수 있을 것으로 판단된다. 다공성 CNF 시트는 공극 특성에 따라 공기 필터뿐만 아니라 복합재의 기재 및 정수 필터로도 활용할 수 있을 것으로 기대한다.

주요어 : 셀룰로오스 나노피브릴, 시트, 공극, 건조, 응집, 화학적 처리, 염, 계면활성제, 유변학적 성질, 탈수, 공기 필터

학번 : 2009-21202